Development of DNA Origami Structures for Application in Single-Molecule Fluorescence Studies

Masterarbeit aus dem Fachgebiet

Physikalische Chemie

von

cand. chem. Kira Bartnik

geboren am 15.01.1991

in Mannheim

für die Masterprüfung in Biochemie an der

Ludwig-Maximilians-Universität München

Datum der mündlichen Prüfung: 06.07.2015

Beginn der Masterarbeit: 01.09.2015

Masterarbeit beim Prüfungsausschuss eingereicht am 01.03.2016

Erklärung

Ich versichere, dass ich die vorgelegte Masterarbeit am Department Chemie, Physikalische Chemie der Ludwig-Maximilians-Universität München unter der Anregung und Anleitung von Prof. Don C. Lamb und Dr. Alvaro H. Crevenna selbstständig durchgeführt und keine anderen als die angegebenen Hilfsmittel und Quellen benützt habe.

München, den 01.03.2016

……..

1. Berichterstatter: Prof. Don C. Lamb
2. Berichterstatter: Prof. Achim Hartschuh

Abstract

Single-molecule experiments have proven a powerful tool to investigate biological systems. Two appropriate methods, which are based on fluorescently labeled molecules, are total internal reflection fluorescence (TIRF) or confocal microscopy. Custom-designed DNA nanostructures (DNA origami) can provide a platform to arrange molecules in close proximity, while the overall molecular concentration is kept low enough for single-molecule detection. In this thesis, DNA origami structures served as scaffolds to elucidate assembly mechanisms and dynamics of macro-molecular complexes. Firstly, it was attempted to assemble sarcomeres, the basic contractile units of the skeletal muscle, in solution. For this purpose, a DNA origami two-layer sheet served as an artificial "Z-disc" with binding sites for the actin-capping protein CapZ. However, even after several modifications of the assembly protocol, sarcomere-like structures could not be observed by TIRF. Secondly, a DNA origami structure was established for DNA double-strand break (DSB) repair studies. DNA DSBs are considered the most cytotoxic form of DNA damage and efficient repair is crucial to maintain genomic integrity. In humans, non-homologous end joining (NHEJ) and homologous recombination (HR) are the main repair pathways. However, the assembly of the repair complex and its dynamics have not been visualized yet. A DNA origami structure was designed and tested for its potential to serve as a platform for DNA DSB repair studies. As a proof of principle, two fluorescently labeled DNA double-strands were bound to the DNA origami and "repaired" with the T4 DNA ligase. The success of the ligation reaction was monitored by Förster Resonance Energy Transfer (FRET). The designed DNA origami system can therefore be used for further DNA DSB repair studies.

Contents

List of Figures

List of Tables

I. Introduction

Artificial models are a common approach to mimic biological systems. DNA origamis have proven a useful tool to position (bio)molecules with nanoscale precision[1-3] and are applied here as model systems to elucidate assembly mechanisms and dynamics of macro-molecular complexes.

I.1. DNA nanotechnology

The term DNA origami refers to the folding of DNA into arbitrary two- and three-dimensional shapes. A DNA origami consists of an even number of parallel bundles of double-stranded DNA (dsDNA), which are built of a roughly 7-kilobase, usually circular single-stranded DNA chain (termed scaffold) and many short DNA single-strands (referred to as staples). Staples bind to the scaffold in a pre-programmed manner through Watson-Crick base-pairing and fold it into the desired shape[4].

A simple method to fold DNA into nanoscale objects was first introduced by Paul W. K. Rothemund in 2006, when he created several two-dimensional DNA origami structures[4]. Rothemund mixed the scaffold with a 100-fold excess of staples and used a temperature gradient for assembly. A famous example is his DNA smiley (figure 1).

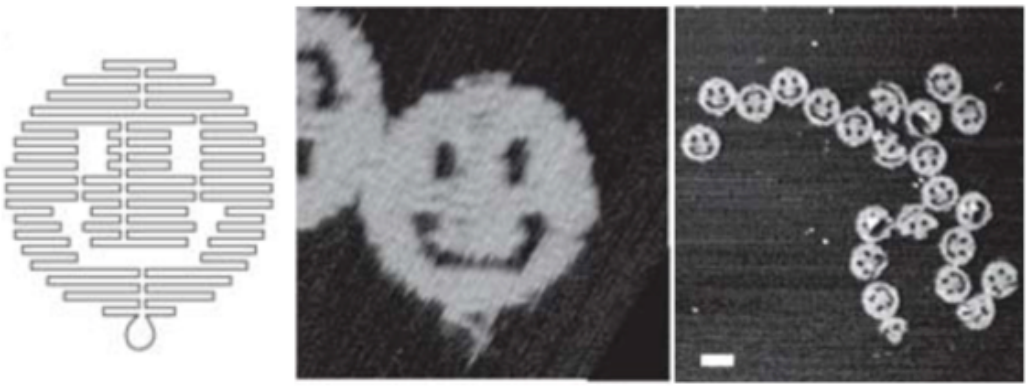

Figure 1: Folding path (left) and AFM images of a DNA smiley. The size of the enlarged AFM image (middle) is 165 nm x 165 nm, the scale bar for the right image is 100 nm. Images taken from[4].

A few years later, the method was extended to three-dimensional shapes and the open-source design software CaDNAno was developed[5]. CaDNAno, and its successor

CaDNAno2, offer the possibility to create objects of various sizes, as the DNA origami design can be based on a honeycomb or a square lattice. On the honeycomb lattice, each double-helix has three neighbors, while each double-helical domain on the square lattice has four direct neighbors. Using the square lattice structure, densely packed structures are created, while the honeycomb lattice leads to more porous structures, enabling to create larger objects[6]. The main steps for designing a DNA origami are summarized in the following chapter.

DNA origamis can be functionalized at specific positions by integrating staple strands with DNA extensions or functional groups. As each staple strand can be functionalized individually, DNA origamis have become a useful tool to position molecules with nanoscale precision[1]. Examples are the attachment of proteins[2] or the incorporation of both biotinylated staples and a fluorescent dye for position-specific single-molecule studies in zero-mode-waveguides[3].

I.2. DNA origami design

To design a DNA origami, it has to be chosen first if the design should be based on the honeycomb or square lattice and if the structure should consist of one or several layers. Based on these decisions, the scaffold has to be brought into the desired shape. The structure should be designed to closely match one of the limited choices of scaffolds. In addition to the commonly used genome derivatives preloaded in CaDNAno and CaDNAno2 (M13mp18 (7249 nucleotides), p7308, p7560, p7704, p8064, p8100, p8634), a scaffold sequence of choice can be uploaded. Scaffold crossovers are introduced to create a singular scaffold path. Crossovers are inter-helix connections, which consist of immobilized Holliday junctions[7]. Next, complementary staple strands are added and cut into shorter parts. The length of the individual staple strands should be in the range of 18 to 50 nucleotides[6]. If staples are shorter than 18 nucleotides, their binding to the scaffold might not be stable at room temperature, while synthesis costs increase with the staple length. There are several rules for the staple paths. The minimal distance to the next crossover should be at least 4 nucleotides to avoid detachment of the staple at this position. If a staple is divided into several parts by crossovers, a short part in between two longer parts should be avoided to prevent energy traps. The longer parts are more stable at higher temperatures and will therefore bind earlier to the

scaffold than the short part of the staple, leaving the short part no chance to attach as well. An example for a bad (left) and good design (right) is shown in figure 2. Furthermore, staple strands should not end at scaffold crossovers[8].

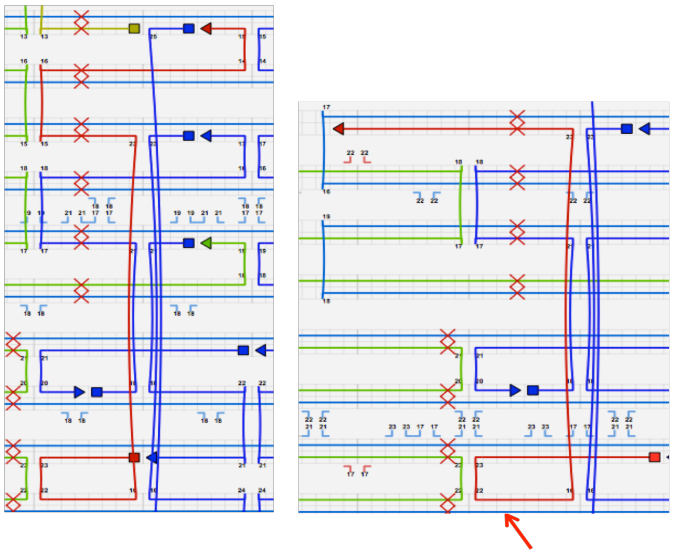

Figure 2: Example for a bad (right) and a good DNA origami design (left) concerning the path for the red staple. In the right image is a medium segment (red arrow) between two longer staple parts.

To improve folding yields, staple strands should contain one large segment of at least 14 nucleotides (without strand breaks or staple and scaffold crossovers) that binds to a complementary continuous segment of the scaffold. The 14 nucleotide segments probably act as seeds which propagate proper folding of the structure[9]. Staple strands at the ends of the structure can stack together through blunt end interaction[4,10]. To avoid aggregation by blunt-end association, Poly-T or Poly-C tails can be added at the ends of the helices. Single-stranded scaffold DNA loops at the helical interfaces serve the same purpose[11].

When the design process is completed, the nucleotide sequences of the scaffold and staple strands are added. Based on these sequences, staple strands can be ordered.

Before synthesizing the staples, the three-dimensional structure of the DNA origami has to be checked. For this purpose the program Computer-aided engineering for DNA origami (CanDo) was developed[6]. Based on CaDNAno files, the 3-D origami shape is computed by applying the finite element method. DNA base pairs are modeled as two-node beam finite elements representing an elastic rod with effective parameters for

geometry and material (e.g. 0.34 nm for the length of a base pair and 2.25 nm for its diameter[12]).

I.3. Biological Background

During this master's thesis, two different DNA origami structures served as platforms for single-molecule fluorescence studies. Firstly, a two-layer rectangular sheet with binding sites for the actin-capping protein CapZ was used to study the assembly of sarcomere-like structures in solution. Secondly, a two-layer sheet with gap harboring two attachment sites for dsDNA substrates was designed for a DNA double-strand break (DSB) repair study. The biological background for both projects involving the most important proteins and enzymes are summarized in the following sections.

I.3.1. Composition and function of sarcomeres

Contraction of skeletal muscles is fundamental for all kinds of movement in animals. Contraction depends on the ATP-driven sliding of highly organized arrays of actin "thin" filaments against arrays of myosin "thick" filaments within the basic contractile units termed sarcomeres[13]. The cross section of actin thin and myosin thick filaments and their hexameric arrangement in the sarcomere is shown in figure 3.

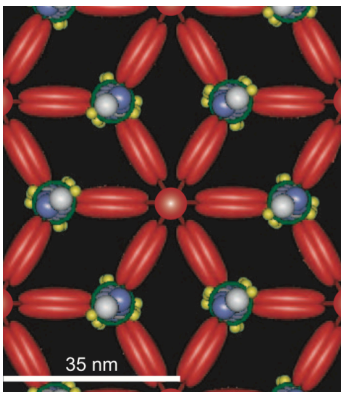

Figure 3: Simulated cross section of a sarcomere with myosin thick filaments (red), actin thin filaments (diffferent shades of blue), troponin (yellow) and tropomyosin (green), adapted from[14].

Several accessory proteins are necessary for the precise arrangement of actin and myosin filaments. The main components of a sarcomere are illustrated in figure 4. CapZ binds the barbed ends of actin filaments and anchors them to the Z-disc, which

seperates two sarcomere units. The length of the actin filaments is controlled by the molecular ruler protein nebulin. Nebulin stretches from the Z-disc to the pointed ends of actin filaments, which are stabilized by the capping protein tropomodulin. Actin filaments are further coated with tropomyosin and troponin, which control the availability of myosin binding sites on actin filaments and therefore muscle contraction in a Ca^{2+}-ion dependent way.

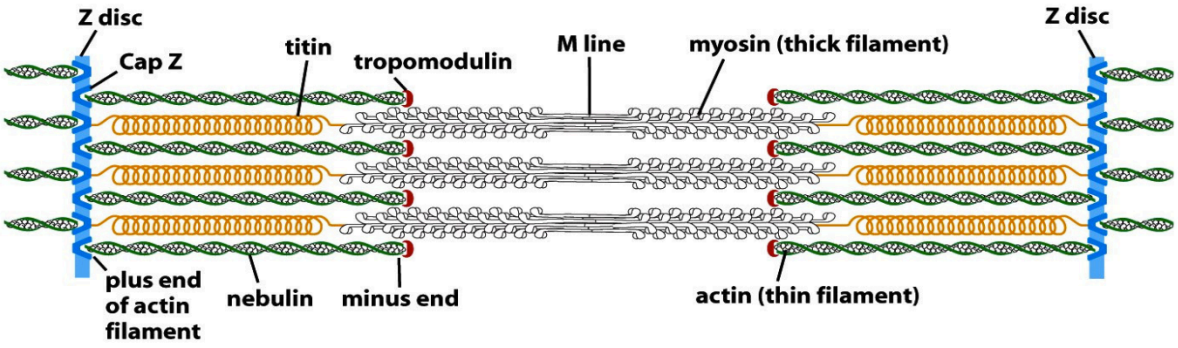

Figure 4: Composition of a sarcomere, the basic contractile unit of skeletal muscle cells, taken from[13].

Myosin thick filaments are composed of specific muscle isoforms of myosin II. They are connected to the Z-disc by titin, which acts as a molecular spring. The spring-like unfolding and refolding of titin's immunoglobulin-like domains keep the myosin thick filaments in the middle of a sarcomere and allows the recovery of muscle fibers after overstretching.[13]

I.3.2. DNA double-strand break repair by NHEJ and HR

DNA DSBs, probably the most cytotoxic from of DNA damage, can be a result of normal cellular processes, ionizing radiation[15], but also of chemotherapeutics[16]. In humans, non-homologous end-joining (NHEJ)[15] and homologous recombination (HR)[17] are the main repair pathways to restore genomic integrity. NHEJ can convert a great diversity of substrates into joined products by removing damaged nucleotides if necessary, while HR depends on an intact copy of the broken chromosome as a template for repair.

During NHEJ, DSB ends are initially recognized and bound by a heterodimer composed of Ku70/Ku80, which leads to the recruitment of the DNA-dependent protein kinase catalytic subunit (DNA-PKcs), the X-ray repair cross-complementing protein 4 (XRCC4),

the XRCC4 like factor (XLF) and DNA ligase IV[18]. DNA ligase IV can ligate incompatible DNA ends and even across gaps and is one of the most flexible ligases known[19]. For DNA ends with complementary overhangs of four nucleotides, it was shown that XRCC4 and DNA ligase IV are the only required components for repair[19]. However, a recent study indicated an even more effective repair in the presence of the Ku heterodimer[20].

HR describes the exchange of genetic information between chromosomes, which is mediated by a conserved class of enzymes termed recombinases. The eukaryotic recombinases Rad51 and Dmc1 are responsible for pairing of homologous DNA sequences via presynaptic filaments, which are filamentous intermediates on single-stranded DNA (ssDNA) ends. Various mediators and accessory proteins are required to enhance formation of these presynaptic filaments and to catalyze pairing of homologous DNA strands and the strand exchange reaction[17].

I.4. Fluorescence Spectroscopy

The incorporation of fluorescent dyes helps to study biological systems. For this thesis, fluorescently labeled proteins or DNA strands were investigated by fluorescence techniques.

The emission of light from excited electronic states is termed luminescence, which is further divided into the phenomena fluorescence and phosphoresence. In both cases, absorption of a photon leads to the excitation to a higher energetic state (excited singlet states for fluorescence and excited triplet states for phosphorescence), followed by relaxation to the ground state by emitting a photon of longer wavelength. A Jablonski diagram illustrates the processes occurring between absorption and emission of photons (figure 5). Upon absorption of a photon, an electron is excited from the singlet ground state S_0 to a higher energetic level S_n, followed by internal conversion, which is the rapid relaxation to the lowest vibrational level of S_1. When returning to the ground state, a photon is emitted. However, the molecule can also relax non-radiatively by dissipating the energy into the solvent. The energy of the emitted photon is lower compared to the energy of the absorbed photon and the fluorescence emission spectrum therefore shifted to longer wavelengths (Stokes shift[21]). The fluorescence emission spectrum does not depend on the excitation wavelength, as all fluorescent transitions start from the lowest vibrational level of S_1 (Kasha's rule[22]). Alternatively to

fluorescence emission, molecules in the first excited state S_1 can undergo a spin conversion to the first triplet state T_1. This intersystem crossing is quantum mechanically forbidden and phosphorescence emission rates are therefore slow.

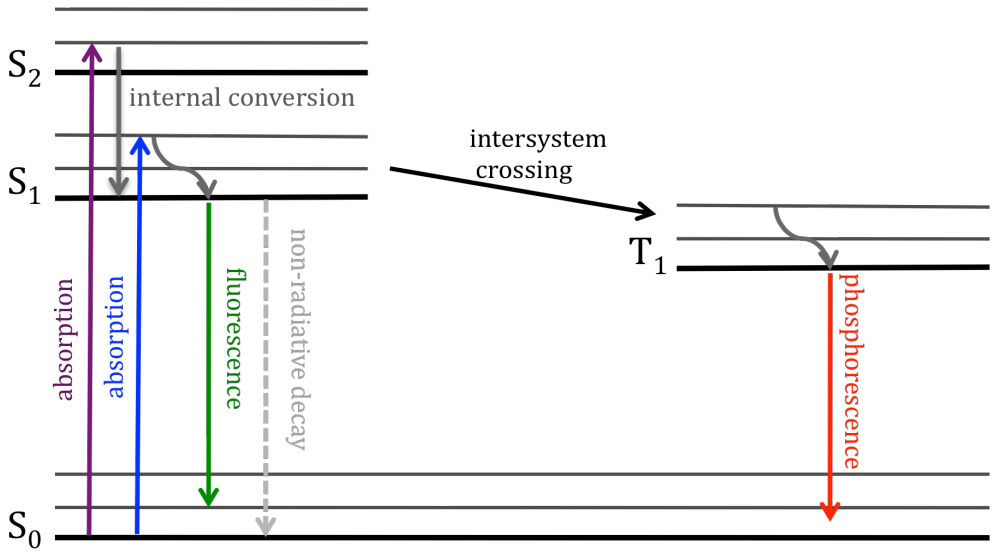

Figure 5: A typical Jablonski diagram with S_n = n^{th} singlet state, and T_1 = first triplet state.

The fluorescence lifetime, τ, and the quantum yield, Φ, are important characteristics of a fluorophore. τ represents the average time which a molecule spends in the excited state before returning to the ground state, with typical values around 10 ns[23]. In the absence of non-radiative transitions to the ground state, the fluorescence lifetime, τ, is defined as

$$\tau = \frac{1}{\Gamma} \qquad \text{(eq. 1)}$$

with the emissive rate of the fluorophore, Γ. This and all following equations in chapter I are adapted from Lakowicz's *Principles of Fluorescence Spectroscopy*[23]. In the presence of non-radiative decay with the rate constant k_{nr}, the equation has to be modified:

$$\tau = \frac{1}{\Gamma + k_{nr}} \qquad \text{(eq. 2)}$$

.

Φ is the ratio of emitted to absorbed photons and defines the efficiency of the fluorescence process:

$$\Phi = \frac{number\ of\ emitted\ photons}{number\ of\ absorbed\ photons} = \frac{\Gamma}{\Gamma + k_{nr}}. \qquad \text{(eq. 3)}$$

I.4.1. FRET

Förster resonance energy transfer (FRET) describes the transfer of energy between a donor molecule in the excited state and an acceptor molecule in the ground state (figure 6). FRET occurs, if the emission spectrum of the donor overlaps with the absorption spectrum of the acceptor[24]. Importantly, the energy transfer does not involve an intermediate photon, which is emitted from the donor and absorbed by the acceptor. FRET is explained by long-range dipole-dipole interactions.

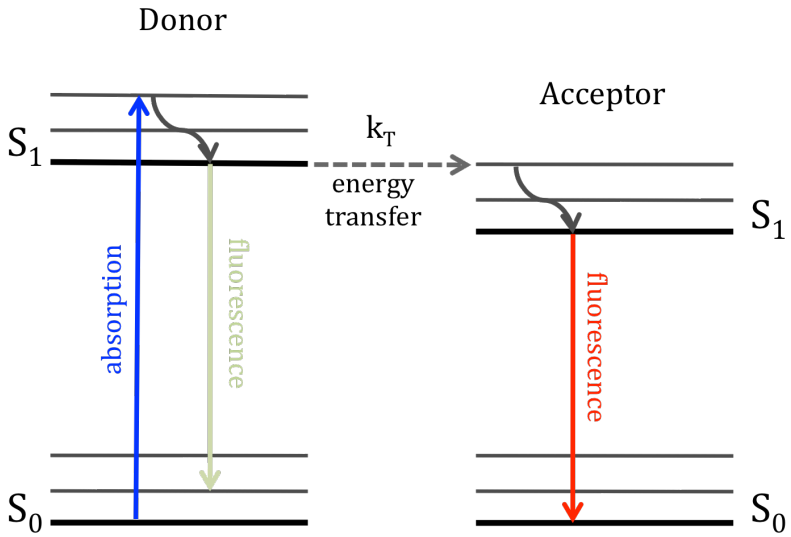

Figure 6: A Jablonski diagram showing a FRET process. k_T is the rate of energy transfer between donor and acceptor.

The energy transfer rate k_T from a donor to an acceptor depends on the donor-acceptor distance, r, the quantum yield of the donor, Q_D, the spectral overlap between the emission spectrum of the donor and the absorption spectrum of the acceptor, $J(\lambda)$, and the relative orientation of the donor and acceptor transition dipoles, κ^2 (often assumed to be 2/3). The energy transfer rate is therefore given by

$$k_T(r) = \frac{1}{\tau_D}\left(\frac{R_0}{r}\right)^6 \qquad \text{(eq. 4)}$$

with the Förster radius R_0:

$$R_0^6 = \frac{9000(\ln 10)\kappa^2 Q_D}{128\pi^5 N_A n^4} J(\lambda). \qquad \text{(eq. 5)}$$

N_A is Avogadro's number and n is the refractive index of the medium. R_0 is the distance at which the energy transfer efficiency is 50%. Typical values for R_0 are between 20 and 60 Å[23]. A common application for FRET is as a "spectroscopic ruler"[25] to determine the distance between two dyes, for example fluorescent labels on biomolecules. The ratio of the transfer rate to the decay rate of the donor in presence of the acceptor is the FRET efficiency, E:

$$E = \frac{k_T(r)}{\tau_D^{-1} + k_T(r)} = \frac{R_0^6}{R_0^6 + r^6}. \qquad \text{(eq. 6)}$$

Thus, the transfer efficiency strongly depends on interdye distance changes in the range of the Förster radius.

I.4.2. FCS

Fluorescence correlation spectroscopy (FCS) is a correlation analysis of fluorescence intensity fluctuations. FCS experiments were first described in the early 1970s[26-28]. The method is based on molecules in solution, which diffuse in and out of a small observation volume of approximately 1 fL size. The small volume is realized by a laser beam, which is focused to a diffraction-limited spot, and a confocal pinhole to discard signal from outside of the desired volume. FCS measurements are best performed when observing a small number of fluorescently labeled molecules, thus fluorophore concentrations should be in the pico- to nanomolar range. When a fluorophore diffuses into the focused laser beam, a burst of photons is emitted. Random diffusion of the molecules leads to time-dependent fluctuations of fluorescence intensity. These temporal fluctuations are analyzed using the signal fluctuation autocorrelation function, given by

$$G(\tau) = \frac{\langle \delta I(t)\delta I(t+\tau)\rangle}{\langle I(t)\rangle^2} = \frac{\langle I(t)I(t+\tau)\rangle}{\langle I(t)\rangle^2} - 1 \qquad \text{(eq. 7)}$$

with I(t) the signal at time t, δI(t) the deviation from the mean intensity and <> the time average. The amplitude of the correlation function is sensitive to the number of molecules in the focus and the time dependent decay of the correlation function reports on the time scale of molecular motion. Usually, the autocorrelation curve for freely diffusion particles in 3D is described using the following model:

$$G(\tau) = \frac{1}{\langle N\rangle} \cdot \frac{1}{1+\frac{\tau}{\tau_D}} \cdot \frac{1}{\sqrt{1+\frac{1}{p^2}\cdot\frac{\tau}{\tau_D}}} \qquad \text{(eq. 8)}$$

where $\langle N\rangle$ is the average number of particles in the focal volume and *p* the ratio of the axial to the lateral width of the, assumed, Gaussian-shaped focal volume. An interaction of two fluorophores can be revealed by cross-correlation[29]. The amplitude of the cross correlation is proportional to the number of the two-color molecules.

I.4.3. TIRF

Besides using a confocal pinhole to restrict the observed volume for single molecule detection, total internal reflection fluorescence (TIRF) microscopy can be performed. This technique is based on the exponential decay of an evanescent field generated by total internal reflection at the boundary between a high refractive index (n_2) to a low refractive index (n_1) medium, for example at the interface between a glass coverslip and water. The basic principle of TIRF is illustrated in figure 7. If the incident angle of the laser beam exceeds the critical angle, θ_C, the beam is totally internal reflected. The critical angle can be calculated using n_1 and n_2:

$$\theta_C = \sin^{-1}\left(\frac{n_1}{n_2}\right) . \qquad \text{(eq. 9)}$$

Although the incident beam is completely reflected, it can still interact with the sample at the interface, as the intensity penetrates a short distance into the sample as an

evanescent wavefront. The evanescent field intensity, *I*, decreases with distance *z* into the low refractive index medium according to

$$I(z) = I(0)\exp(-z/d) \qquad \text{(eq. 10)}$$

with the intensity at the interface, *I(0)*, and the decay constant, *d*.

The restricted illumination distance alonge the z-axis limits the observation volume, as only fluorophores located within the evanescent field are excited.

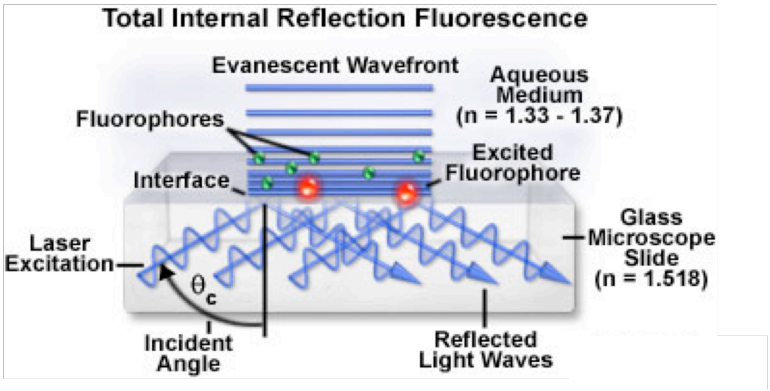

Figure 7: Schematic representation of TIRF at the interface between a microscope coverslip and an aqueous sample. Figure taken from http://www.microscopyu.com/articles/fluorescence/tirf/tirfintro.html (2016-02-02).

There are two experimental methods to perform TIRF microscopy: the prism-type and the objective-type (figure 8).

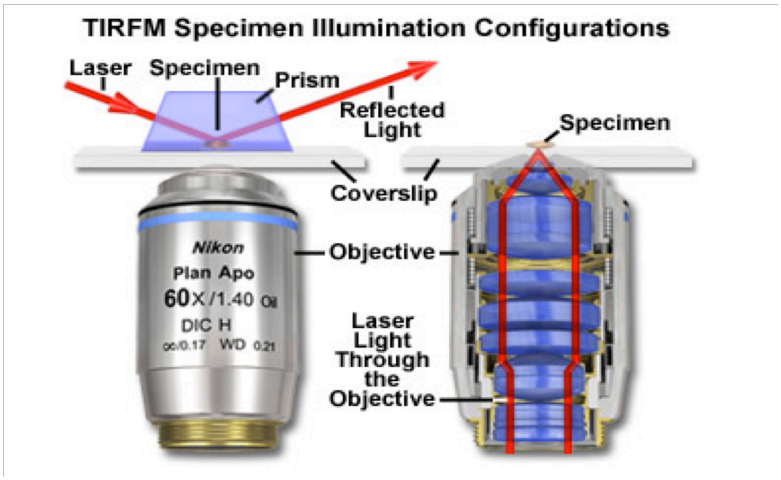

Figure 8: Prism (left) and objective methode (right) for TIRF microscopy. Figure taken from http://www.microscopyu.com/articles/fluorescence/tirf/tirfintro.html (2016-02-02).

For the prism-type method, the incoming laser beam is directed into a glass prism and the incidence angle is adjusted to the critical angle. Using the objective-type method, the excitation beam is focused on the back focal plane of the objective. When this beam is delocalized from the center of the objective, it leaves the objective under a certain angle. An incident angle higher than the critical angle can be achieved with objectives of high numerical aperture. Excitation and emission pass through the same objective.

II. Materials and Methods

II.1. Materials

Buffer compositions are described in the following materials chapter. If not stated otherwise, buffers were stored at room temperature.

A p7560 scaffold was kindly provided by the group of Prof. Liedl. Staple strands were produced by Eurofins Genomics, Ebersberg, Germany. The DNA strands which served as dsDNA substrates for the repair study as well as biotinylated handles for the two-layer sheet with gap were ordered from Purimex, Grebenstein, Germany. All used DNA sequences are listed in the appendix (tables A.1. and A.2.).

Rabbit skeletal muscle α-actin, rabbit skeletal muscle α-actin labeled with atto488, myosin, myosin thick filaments and CapZ were purchased from Hypermol, Bielefeld, Germany. Streptavidin was purchased from Sigma-Aldrich, Taufkirchen, Germany.

II.2. Experimental setups

FCS and FRET measurements were performed on a home-built confocal microscope with a 60x 1.27 NA water immersion objective (Plan Apo IR 60x 1.27 WI, Nikon). A 480 nm laser was used for blue excitation and a 640 nm laser was used for red excitation. Typical laser powers before the objective were 120 µW for the blue and 40 µW for the red laser. Fluorescence was filtered by a 525/50 (blue channel) and a 705/100 emission filter (red channel).

FCS measurements were also performed on a second home-built confocal microscope with a 60x 1.27 NA water immersion objective (Plan Apo IR 60x 1.27 WI, Nikon). For blue excitation, a 475 nm laser was used, while 561 nm and 635 nm lasers were used for yellow and red excitation, respectively. Laser powers were adjusted to 10 µW before the objective. Fluorescence was filtered by a 635 nm long-pass filter (red channel), a 595/50 (yellow channel) and a 520/40 emission filter (blue channel).

TIRF experiments were performed on a home-built WF-TIRF setup with a 60x. 1.45 NA oil immersion objective (Plan Apo TIRF 60x 1.45, Nikon). For blue and red excitation, 488 nm and 642 nm lasers were used, respectively. Typical laser powers before the objective were around 1 mW for both lasers. Fluorescence was filtered by a 525/50

(blue channel) and a 680/42 emission filter (red channel). The exposure time was set to 100 ms.

II.3. DNA origami

II.3.1. DNA origami design

CaDNAno2, which is based on CaDNAno[5], was used for DNA origami design. The design details for the two different DNA origamis are described below. Before ordering the DNA strands, the 3-D structure of the design was analyzed by CanDo[6] at http:// cando.dna-origami.org/. For analysis, the default parameters (DNA geometry: axial rise per base-pair 0.34 nm, helix diameter 2.25 nm, crossover spacing 10.5 bp; DNA mechanical properties: axial stiffness 1100 pN, bending stiffness 230 pN nm^2, torsional stiffness 460 pN nm^2, nick stiffness factor 0.01) were used.

II.3.2. Design details

The two-layer sheet for the sarcomere project was designed by the group of Prof. Liedl. The design is based on the square lattice. p7560 was chosen as the scaffold. Dominik Böhm further added 12 biotin- and 4 Cy5-staples[30]. The respective staples were elongated with a T_5-spacer and modified with biotin or Cy5 at the 5'-end. The biotinylated handles served as binding sites for the actin-binding protein CapZ, which was also biotinylated. Biotinylated staples were positioned in an hexameric form on both sides of the structure to get an arrangement of actin filaments similar to those at a z-Disc[14].

As the tetrameric protein streptavidin has four binding sites for biotin, more than one biotinylated CapZ can bind to a single biotinylated DNA staple. Furthermore, streptavidin can link two biotinylated DNA strands or two biotinylated proteins. In order to make CapZ-DNA binding more specific, I replaced the biotinylated handles with staples containing a 5'-$(ACC)_5$-3' sequence, while CapZ was crosslinked with a complementary ssDNA. To reduce aggregation of the folded DNA origami, I added staples at the ends of the DNA helices, so-called endcaps, and elongated them with T_4-tails.

For the DNA DSB repair study, I designed a DNA origami two-layer sheet with gap (figure 9) based on the square lattice with p7560 as scaffold. The frame is composed of two layers for better stability in solution.

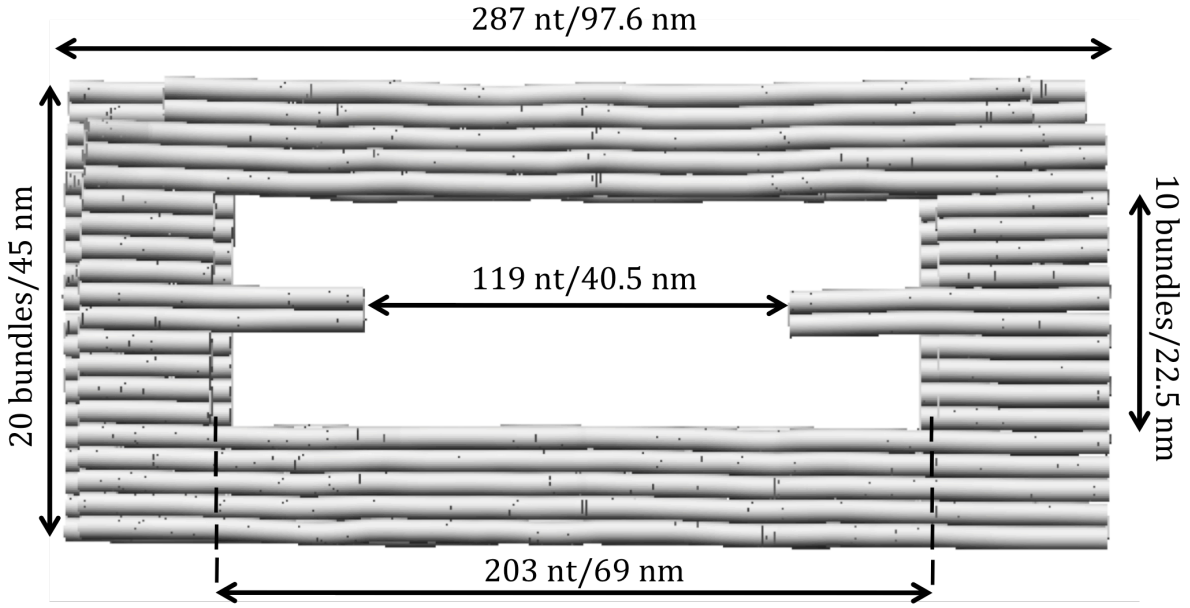

Figure 9: Dimensions of the two-layer sheet with gap. Distances in nm were calculated assuming 0.34 nm for the length of a base pair and 2.25 nm for its diameter.

Inside the 69 nm gap are two protrusions, which serve as attachement sites for the DNA repair substrates. Two roughly 80 nucleotide (nt) long dsDNA can be bound inside the gap. This DNA length is similar to the DNA substrates used in the NHEJ FRET experiments by Reid et al.[20], where a biotinylated 80 nt dsDNA bound to a surface and a 80 nt dsDNA in solution were used. In order to bind the origami to a surface, four biotinylated strands can be incorporated. The 5'-ends of the biotinylated staples were chosen to be at positions were the scaffold of one layer can be connected to the scaffold of the other layer via a crossover. This ensures an orthogonal arrangement of the biotinylated handles with respect to the origami.

II.3.3 Assembly of DNA origami

For each DNA origami structure, a staple stock was prepared by mixing all required staple strands. The concentration of the single DNA staples in the ordered plates was 50 µM, the final concentration in the staple stock depended on the total number of staples. For example, the number of staple strands for the two-layer sheet with gap was

225, therefore the concentration of a single strand in this mix was 50 µM/ 225 = 222 nM. For assembly, 10 nM of the p7560 scaffold (stock concentration 100 nM) were mixed with a 10-fold molar excess of staple strands. The folding buffer contained 1x TE (10 mM Tris, 1 mM EDTA, pH 8.0). The $MgCl_2$ concentration for the two-layer sheet (sarcomere project) was 14 mM. For the two-layer sheet with gap (DNA DSB repair study), $MgCl_2$ concentrations were varied between 10 mM, 12 mM, 14 mM, 16 mM, 18 mM and 20 mM to find the optimal folding condition (12 mM $MgCl_2$). The folding batches (typically 100 µL) were subjected to a thermal annealing protocol using an eppendorf mastercycler personal. The thermocycler programs for the two DNA origami structures are shown in table 1.

Table 1: Thermocycler programs for the folding of the DNA origami two-layer sheet (program name "KIRA") and the two-layer sheet with gap (program name "KIRANEW").

two-layer sheet		**two-layer sheet with gap**	
65° C	15 min		
65-60° C	-1° C/5 min, 5x	65° C	5 min
60-37° C	-1° C/30 min, 23x	65-20° C	-1° C/30 min, 45x
37-6° C	-1° C/5 min, 31x	20° C	for ever
6° C	for ever		

II.3.4. Purification of DNA origami with PEG

The assembled structures were purified by adding poly(ethylene glycol) (PEG) polymers as a precipitating agent. Self-assembly reaction mixtures were mixed 1:1 (v/v) with PEG buffer containing 15% (w/v) PEG8000, 5 mM Tris, 1 mM EDTA and 500 mM NaCl. The pH of the precipitation buffer was adjusted to 8.0 and the buffer was filter-sterilized with a 0.45 µm filter before use. The solution was mixed by tube inversion and centrifuged at 12300 rpm (16000 rcf) and 25° C for 30 min using an eppendorf centrifuge (model 5417R). The supernatant was removed, the pellet was dissolved in target buffer and incubated for at least 30 min on a shaker at 650 rpm and 25° C. Afterwards, a second PEG precipitation step was performed. The pellet was dissolved in target buffer and incubated over night under shaking conditions. To concentrate the DNA origami solution, a smaller volume of target buffer was added to the pellet compared to the original volume of the folding batch (for example 25 µL target buffer compared to a 100 µL folding batch gives a 4-fold concentrated DNA origami solution). The

concentration of the DNA origami solution in ng/µL was determined via the absorbance at 260 nm. To convert µg DNA into pmol DNA, equation 11 was applied, where 660 pg/pmol is the average molecular weight of a nucleotide pair in double-stranded DNA, and 7560 the length of the scaffold DNA:

$$\mu g(DNA) * \frac{pmol}{660\,pg} * \frac{10^6\,pg}{1\mu g} * \frac{1}{7560} = pmol(DNA). \qquad \text{(eq. 11)}$$

II.3.5 Analysis of the DNA objects with gel electrophoresis

Electrophoresis of the folded and purified DNA objects was carried out in 1% agarose gels containing electrophoresis buffer (1x TAE (40 mM Tris, 0.1% (v/v) acetic acid, 1 mM EDTA, pH 8.5), 11 mM $MgCl_2$). The concentration of the DNA samples was typically 10 nM. As a standard, a 1 kb DNA ladder (GeneRuler 1kb DNA ladder, Thermo Fisher Scientific) was used. The gel was run on ice for 90 min at 80 V. For visualization of the DNA bands, the gel was stained with SYBR gold (Thermo Fisher Scientific, 10 µL of 10000x concentrate in DMSO in 100 µL 1xTAE) for 40 min under shaking. For imaging, a Biorad Gel Doc™ EQ Imager with trans-UV illumination was used.

II.3.6 Analysis of the DNA objects with TEM

The shape of the folded DNA origamis was vizualized by transmission electron microscopy (TEM) using the transmission electron microscope JEM-1011 (Jeol). The carbon coated Cu-grids were plasma cleaned at 240 V for 60 s to ensure a hydrophilic grid surface. For staining, two droplets of 7 µL uranyl acetate (1% in H_2O) were placed on parafilm. 7 µL of a 2 nM DNA origami solution was pipetted on the grid surface. After 60 s, the excess liquid was removed with a filter paper. The grid was briefly submerged into the first droplet of uranyl acetate and the excess liquid immediately removed. After submerging the grid in the second droplet of uranyl acetate for 15 s, the excess liquid was removed and the grid air-dried for 30 min.

II.4. Sarcomere project

II.4.1. Biotinylation of CapZ

To bind CapZ to the biotinylated staples on the DNA origami two-layer sheet, the protein was biotinylated with the EZ-Link™ Sulfo-NHS-LC-Biotinylation Kit (Thermo Fisher Scientific). A 50 µg aliquot of lyophilized CapZ (non-muscle, human recombinant, Hypermol) was dissolved in 50 µL ddH_2O and incubated for 30 min on ice. The buffer delivered with the protein contained 150 mM NaCl, 20 mM HEPES pH 7.4, 1 mM DTT and 1% disaccharides.

The protein concentration was determined via the absorbance at 280 nm with the extinction coefficient $\varepsilon_{280} = 76810\ M^{-1}\,cm^{-1}$ [the extinction coefficient was determined with the ProteinCalculator (http://protcalc.sourceforge.net/) and the sequences for the α- and β-subunit of CapZ (http://www.ncbi.nlm.nih.gov/protein/5453597?report=fasta and http://www.ncbi.nlm.nih.gov/protein/330864679?report=fasta, respectively, sites accessed on 15-12-28)]. A 10-fold molar excess of Sulfo-NHS-LC biotin was added to CapZ and incubated for 2 h on ice. During the biotinylation reaction, N-Hydroxy-succinimide (NHS) ester-activated biotins and primary amino groups (e.g. of lysines) form stable amide bonds at pH 7-9, while Sulfo-NHS is released (figure 10).

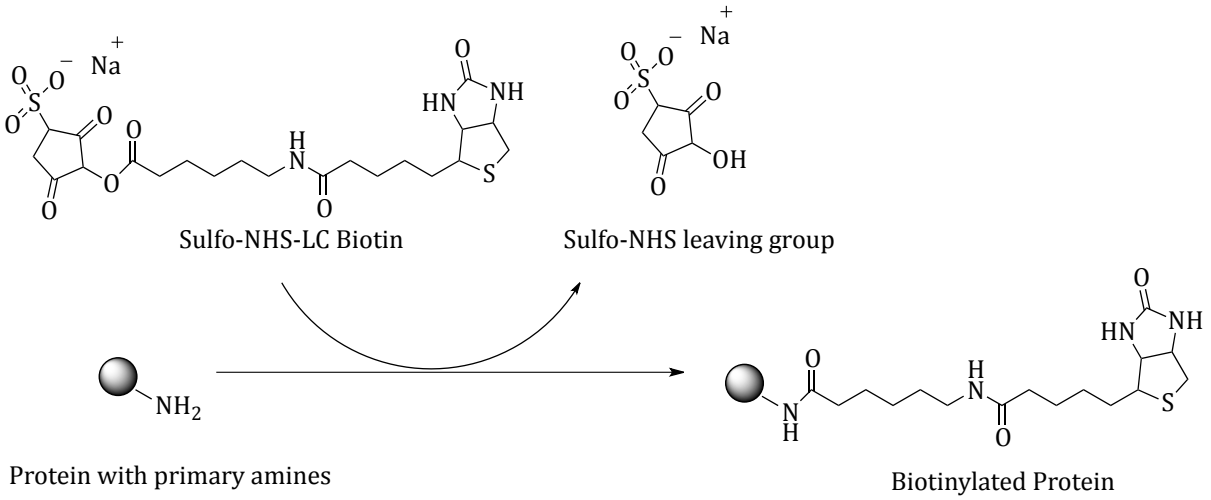

Figure 10: Reaction of Sulfo-NHS-LC-Biotin with a primary amine. Sulfo-NHS ist the leaving group.

Sulfo-NHS leaving groups and excess biotin reagents were removed with Zeba™ Spin Desalting Columns, 7K MWCO, 0.5 mL (Thermo Fisher Scientific) according to the manufacturer's instructions. For equilibration of the column and elution of the protein, BupH™ PBS (0.1 M Na_3PO_4, 0.15 M $NaCl_2$, pH 7.2) was used.

To estimate the mole-to-mole ratio of biotin to CapZ, the biotinylated CapZ solution was added to a mixture of 1 mg avidin and 60 µL HABA (4'-hydroxyazobenzene-2-carboxylic acid, 10 mM in 0.01 N NaOH) in 1.94 mL BupH™ PBS. The absorption at 500 nm, A_{500}, was measured for HABA/avidin alone (H/A) and with 10% (v/v) biotinylated CapZ (H/A/B). Biotin has a higher affinity for avidin than HABA. Therefore, binding of biotin to avidin releases HABA and the absorption at 500 nm decreases[31]. To calculate the concentration of biotin in the reaction mixture, the following equation was used:

$$\frac{mmol\ \ biotin}{mL\ \ reaction\ \ mixture} = \frac{\Delta A_{500}}{\varepsilon_{500}(H/A) * d} = \frac{[0.9 * A_{500}(H/A)] - A_{500}(H/A/B)}{34000 M^{-1} cm^{-1} * 0.1 cm}. \qquad \text{(eq. 12)}$$

The correction factor 0.9 considers the dilution of the HABA/Avidin solution by the addition of protein. The extinction coefficient for a HABA/Avidin solution is ε_{500} = 34000 M^{-1} cm^{-1}. The ratio of biotin to CapZ was determined with

$$\frac{mmol\ \ biotin\ \ in\ \ original\ \ sample}{mmol\ \ protein\ \ in\ \ original\ \ sample} = \frac{(mmol/mL\ \ biotin\ \ in\ \ reaction\ \ mixture) * 10}{mmol/mL\ \ protein\ \ in\ \ original\ \ sample}. \text{ (eq. 13)}$$

The factor 10 is necessary, as CapZ-Biotin was diluted 1 to 10 in the HABA/Avidin reaction mixture. Eq. 12 and 13 are adapted from the manufacturer's instructions for the EZ-Link™ Sulfo-NHS-LC-Biotinylation Kit.

II.4.2 Modification of CapZ with Thio-TAMRA-DNA

- Crosslinker 1: SPDP (succinimidyl 3-(2-pyridyldithio)propionate)

The idea to modify CapZ with a Thiol-DNA is based on a study by Fu et al.[32], where DNA was conjugated to enzymes via the crosslinker SPDP and later bound to complementary handles on a rectangular DNA origami. SPDP is a heterobifunctional crosslinker with an NHS ester as the amine-reactive portion (figure 11, A) and a 2-pyridyldithio group as the sulfhydryl-reactive part. The reaction results in the release of pyridine 2-thione (figure 11, B) and an increase in absorbance at 343 nm[33].

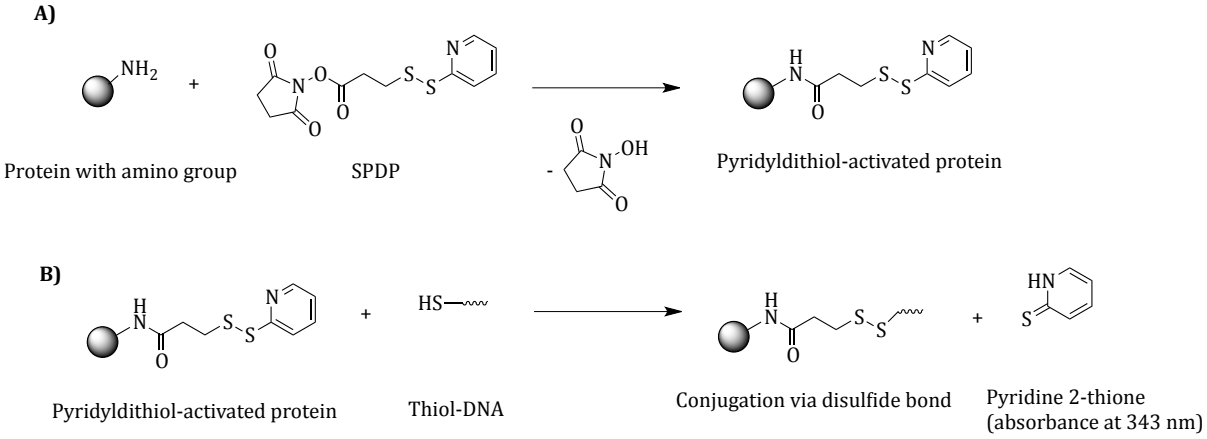

Figure 11: Reaction of SPDP with amino groups (**A**) and thiol-groups (**B**).

A 50 µg aliquot of lyophilized CapZ (non-muscle, human recombinant, Hypermol) was dissolved in 50 µL ddH_2O and incubated for 30 min on ice. CapZ was incubated with a 20-fold molar excess of SPDP in 1xPBS (137 mM NaCl, 2.7 mM KCl, 10.1 mM $Na_2HPO_4 \cdot 2H_2O$, 1.75 mM KH_2PO_4, pH 7.0) for 2.5 h on ice. Unbound SPDP was removed with Zeba™ Spin Desalting Columns, 7K MWCO, 0.5 mL (Thermo Fisher Scientific) according to the manufacturer's instructions. For equilibration of the column and elution of the protein, 1x PBS was used. A 10-fold molar excess of 5'-SH-GGTGGTGG[TAMdT]GGTGGT-3' ssDNA (Thio-TAMRA-DNA, produced by Eurofins Genomics) in 1x PBS was added to the pyridyldithiol-activated CapZ and incubated on ice over night. Before use, the DNA was reduced by adding 200 µL 10 mM TCEP (2.9 mg TCEP-HCl in 1x TE buffer). The DNA solution was incubated under shaking at 25° C, 600 rpm for 1 h and precipitated by adding 150 µL 3M NaAc (2.46 g NaAc and 0.032 g $MgAc^*4H_2O$ in 10 mL ddH_2O). The tube was filled with ethanol, shaked gently and incubated for 20 min at -20° C. The solution was spinned for 5 min at 13000 rcf (eppendorf centrifuge 5417R), the supernatant discarded and the pellet dried at RT. The DNA was then dissolved in an appropriate volume of 1x TE, pH 8.0. To estimate the coupling efficiency of DNA and CapZ, the absorbance at 343 nm was measured, as an efficient coupling should result in the release of pyridine-2-thione (ε_{343}= 8080 M^{-1} cm^{-1}, value given in the manufacturer's instructions).

- Crosslinker2: SMPH(Succinimidyl 6-((beta-maleimidopropionamido)hexanoate)

SMPH is another amine-to-sulfhydryl crosslinker with NHS ester and maleimide reactive groups (figure 12). SMPH was tested as crosslinking experiments with SPDP were not successful.

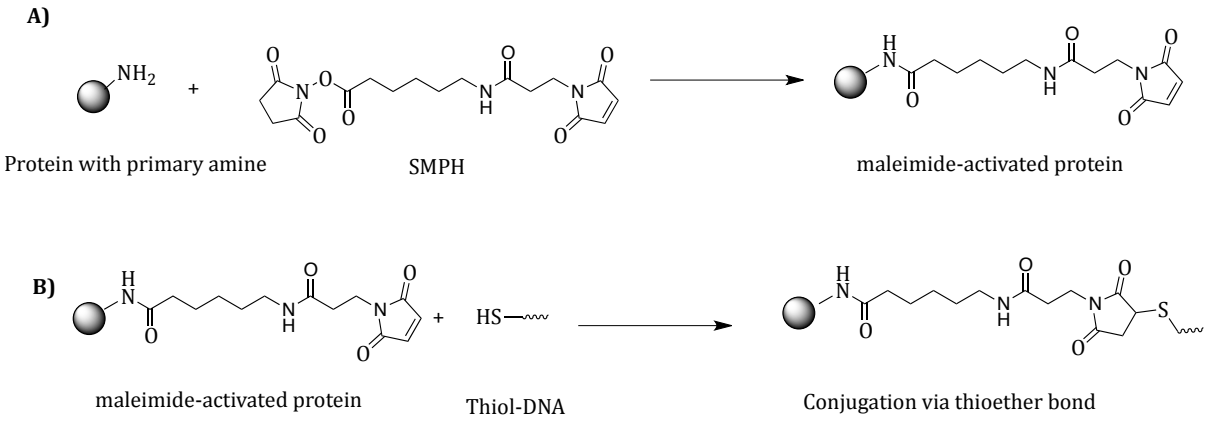

Figure 12: The NHS ester part of SMPH reacts with amino groups (**A**), while the maleimide part reacts with thiol groups (**B**).

A 50 µg aliquot of lyophilized CapZ (non-muscle, human recombinant, Hypermol) was dissolved in 50 µL ddH_2O and incubated on ice for 30 min. CapZ was incubated with a 10-fold molar excess of SMPH in 1xPBS for 2 h on ice. Excess crosslinker was removed with Zeba™ Spin Desalting Columns, 7K MWCO, 0.5 mL (Thermo Fisher Scientific) according to the manufacturer's instructions. For equilibration of the column and elution of the protein, 1xPBS was used. Thio-TAMRA-DNA was reduced as described above. The maleimide-activated protein was incubated with a 2-fold molar excess of DNA on ice over night.

In a second crosslinking experiment, reduced Thio-TAMRA-DNA was incubated with SMPH at a molar ratio of 1:1 for 10 min at RT. Afterwards, CapZ was added and incubated with a 3-fold molar excess of DNA and SMPH on ice over night.

II.4.3. Polymerization of actin with and without CapZ

Actin polymerization and sarcomere assembly experiments were carried out in flow cells[34], which were made of a cover glass (20 mm x 20 mm) glued to a glass slide with parafilm. The surface of the flow cells was passivated with 10% (w/v) BSA in PBS (stored at 4° C) for 10 min. After two washing steps with 90 µL G-buffer (5 mM Tris

pH 7.8, 0.1 mM $CaCl_2$, 0.2 mM ATP, 1 mM DTT, stored at 4° C) each, myosin was added as a tethering protein and incubated for 5 min. After an additional washing step with 90 µL G-buffer, the protein mix was flushed into the flow cell, which was sealed with grease.

The concentration of actin (33% atto488-actin) was determined via the absorbance at 290 nm (with $\varepsilon_{290} = 26600\ M^{-1}\ cm^{-1}$)[35]. The final concentration of actin in the polymerization mix was varied between 0.5-1.5 µM. Actin was incubated with G-buffer and 1/10 volume exchange buffer 10xME (500 µM $MgCl_2$, 2mM EGTA) for 5 min on ice. Afterwards, a polymerization mix was added, which contained G-buffer, 1/10 volume polymerization buffer 10xKMEI (500 mM KCl, 10 mM $MgCl_2$, 10 mM EGTA and 100 mM imidazole HCl, pH 7.0), 0.25% (wt/v) methylcellulose and the photococktail[36] composed of 1 mM Trolox (6–hydroxy–2,5,7,8–tetramethylchroman–2–carboxylic acid), 250 nM PCD (protocatechuate deoxygenase) and 2.5 mM PCA (3,4-dihydroxybenzoic acid).

If actin polymerization was studied in the presence of CapZ (unmodified or modified), CapZ was added to the actin mix before adding the polymerization mix. The final concentration of CapZ was 10 nM.

II.4.4. Sarcomere assembly

- With biotinylated CapZ and biotin-handles on the DNA origami

The DNA origami solution was incubated with a 15-fold molar excess of streptavidin for 1 h on ice. In some cases, unbound streptavidin was removed with an Amicon Filter 100 kDa MWCO (Merck Millipore) by centrifugation for 30 min at 14000 g and 4° C. The centrifugation tube was inverted and the sample recovered by a short centrifugation step at 1000 g for 2 min. Biotinylated CapZ was added to the DNA-streptavidin mix in a 12-fold molar excess with respect to the DNA (because the DNA two-layer sheet has 12 biotin positions) and incubated between 10 min and 1 h. In another experiment, DNA, CapZ and streptavidin were directly mixed and incubated for 1 h on ice. As described above, actin was mixed with G-buffer and 1/10 volume 10xME for 5 min on ice. The actin solution was then added to the DNA-streptavidin-CapZ mix and the solution incubated between 10 min and 1 h on ice. Afterwards, the polymix and myosin thick filaments were added and the sample was flushed into a flow cell. The final concentration of DNA was 500 pM and the concentration of myosin thick filaments between 250 pM and 5 nM. The actin concentration was 1 µM, 1.2 µM or 1.5 µM.

- With DNA-modified CapZ and complementary handles on the DNA origami

DNA and a 12-fold molar excess of DNA-modified CapZ were incubated for 1 h at RT. An actin solution was then added to this mix and incubated for 1 h on ice. After adding the polymix and myosin thick filaments (final concentration 500 pM), the sample was flushed into a flow cell and analyzed by TIRF microscopy.

II.5. DNA DSB repair study

II.5.1. Annealing of ssDNA

Following DNA oligonucleotides were used to create dsDNA for the DSB repair study:

oligo 1:
5' - TTCTGACCTGAAAGCGTAAGCTATGTATGCTCCCATGCTAAATACAACAAGCGGGCGTGA GACAGAGGAT/T-Atto647N/ATGC - 3' (75 nt)

oligo 2 (complementary to oligo 1):
5' - CACGGCATAATCCTCTGTCTCACGCCCGCTTGTTGTATTTAGCATGGGAGCATACATAGA ATACGTGGCACAGACAATATTTTTGAAT - 3' (88 nt)

oligo 3:
5' - CGTGAGATAATTCGTCGGTATGCTATGTATGCTCCCATGCTAAATACAACAAGCGGCGCG CGTGCGCATCGTAACCGTGCATCTGCCAGTT - 3' (91 nt)

oligo 4 (complementary to oligo 3):
5' - GGTCACGTTGGTGTAGATGGACGCGCGCCGCTTGTTGTATTTAGCATGGGAGCATACATA GCATACCGACGAAT/T-Alexa488/ATCT – 3' (79 nt)

Complementary DNA oligonucleotides 1+2 and 3+4 were annealed in 1xTE, 12 mM $MgCl_2$ at concentrations of 10 µM per oligo (for oligos 2 and 3 without 5'-phosphate) or 3 µM per oligo (if 5'-termini of oligo 2 and 3 were phosphorylated) using a temperature gradient. The nucleotides were heated to 99° C for 5 min and then cooled to 9° C with a rate of -1° C/min.

II.5.2. Binding dsDNA to the DNA origami

The binding of dsDNA substrates to the DNA origami is presented in figure 13. Each dsDNA has two single-stranded overhangs, which are complementary to the origami scaffold at the protrusions. Oligos 2 and 3 each have an additional overhang of four nucleotides, which are complementary to each other. The fluorescent labels are positioned four bases upstream of the 3'-ends in oligos 1 and 4. To bind the dsDNA to the DNA origami two-layer sheet with gap, the DNA origami was typically incubated with a 5x molar excess of dsDNA for 4 h at room temperature. The volume was adjusted to 100 µL with 1xTE, 12 mM $MgCl_2$ buffer. After 4 h, unbound dsDNA was removed with an Amicon Filter 100 kDa MWCO (Merck Millipore).

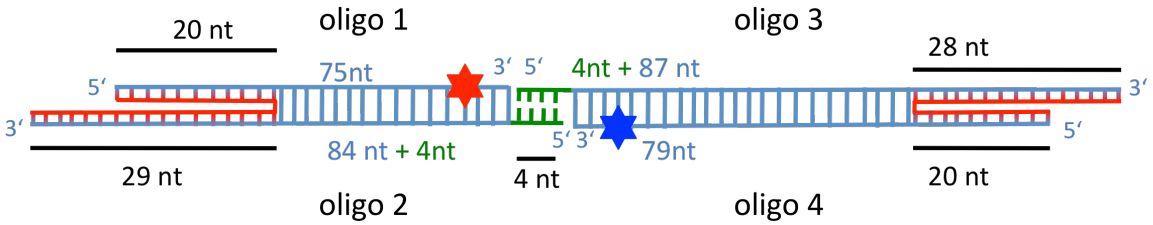

Figure 13: Schematic representation of the dsDNA substrates bound to the DNA origami two-layer sheet with gap. The protrusions of the origami, which are the binding sites for the DNA strands, are colored red. ssDNA oligos are colored blue, while the complementary overhangs of 4 bases in oligos 2 and 3 are shown in green. The red and blue stars represent the positions of the fluorescent labels Atto647N and Alexa488, respectively.

The DNA sample was centrifuged four times at 11500 rpm (14000 rcf) and 25° C for 10 min in an eppendorf centrifuge (model 5417R). After the first three centrifugation steps, the volume of the sample was adjusted to 100 µL with 1xTE, 12 mM $MgCl_2$. The centrifugation tube was inverted and the sample recovered by a short centrifugation step at 3100 rpm (1000 g) for 2 min.

II.5.3. Ligation of dsDNA

To ligate the sticky ends of the dsDNA in solution or bound to the DNA origami, a T4 DNA ligase (New England BioLabs® Inc., 400.000 units/mL) was used. The T4 DNA ligase catalyzes the formation of a phosphodiester bond between neighboring 5'-phosphate- and 3'-OH-ends[37]. Therefore, the 5'-termini of oligo 2 and 3 had to be phoshorylated using a T4 polynucleotide kinase (PNK, New England BioLabs® Inc.,

10.000 units/mL) and ATP. The phosphorylation reaction was set up with 300 pmol DNA (table 2) and incubated for 30 min at 37°C. As the single-stranded DNA oligos were annealed afterwards, an additional heat inactivation step at 65° C was skipped.

Table 2: Overview of the components required for the phosphorylation of 5'-termini of DNA nucleotides using a T4 polynucleotide kinase.

component	50 µL reaction
DNA oligo 2 or 3 (100 µM)	3 µL
10x T4 DNA ligase buffer (with 10 mM ATP)	5 µL
T4 PNK	1 µL
H_2O	41 µL

The ligation reaction was set up with 0.04 pmol DNA according to table 3 and incubated for 20 min at room temperature.

Table 3: Overview of the components required for the ligation reaction with T4 DNA ligase.

component	20 µL reaction
4 nM DNA origami+dsDNA	10 µL
or	
8 nM oligo1+2 and	5 µL
8 nM oligo3+4	5 µL
10x T4 DNA ligase buffer	2 µL
ddH_2O	7 µL
T4 DNA Ligase	1 µL

For FCS and FRET experiments, the samples were diluted to pM concentrations using 1xTE, 12mM $MgCl_2$ buffer containing 1 mM Trolox to reduce photobleaching and blinking[38]. The Trolox buffer was activated for 5 min with UV light to create its oxidized form, quinone Trolox. Trolox and the quinone derivative act as a reducing and oxidizing system (ROXS).

II.6. Data Analysis for FCS and FRET

For FCS, additionally a triplet term was included into the model:

$$G(\tau) = \frac{1}{\langle N \rangle} \cdot \left(1 + \frac{T}{1-T} \cdot e^{-\frac{\tau}{\tau_T}}\right) \cdot \frac{1}{1+\frac{\tau}{\tau_D}} \cdot \frac{1}{\sqrt{1+\frac{1}{p^2} \cdot \frac{\tau}{\tau_D}}} \qquad \text{(eq. 14)}$$

with *T* as the equilibrium fraction of particles that have entered the triplet state with the relaxation time τ_T. The value for *p* was determined from a measurement of reference dyes.

For burst analysis, burst selection was performed using the all-photon burst search algorithm, which is based on a sliding time window approach[39]. Fixed parameters for DNA origami-bound DNA double-strands were minimum 500 photons per burst, 2500 µs as time window and 50 photons per time window. For unbound dsDNA, minimum 100 photons per burst, a time window of 500 µs and 10 photons per time window were chosen. The FRET efficiency of each photon burst was calculated according to[40]

$$E = \frac{F_{BR}}{F_{BR} + F_{BB}}, \qquad \text{(eq. 15)}$$

with F_{BR} the fluorescence signal in the red channel after blue excitation and F_{BB} the fluorescence signal in the blue channel after blue excitation. Plots of stoichiometry versus FRET efficiency are commonly used to distinguish double-labeled molecules from donor- or acceptor-only species. The stoichiometry is defined as the ratio of signal after donor excitation to the total detected signal[40]:

$$S = \frac{F_{BB} + F_{BR}}{F_{BB} + F_{BR} + F_{RR}}. \qquad \text{(eq. 16)}$$

The stoichiometry value of double-labeled molecules is around 0.5, while donor-only molecules display stoichiometry values of around 1 and FRET efficiency values of roughly zero. Acceptor-only molecules show stoichiometry values close to zero and undefined FRET efficiency values. A Two-Channel Kernel-Density Estimator[41] (2CDE)-filter was used to remove donor- and acceptor-only species.
Equations for corrected FRET efficiency, *E*, and stoichiometry, *S*, read as follows[40]:

$$E = \frac{F_{BR} - \alpha F_{RR} - \beta F_{BB}}{F_{BR} - \alpha F_{RR} - \beta F_{BB} + \gamma F_{BB}}, \qquad \text{(eq. 17)}$$

$$S = \frac{F_{BR} - \alpha F_{RR} - \beta F_{BB} + \gamma F_{BB}}{F_{BR} - \alpha F_{RR} - \beta F_{BB} + \gamma F_{BB} + F_{RR}} \quad \text{(eq. 18)}$$

with the correction factor for direct excitation of the acceptor, α, the correction factor for donor crosstalk in the acceptor channel, β, and the detection correction factor, γ. For correction of the data, 1% crosstalk and 0.5% direct excitation were assumed. A γ-factor of 0.6 was used.

III. Results and Discussion

For this thesis, two different DNA origami structures served as scaffolds to elucidate assembly mechanisms and dynamics of macro-molecular complexes. Firstly, a DNA origami two-layer sheet served as a platform for sarcomere assembly. Secondly, a DNA origami structure two-layer sheet with attachment sites for two DNA double-strands was established for DNA DSB repair studies.

III.1. Assembly of sarcomere-like structures

The basic idea of this project was to assemble sarcomere-like structures in solution. For assembly, I attempted to use a DNA origami as a "Z-disc", the actin-capping protein CapZ bound to the origami, actin and myosin thick filaments. Preliminary data (aquired during a bachelor's thesis) suggested that sarcomere-like structures could be formed in solution using a DNA origami two-layer sheet with biotin-handles and biotinylated CapZ[30]. The same DNA origami structure was used in this study and modified by adding endcaps. Besides using biotin-streptavidin-bonds to connect CapZ to the DNA origami, a different binding strategy based on complementary ssDNA was tested.

III.1.1. Reducing aggregation of the DNA origami structure

The DNA origami two-layer sheet was assembled in the presence of biotinylated staples or staples containing a ssDNA extension (5'-$(ACC)_5$-3'). In both cases, Cy5-labeled strands were incorporated as well. As staples were added at 10-fold molar excess compared to the scaffold, unbound strands had to be removed after folding. It was shown that single- and multi-layer DNA can be purified by PEG without any damage and that two cycles of PEG purification remove 99.4% of excess staples[11]. While the folded DNA origami precipitates upon addition of PEG, the lower molecular weight staples remain in solution. For the DNA origami two-layer sheet, nearly all unbound staple strands were removed after the first cycle of PEG purification (figure 14). In the first lane of both agarose gels, the scaffold p7560 appears as a sharp band. PEG purified DNA origamis with incorporated biotin-staples (figure 14, A) or ACC_5-staples (figure 14, B)

display a band similar to the scaffold. In the third lane of both gels, the supernatant after the first PEG precipitation step was loaded. Unbound staple strands are detected as a blurry, broad band below the origami band. In the supernatant after the second PEG precipitation, nearly no unbound staples are left.

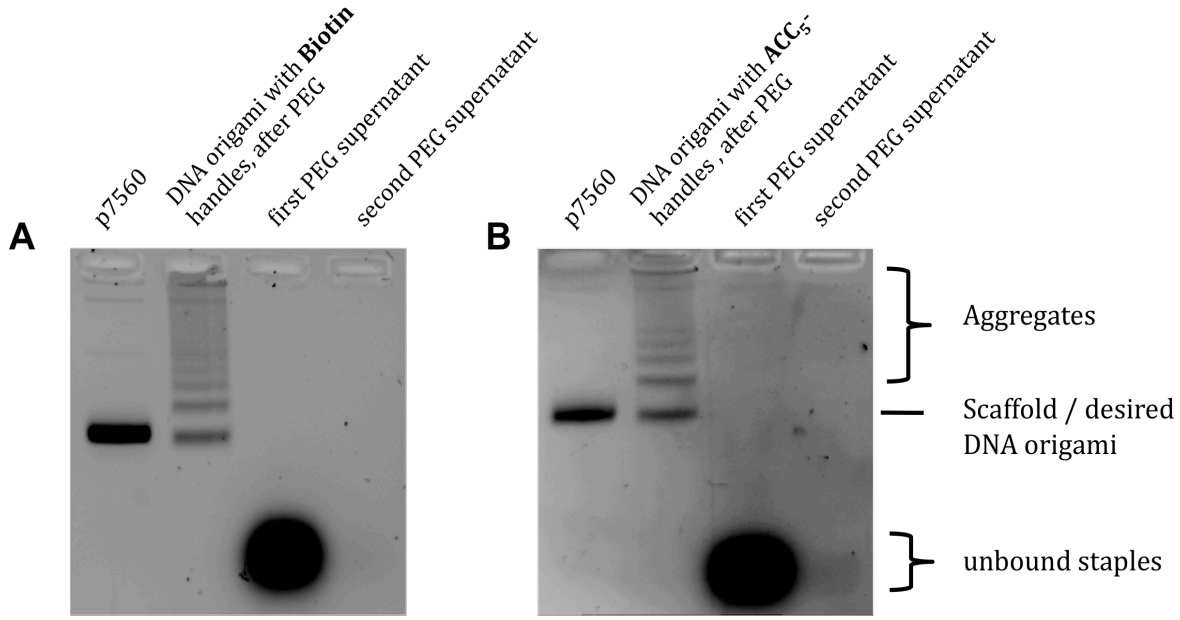

Figure 14: Addition of PEG as a precipitating agent removes unbound staple strands. Agarose gels display bands of PEG purified DNA origami two-layer sheets with incorporated Biotin-staples (**A**) or ACC_5-extended staples (**B**). Unbound staples are detected in the first PEG supernatants.

Additional higher molecular weight bands are visible above the DNA origami band. These bands correspond to aggregated structures. When comparing the two agarose gels, there seems to be slightly more aggregation for DNA origamis with biotin-handles than with ACC_5-extended staples.

In order to reduce aggregation of the DNA origami two-layer sheets, the design was slightly modified. Staples were added at the helical interfaces and elongated with T_4-tails, as these so-called endcaps shall prevent aggregation by blunt-end association[11]. Aggregation tests were performed with the DNA origami containing biotin-handles, as this structure has shown slightly more aggregation than the origami with ACC_5-handles (figure 14). A possible reason for the increased aggregation could be the use of different scaffold batches. For the biotin-origami, two faint bands above the scaffold are visible, which indicates aggregation of the scaffold even in the absence of staples. To investigate the influence of the scaffold on DNA origami aggregation, the assembly of the two-layer

sheet was performed with a freshly prepared p7560 scaffold or a scaffold from an older batch. The structure was assembled in the presence or absence of endcaps in the staple mix. After assembly, the DNA samples were purified by PEG precipitation and separated on an agarose gel (figure 15). The scaffolds from the two different batches show no significant difference after exposure to the temperature gradient. However, when folded in the presence of staple strands with or without endcaps, the origami containing the "old" scaffold forms many aggregates. Using the "new" scaffold, aggregation of the DNA origami considerably decreases. Addition of endcaps during the assembly process further reduces aggregation, but the difference is not as striking as with the different scaffolds. Therefore, the p7560 scaffold from the freshly prepared batch and a staple stock containing the endcaps were used for further assemblies of the DNA origami-two-layer sheet.

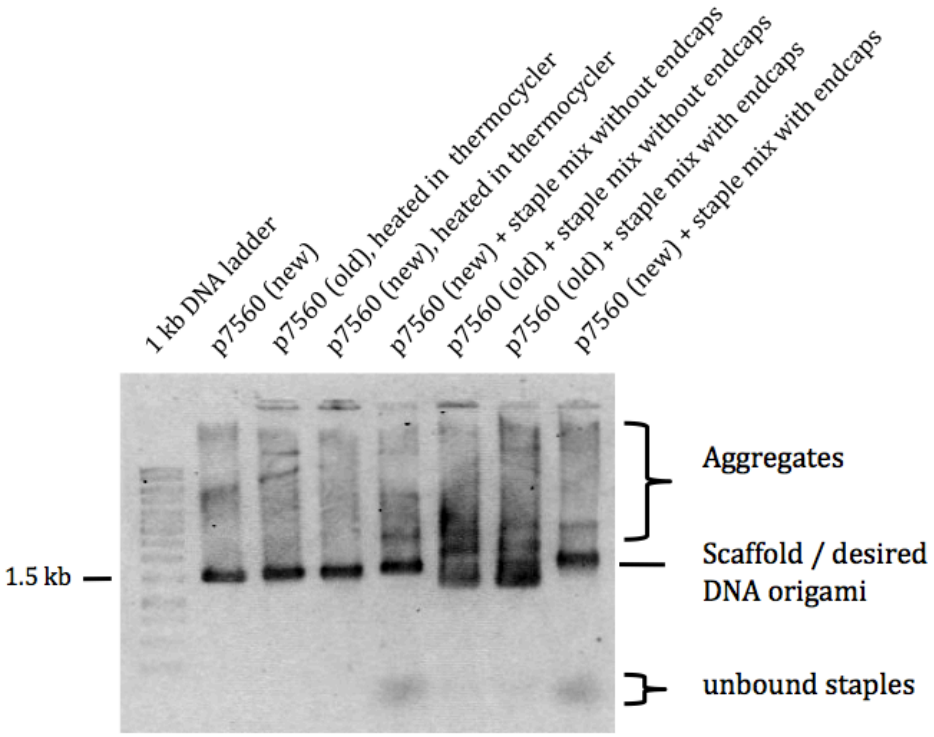

Figure 15: The scaffold and the addition of endcaps have an influence on the aggregation behavior of DNA origamis. An agarose gel detects bands of purified DNA origami two-layer sheets with biotin-staples, which were assembled under different conditions. A freshly prepared scaffold (new) causes considerably less aggregation during folding than a scaffold from an older batch (old). Addition of endcaps further decreases aggregation.

III.1.2. Visualization of the DNA origami with TEM

To confirm the correct folding of the DNA origami two-layer sheets, PEG purified DNA origamis containing ACC_5-staples were visualized by TEM. TEM images (figure 16) show that the DNA origamis have the desired structure. Some of the rectangular DNA objects may appear to stick together (left panel), which could be due to some aggregation or an effect of the sample staining.

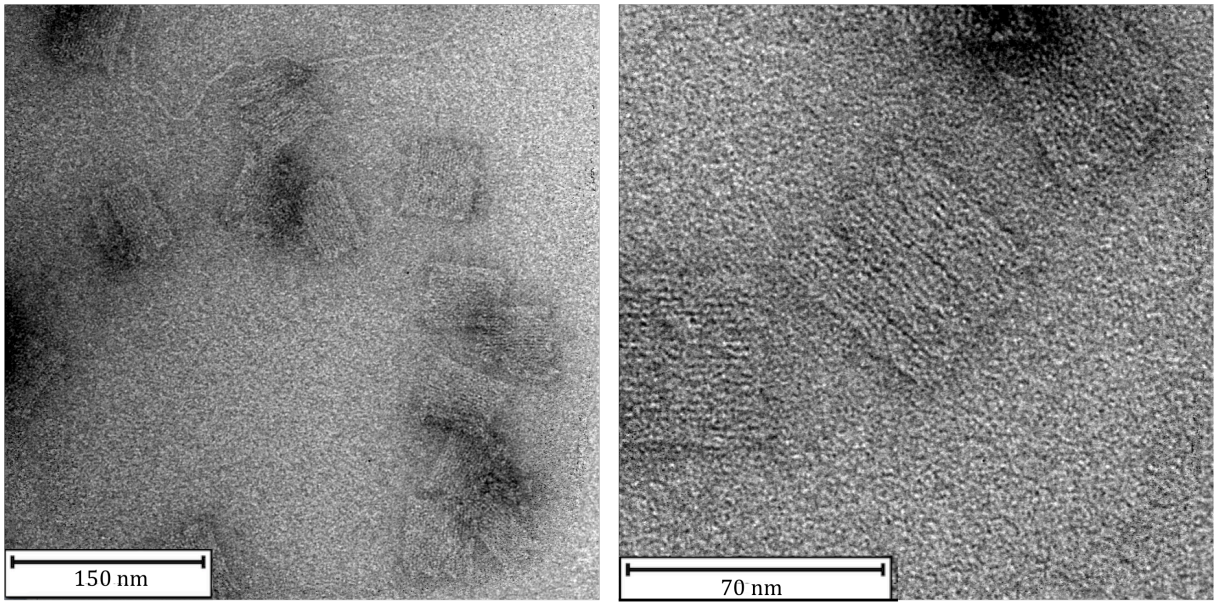

Figure 16: TEM images of the correctly folded DNA origami two-layer sheets with ACC_5-staples.

III.1.3. Modification of CapZ

To build sarcomere-like structures, the actin-binding protein CapZ had to be connected to the DNA origami two-layer sheet. One already applied binding strategy was based on biotin-handles on the DNA origami and biotinylated CapZ[30].

For biotinylation, the protein was incubated with NHS-activated biotin molecules. The mole-to-mole ratio of biotin to CapZ was estimated by a HABA/Avidin assay. The absorption values at 500 nm for HABA/Avidin alone and with modified protein are listed in table 4. As expected, the values are lower in the presence of biotinylated CapZ, as binding of biotin to avidin releases HABA and causes a decrease in absorption at 500 nm[31].

Table 4: Measured absorption values at 500 nm for the HABA/Avidin solution with and without biotinylated CapZ.

	A_{500} values	**mean A_{500} value**
HABA/Avidin	0.117 0.117 0.119 0.117 0.120	0.118
HABA/Avidin with Biotin-CapZ	0.100 0.098 0.097 0.094 0.095	0.096

Assuming a CapZ concentration of 9 µM (determined via A_{280}), the ratio of biotin to CapZ was 3.3 biotin molecules per CapZ molecule. Thus, a successful biotinylation reaction had occured.

To test the function of the protein after the biotinylation reaction, actin polymerization assays were carried out using unmodified or modified CapZ (figure 17).

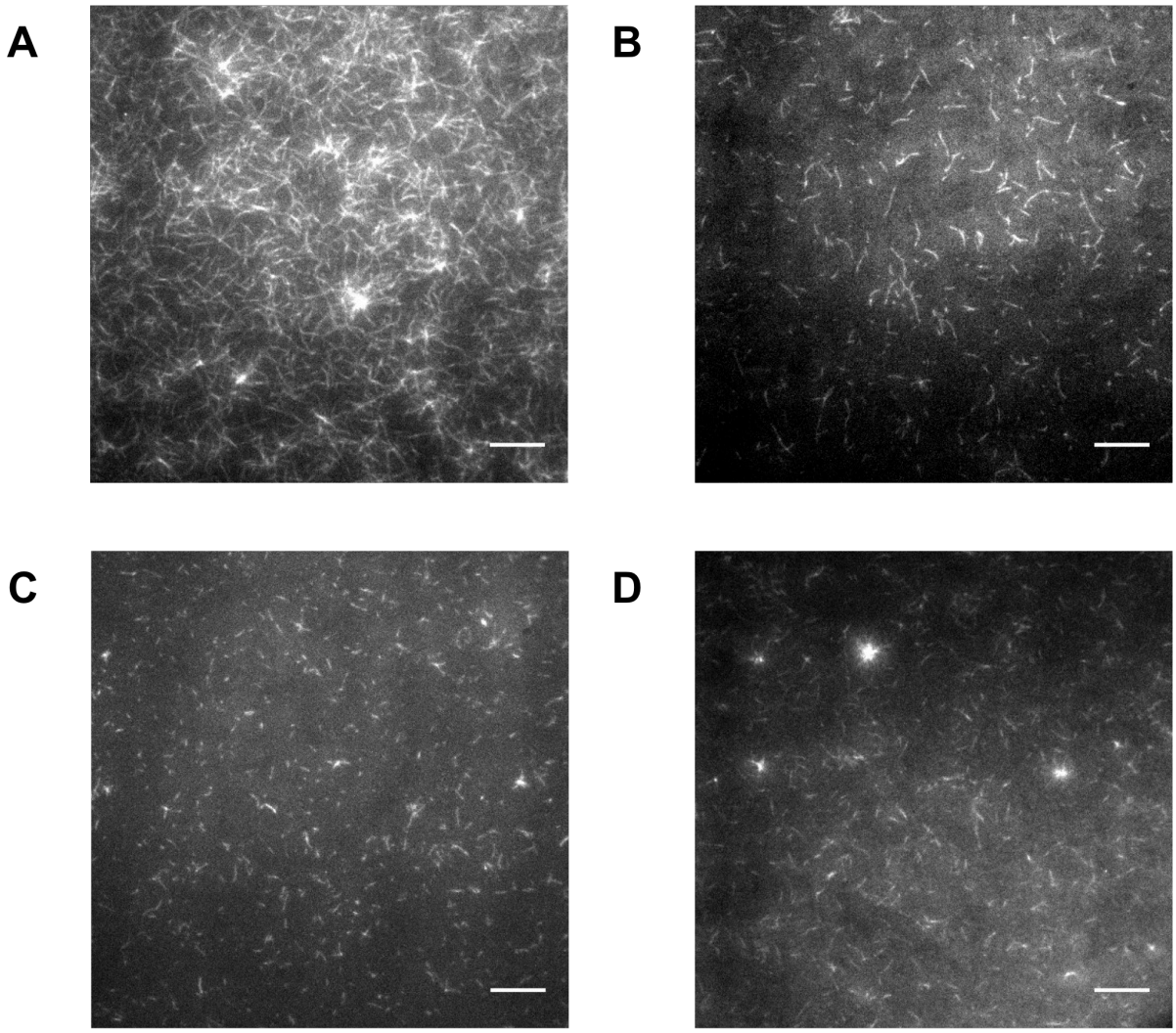

Figure 17: Modified CapZ binds to actin filaments. TIRF images of actin filaments (**A**, actin concentration 1.5 µM), and actin in the presence of 10 nM unmodified CapZ (**B**), biotinylated CapZ (**C**) or CapZ incubated with SMPH and ssDNA (**D**) show, that actin filaments are considerably shorter in the presence of both unmodified and modified CapZ. Scale bar: 10 µm.

As CapZ binds to the barbed end of actin filaments, it inhibits further polymerization[42]. Thus, shorter actin filaments are expected when actin polymerizes in the presence of CapZ. In the absence of CapZ, actin forms a filamentous network, which can be visualized by TIRF (figure 17, A). Bright spots indicate the presence of myosin, which was used as a tethering protein. As expected, the addition of unmodified CapZ leads to considerably shorter actin filaments (figure 17, B). In the presence of biotinylated CapZ, the actin filaments appear even shorter (figure 17, C). As it was already shown that the actin length distribution in the presence of unmodified and biotinylated CapZ is nearly identical[30], the actin length distribution was not further investigated here. Taken together, TIRF experiments confirm the expected function of CapZ even after the modification with biotin and its potential as a component for sarcomere assemblies.

Despite its simple experimental realization, the modification of CapZ with biotin has some drawbacks, as streptavidin, a tetrameric protein with four biotin-binding sites, has to be used to connect biotinylated CapZ to the biotinylated DNA origami handles. Therefore, the binding of more than one biotinylated CapZ to a single biotinylated DNA staple is possible. Furthermore, streptavidin cannot only link DNA and CapZ, but also two biotinylated DNA strands or two biotinylated proteins.

In order to circumvent these drawbacks and to make the binding of CapZ to the handles on the DNA origami more specific, another binding strategy was tested, which was based on complementary DNA single-strands on the protein and on the DNA origami[32]. Instead of biotin-handles, staples with a ssDNA-extension were incorporated during folding of the DNA origami two-layer sheet. Further, it was attempted to modify CapZ with a DNA single strand, complementary to the handles on the DNA origami. Two coupling reagents, SPDP and SMPH, were chosen to modify CapZ with a TAMRA-labeled 5'-SH-(GGT)-3'-DNA. SPDP and SMPH are amine-to-sulfhydryl-crosslinkers with a NHS ester as the amine-reactive part, and a 2-pyridyldithio (for SPDP) or maleimide group (for SMPH) as the thiol-reactive portion.

After the crosslinking reactions with SPDP were performed, the absorbance at 343 nm was measured, which allows estimating the coupling efficiency of DNA and CapZ. An efficient coupling should result in the release of pyridine-2-thione and an increased absorption at 343 nm[33]. However, the absorbance at 343 nm did not change considerably after the crosslinking reactions. Thus, crosslinking with SDPD was not successful.

The experiments were repeated with SMPH, as this crosslinker binds the thiol-group of the DNA oligonucleotide covalently to its maleimide part and not via a disulfide-bond. Disulfide-bonds are sensitive to reduction and could be a possible explanation, why the crosslinking with SPDP did not work. The length of actin filaments in the presence of CapZ, which was incubated with SMPH and 5'-SH-(GGT)-3'-DNA, is similar to the actin filaments bound by unmodified CapZ (figure 17, D). Thus, the crosslinking reaction did not seem to have an influence on the biological activity of CapZ. For a successfully DNA-modified CapZ, TAMRA-DNA signals would be expected at the binding positions of CapZ, which are supposed to be at the barbed ends of actin filaments. However, as nearly no signal for the TAMRA-labeled DNA could be detected by TIRF despite many capped actin filaments (figure 18), it is not clear if DNA was successfully bound to CapZ.

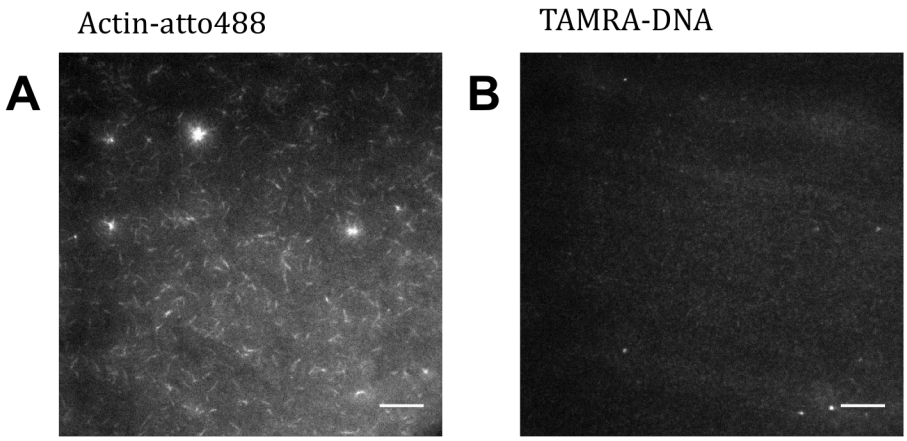

Figure 18: TIRF image of actin filaments in the presence of CapZ, which was incubated with SMPH and TAMRA-labeled DNA single-strands. (**A**) Actin forms short filaments in the presence of CapZ. (**B**) Only a few signals of the TAMRA-labeled DNA are detected. Scale bar: 10 µm.

To check if DNA is really crosslinked to the protein, the diffusion of the TAMRA-DNA single-strand before and after crosslinking with CapZ was measured in solution. With the molecular weights of 5.5 kDa for the DNA strand and 66 kDa for CapZ[43], a slower diffusion is expected for a DNA oligonucleotide successfully bound to CapZ. However, the autocorrelation curves for free DNA and DNA after the labeling reaction are nearly identical and independent of the crosslinker choice (figure 19, A and B). For both crosslinker reactions, the diffusion of TAMRA-labeled DNA is slower than the diffusion of the dye atto565. Therefore, it can be excluded that the correlation curves are based on free TAMRA dye in solution. Assuming DNA bound to CapZ, addition of actin should furthermore lead to a much slower diffusion, as CapZ would connect the DNA to a capped actin-filament. However, even in the presence of 1.5 µM actin under

polymerizing conditions, diffusion of the DNA oligonucleotide was unchanged (figure 19, C).

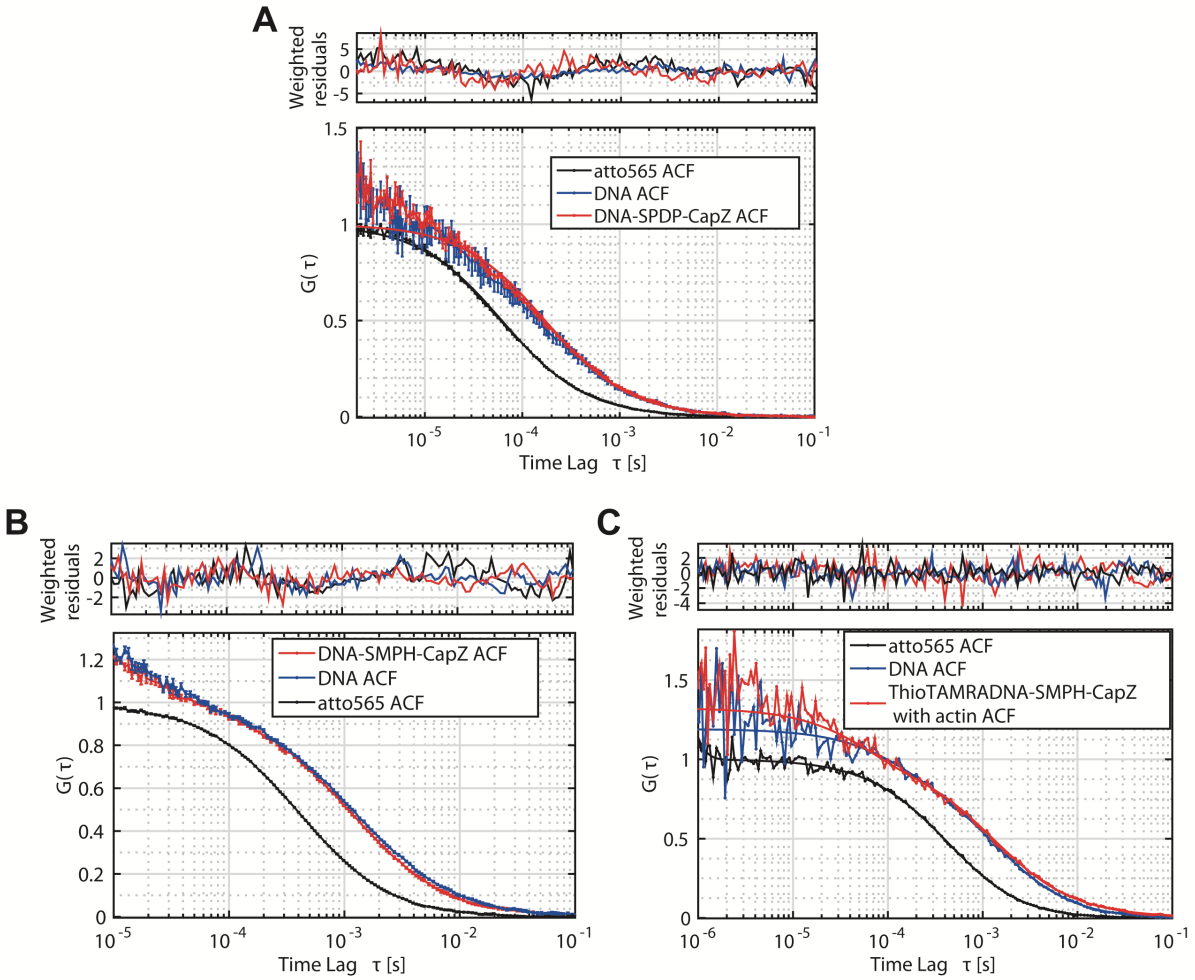

Figure 19: FCS results strongly indicate that the modification of CapZ with DNA is not successful using either the crosslinker SPDP (**A**) or SMPH (**B**). Autocorrelation functions (ACF) of DNA strands before (in blue) and after crosslinking (in red) are nearly identical. Even in the presence of actin, the DNA does not diffuse slower (**C**).

Thus, FCS results strongly indicate that neither SPDP nor SMPH could crosslink CapZ to the thiol-modified DNA single-strands.

III.1.4. Sarcomere assembly

Assembly reactions were mainly performed in the presence of biotin-handles on the DNA origami and biotinylated CapZ, as the success of this protein modification was confirmed by the HABA/Avidin assay. Incubation times and the concentrations of the single components were varied (for details, see II.4.4 sarcomere assembly). DNA

origamis containing staples with ACC_5-extensions and CapZ, which was incubated with SMPH and GTT_5-DNA oligonucleotides, were only used in one experiment.

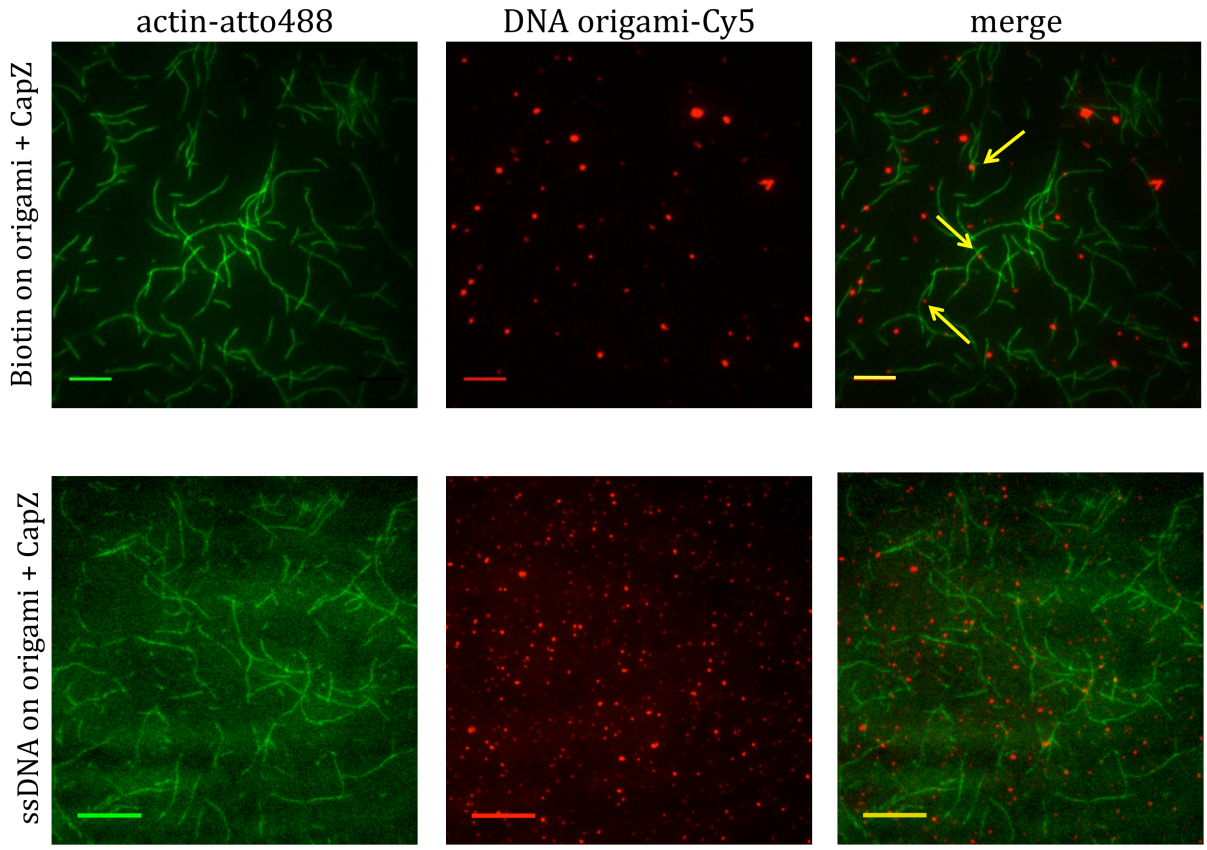

Figure 20: Sarcomere-like structures do not form in solution under different assembly conditions. **Upper panel**: Actin forms short filaments after incubation with biotinylated CapZ, biotin-modified DNA origami two-layer sheets and myosin thick filaments. Cy5-labeled DNA origamis are visible as dots, which colocalize with some of the actin filaments (examples are indicated with a yellow arrow). However, no sarcomere-like structures can be detected. **Lower panel**: The same experiment was repeated with DNA origamis with ACC_5-handles and DNA-modified CapZ. Again, actin forms short filaments and Cy5-labeled DNA origamis are visible as dots. However, nearly no colocalization of both structures can be observed. Scale bars: 10 µm.

Representative TIRF images of assembly reactions based on biotin-streptavidin-bonds between CapZ and DNA origami (upper panel) or on complementary DNA strands (lower panel) with 1.5 µM actin, 500 pM DNA origami, 6 nM modified CapZ and 500 pM myosin thick filaments are presented in figure 20. Actin seems to form relatively short filaments, which indicates the presence of functional CapZ. Without CapZ, actin polymerizes into a dense network of filaments (data not shown). Cy5-labeled DNA origamis are detected as dots. Compared to ACC_5-modified DNA origamis, biotinylated origamis are observed as slightly larger spots, which may be due to aggregation. Some biotinylated DNA origamis colocalize with actin filaments (left image in the upper panel,

examples indicated by yellow arrows). However, arrays of DNA origamis with bound actin filaments in between cannot be detected. DNA origamis with ACC_5-handles do not colocalize with actin filamnents, but seem to be randomly distributed. It surprises, that fluorescence signals of ACC_5-modified DNA origamis can be detected at all, as the DNA-modification of CapZ seemed to be unsuccessful. DNA origamis should only be visible when bound to the actin-capping protein CapZ. As this is probably not the case, DNA origamis appear to stick to the cover glass of the flow cells. This gives rise to the question if the colocalization of biotinylated DNA origamis and actin is only due to random sticking of the DNA to the surface or actually a proof for actin-binding via CapZ. Taken the results together, a nonambiguous and reproducible observation of sarcomere-like structures was not possible.

III.2. Using a DNA origami two-layer sheet with gap as a platform for DNA DSB repair studies

For this project, a DNA origami structure was designed in order to bring two dsDNA oligonucleotides in close proximity in a defined geometry. dsDNA were labeled with either Alexa488 or Atto647N and served as substrates for a DNA DSB repair study. The repair process was mimicked - in a simplified approach - by the addition of the commercially available T4 DNA ligase.

III.2.1. Analyzing the DNA origami structure with CanDo

For the DNA DSB repair study, a DNA origami two-layer sheet with gap was designed. Two protrusions inside the gap served as attachment sites for two DNA double-strands. To check the stability of the design, fluctuations at 25° C were calculated with the program CanDo (figure 21). CanDo analysis confirms that the DNA origami has the desired shape at room temperature and accessible dsDNA binding sites, which are – together with the edges of the structure- the most flexible parts.

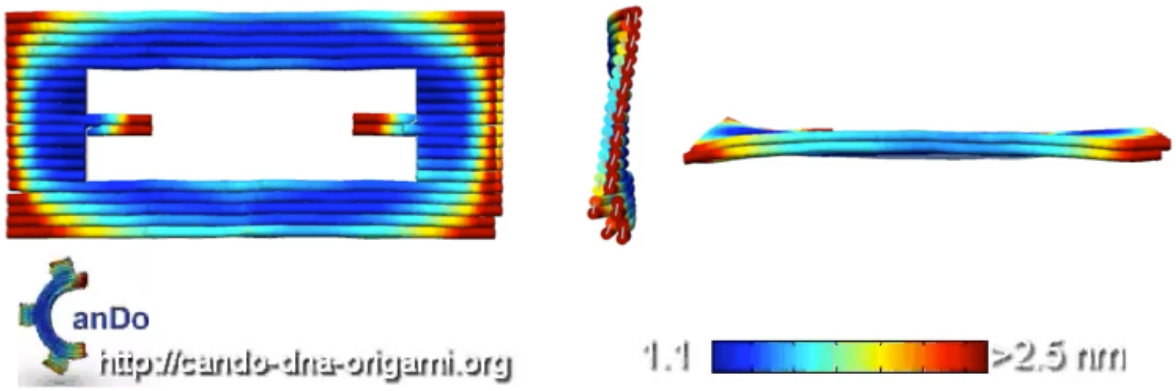

Figure 21: The DNA origami two-layer sheet with gap is stable at 25° C. Fluctuations were calculated using CanDo. The flexibility in nm is shown for the top, side and front view of the structure.

III.2.2. Assembly the DNA origami

Positively charged Mg^{2+}-ions screen the electrostatic repulsion between negatively charged phosphate groups of the DNA backbone and are therefore a crucial component of the folding buffer. To find the optimal folding condition for the DNA origami two-layer

sheet with gap, $MgCl_2$ concentrations were varied between 10 and 20 mM during the assembly process, as theses are typical salt concentrations for the folding of DNA origami structures[9]. The result of the salt screening is shown in figure 22. All structures were assembled in the presence of endcaps containing T_4-tails. Each folding batch led to the desired DNA origami structure, as each lane displays a band comparable to the scaffold alone. The broad, blurry bands below the origami band are unbound staple strands, which were added at 10-fold molar excess with respect to the scaffold. The unbound staples are visible, as the origami samples were not purified by PEG precipitation. During PEG purification, some loss of DNA cannot be avoided. In order to compare equally concentrated DNA samples, this purification step was skipped. There are remarkable differences in terms of aggregation indicated by (smeared) bands above the origami band, which vary in intensity. Most aggregation is observed at 20 mM $MgCl_2$, while nearly no aggregation can be detected with 12 mM $MgCl_2$. Therefore, 12 mM $MgCl_2$ was chosen as the optimal salt concentration for DNA origami assembly.

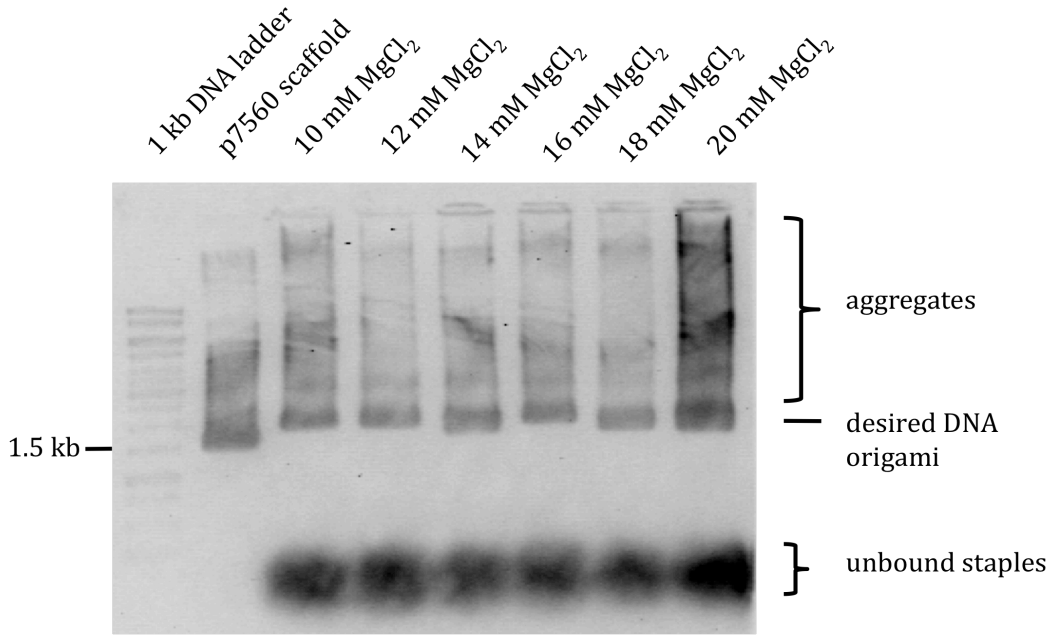

Figure 22: The DNA origami two-layer sheet with gap folds best in the presence of 12 mM $MgCl_2$. An increase in aggregation can be observed in the presence of less or more $MgCl_2$.

III.2.3. Visualization of the DNA origami with TEM

Next, TEM images (figure 23) reveal that most of the DNA origamis have the desired shape and dimension. Only a few aggregated or misfolded structures are detected. In the zoomed out image (left panel) a twisted origami is visible. This indicates both the flexibility of the origami, as it could rotate with one part already attached to the TEM grid, and the stability of the structure, as it was not torn apart during this process.

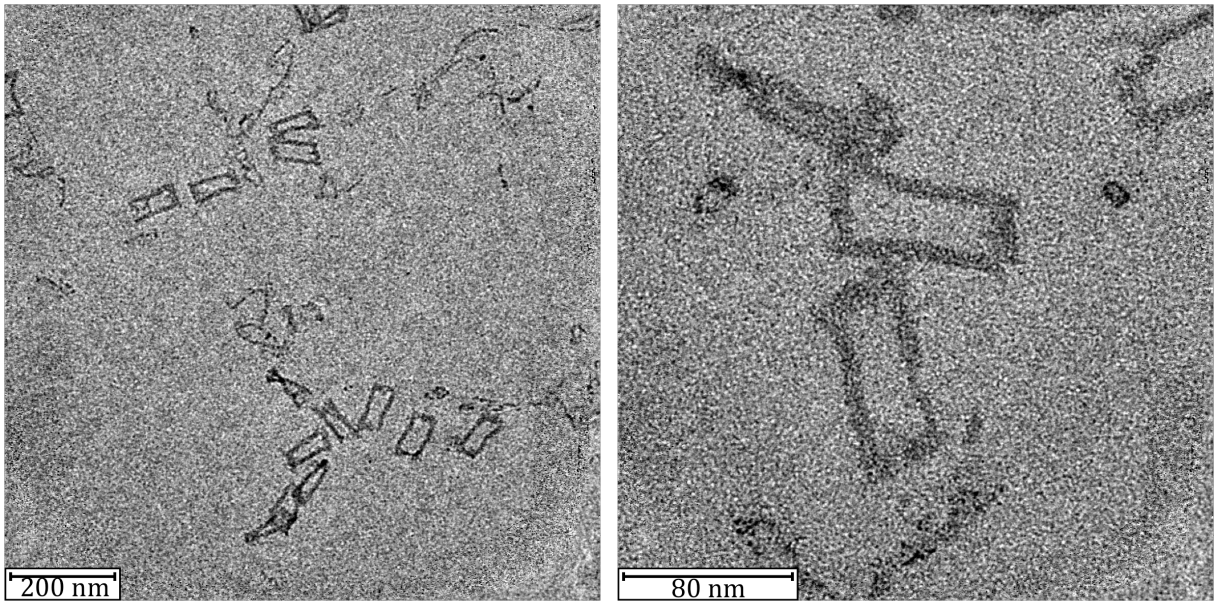

Figure 23: TEM images of the correctly folded DNA origami two-layer sheet with gap.

III.2.4. Binding dsDNA to the DNA origami

After the correct folding of the DNA origami two-layer sheet with gap was confirmed, complementary DNA single-strands were annealed to create dsDNA repair substrates. The successful hybridization of the ssDNA was confirmed by a slower diffusion of the double-strands compared to the Alexa488- or Atto647N-labeled single-strands (figure A.1. in the appendix). The auto- and cross-correlation functions (ACF and CCF, respectively) for phosphorylated dsDNA before and after incubation with the DNA origami two-layer frames are shown in figure 24. For the autocorrelation functions, the photons after red or blue excitation were correlated (RR1xRR2 and BB1+BR1xBB2+BR2, respectively), while the combined channels RR1+RR2 and BB1+BB2+BR1+BR2 were correlated for the cross-correlation functions. For simplicity, data were fitted using a one-component fit, assuming a single diffusional species.

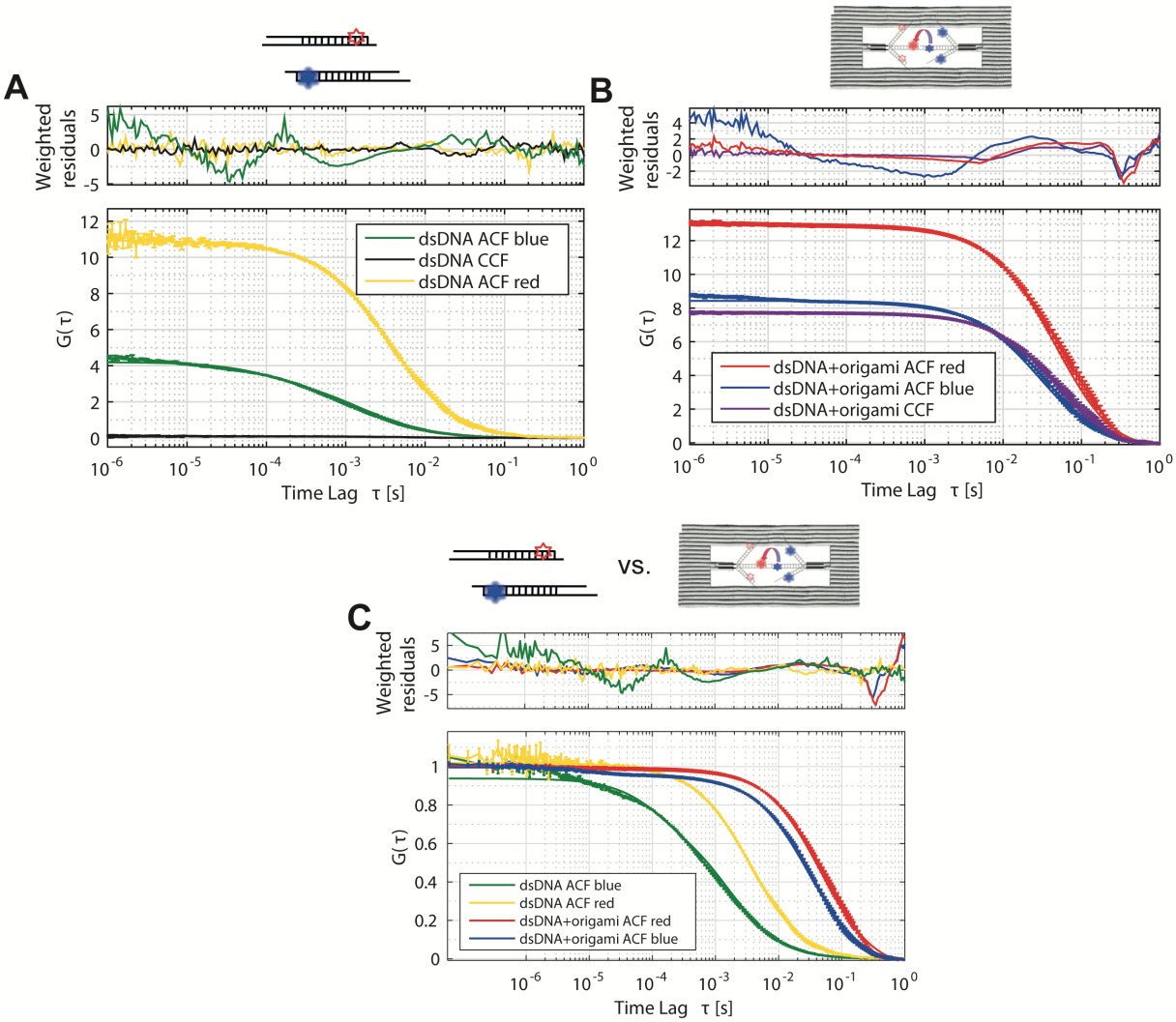

Figure 24: FCS measurements indicate binding of dsDNA to the DNA origami two-layer sheet with gap. (**A**) Alexa488-(blue) and Atto647N-(red) labeled dsDNA do not diffuse together in the absence of the DNA origami. (**B**) Upon binding to the DNA origami, cross-correlation of the two species can be detected. (**C**) dsDNA oligonucleotides diffuse much slower when bound to the DNA origami.

In the absence of DNA origami, there is no co-diffusion of the two DNA double-strands, as the cross-correlation amplitude is zero (figure 24, A). Apparently, the complementary overhangs of four nucleotides on the two oligonucleotides are not sufficient to stably connect them in solution. Weighted residuals show, that the fit does not describe the blue ACF for the Alexa488-labeled dsDNA well. Possible reasons could be a second component, which diffuses slower, or photophysical effects like blinking. Incubation with the DNA origami leads to a considerably slower diffusion of the DNA double-strands compared to the free DNA strands in solution (figure 24, C). Furthermore, the origami-bound DNA strands now diffuse together as indicated by their cross-correlation amplitude (figure 24, B). Thus, FCS results indicate the attachment of the two double-strands to the DNA origami two-layer sheet with gap.

III.2.5. Ligation of dsDNA in solution

The commercially available T4 DNA ligase was chosen to "repair" the dsDNA substrates. It ligates both sticky and blunt ends by catalyzing the formation of a phosphodiester bond between 5'-phosphate and 3'-hydroxyl termini[37]. It is important to keep in mind, that synthetic DNA oligonucleotides contain a 5'-OH group after the solid phase phosphoramidite synthesis cycle and the removal of the 5'-dimethoxytrityl protecting group[44]. Thus, ligation is only possible after phosphorylation of the 5'-termini

The complementary overhangs of dsDNA with phosphorylated 5'-termini (of DNA oligos 2 and 3) were first ligated in the absence of the DNA origami (figure 25).

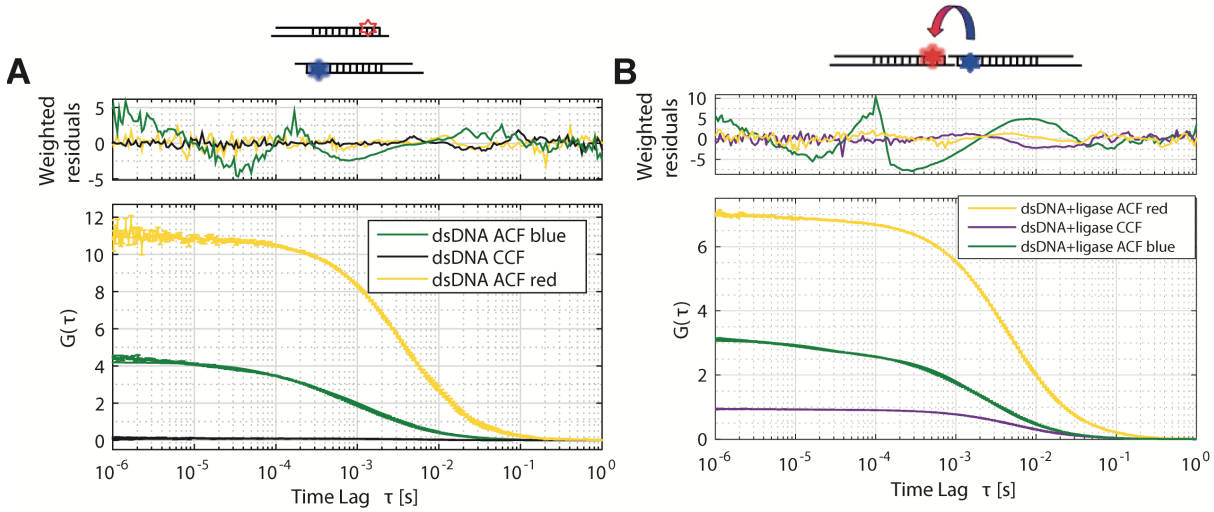

Figure 25: FCS measurements indicate ligation of dsDNA in solution using the T4 DNA ligase. (**A**) The two DNA double-strands show nearly no cross-correlation in solution. (**B**) After incubation with the ligase, cross-correlation is detected.

In contrast to the unligated dsDNA (figure 25, A), co-diffusion of the two DNA species can be observed after ligation even without being attached to the DNA origami (figure 25, B), which indicates a connection of the two dsDNA substrates. However, the cross-correlation amplitude is relatively small compared to the auto-correlation amplitudes, which could be explained by the several possible ligation combinations. Besides linking one Alexa488-labeled DNA double-strand to a Atto647N-labeled dsDNA, two additional 3'-OH termini of the single-stranded overhangs were available, as the DNA strands were not bound to their complementary sequences on the DNA origami scaffold. Therefore, several identical labeled DNA double-strands could have been ligated, which would not contribute to the cross-correlation amplitude.

The successful ligation of the DNA substrates, which are either labeled with Alexa488 or Atto647N, should bring the two fluorescent dyes together within a distance of 12 nucleotides (around 4 nm). Once ligated, FRET should occur from the Alexa488-labeled donor to the Atto647N-labeled acceptor DNA double-strand.

Plots of stoichiometry, S, versus FRET efficiency, E, illustrate the effect of ligation of dsDNA in solution (figure 26). In the absence of DNA origami structures, unligated dsDNA substrates display a donor-only (S = 1, E = 0) and an acceptor-only species (S around zero). The dyes were not close enough for FRET as the complementary overhangs of the DNA strands were not connected to each other.

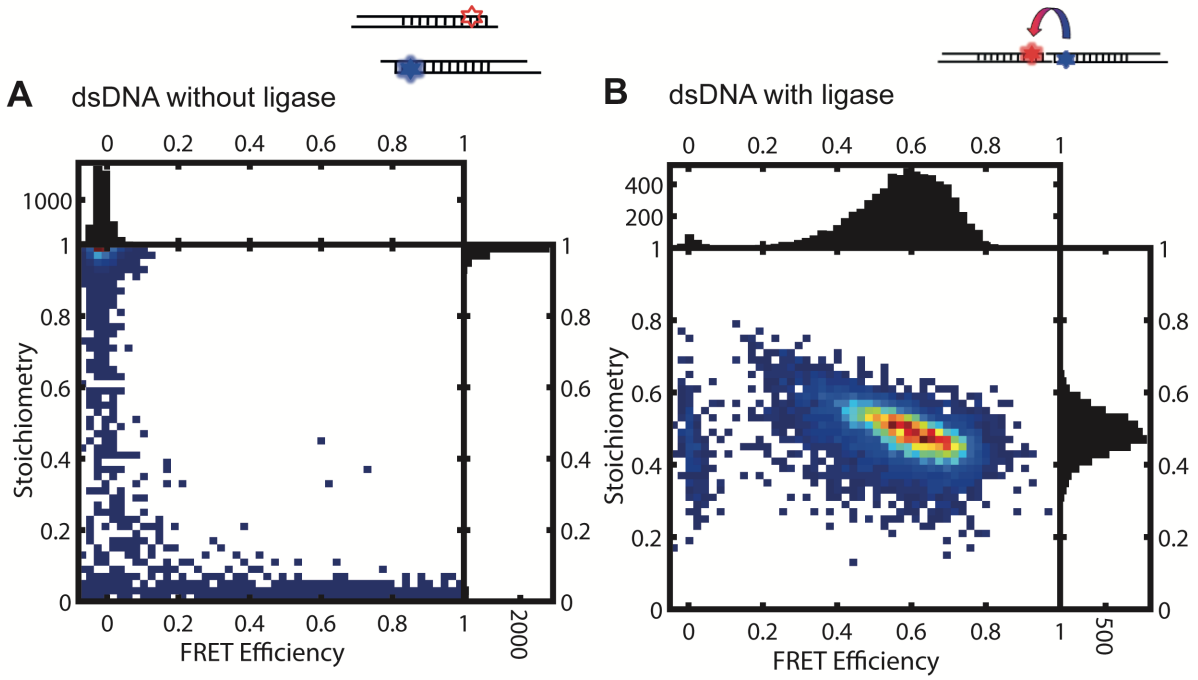

Figure 26: 2D histograms of the stoichiometry versus FRET efficiency for free DNA double-strands in the absence (**A**), or presence of the T4 DNA ligase (**B**). Double-labeled species in **B** were selected using a 2CDE-filter ($ALEX_{2CDE} < 5$). Additional lifetime and anisotropy plots can be found in the appendix (figures A.3 and A.4).

Only after incubation with a T4 DNA ligase, a FRET population appears, indicating a successful ligation of donor- and acceptor-strands. Double-labeled species were selected using a Two-Channel Kernel-Density Estimator[41] (2CDE)-filter, which removed donor- and acceptor-only populations. The original plot without the 2CDE filter is listed in the appendix (figure A.2.). The FRET population has a FRET efficiency peak at around E = 0.6. However, the population is relatively broad and smeared towards the donor-only species. This should not be a result of photobleaching, as measurements were performed in the presence of Trolox. More likely, it is an effect of the several ligation

possibilities of unbound dsDNA. As already mentioned above, the single-stranded overhangs of dsDNA, which are complementary to the scaffold, provide additional 3'-OH-termini for ligation. Therefore, several double-strands can be ligated, for example two donor- and one acceptor-strand. The presence of additional donor-strands influences the FRET efficiency and shifts it towards the donor-only species.

III.2.6. Ligation of dsDNA bound to the DNA origami

Next, the complementary overhangs of dsDNA with phosphorylated 5'-termini (of DNA oligos 2 and 3) were ligated while bound to the DNA origami.

The diffusion behavior of dsDNA bound to the DNA origami did not change after the ligation process (figure 27), as the origami-bound DNA double-strands had already co-diffused in the absence of the ligase.

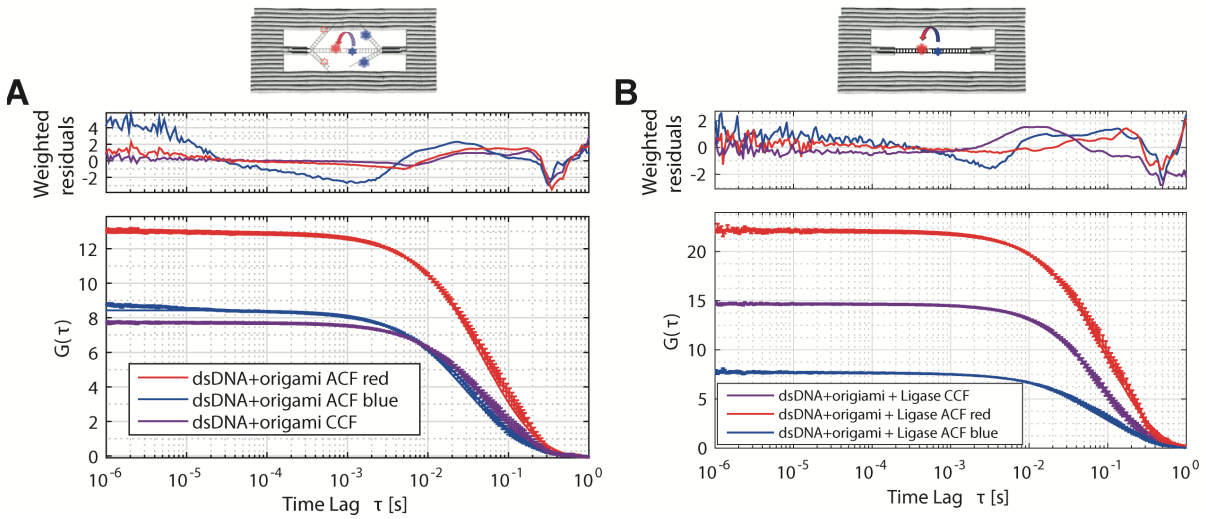

Figure 27: FCS measurements show co-diffusion of DNA origami-bound DNA double strands both in the absence (**A**) and the presence of the T4 DNA ligase (**B**).

Even in the absence of a ligase, some FRET bursts can be observed for DNA double-strands bound to DNA origamis (figure 28, A). Donor- and acceptor-only species were removed using a 2CDE-filter (unfiltered data can be found in the appendix, figure A.2.) Binding of the DNA double-strands to the protrusions of the DNA origami two-layer sheets with gap brings their complementary single-stranded overhangs of four nucleotides in close proximity, which increases their local concentration and therefore the probability of strand pairing. However, the low FRET population is much more

pronounced than the higher FRET one, suggesting only a transiently populated species in the absence of the ligase.

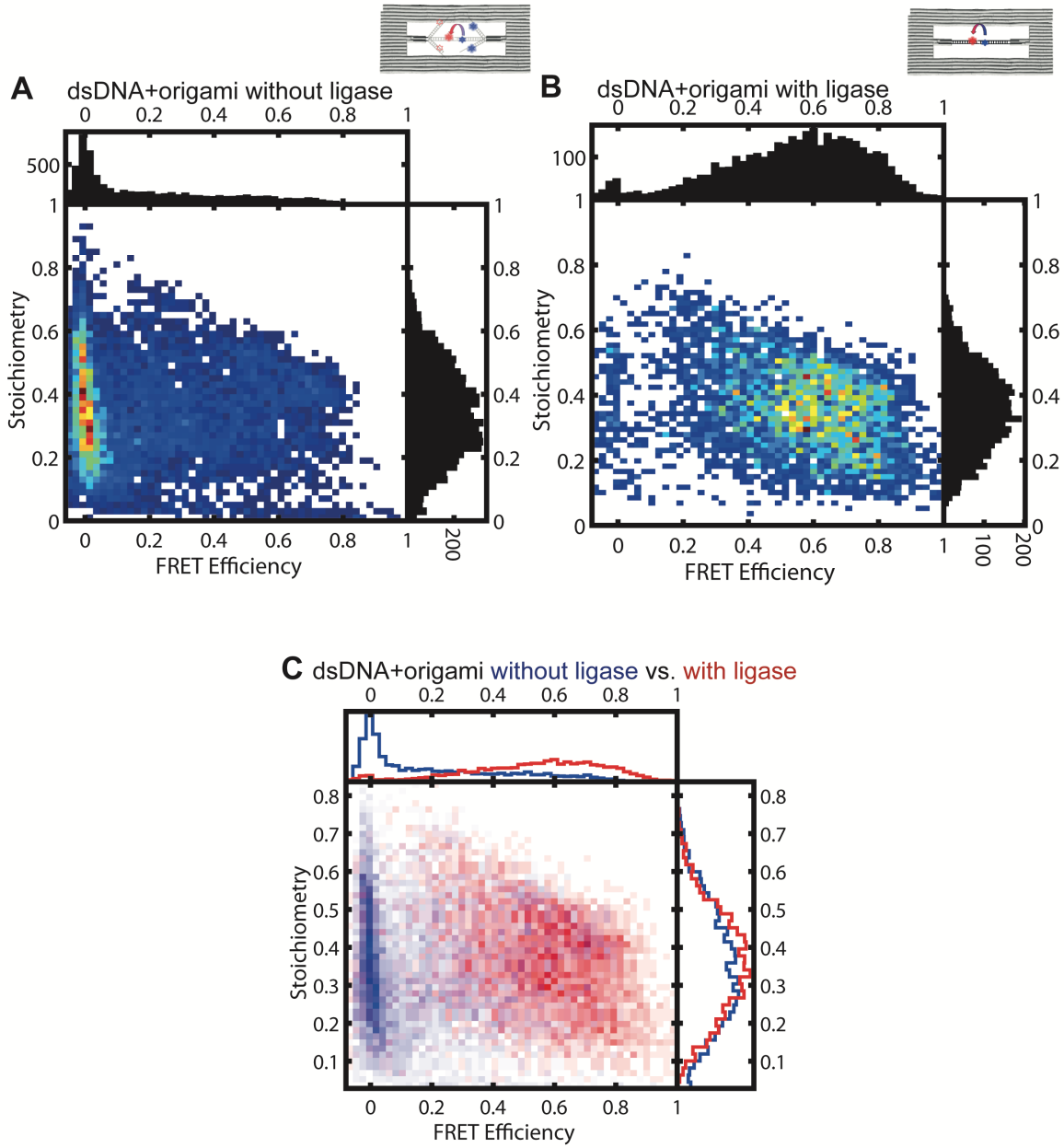

Figure 28: 2D histograms of the stoichiometry versus FRET efficiency for DNA double-strands bound to DNA origami two-layer sheets with gap in the absence (**A**), or presence of the T4 DNA ligase (**B**). Data are directly compared in (**C**) with bursts detected without the ligase in blue and bursts detected with the ligase in red. Double-labeled species were selected using a 2CDE-filter ($ALEX_{2CDE} < 20$). Lifetime and anisotropy plots can be found in the appendix (figures A.5 and A.6).

After incubation with the T4 DNA ligase, the low FRET species nearly disappears and a high FRET species can be detected instead (figure 28, B). The high FRET population is even broader than the one for unbound, ligated double-strands. It needs to be discussed

why this population is so broad and how experimental conditions could be improved. Possible reasons for the broad population could be photobleaching, which might be reduced by the use of other photococktails than Trolox, or aggregation of DNA origami structures. The latter could be decreased by further modification of the assembly protocol, for example by using another temperature gradient or by fine-tuning the $MgCl_2$ concentration. Furthermore, unspecific binding of dsDNA to the DNA origami might also contribute to the broad FRET species. Although the DNA origami was designed to only display two dsDNA binding sites, it is possible that some staple strands were not incorporated during folding and left some parts of the scaffold unoccupied. The single-stranded overhangs of the dsDNA substrates might have bound to these parts if their sequence was complementary to at least a few nucleotides of the scaffold.
In order to visualize the origami-bound DNA double-strands and their binding positions, TEM images of DNA origamis with bound dsDNA were aquired in the presence and absence of a T4 DNA ligase. However, single DNA double-strands, which are not surrounded by other double-strands, could not be visualized by TEM. Instead of TEM, AFM might be a useful technique to show how the dsDNA substrates are bound to the DNA origami.
Nonetheless, the difference between the FRET data obtained for DNA origami-bound double-strands in the presence or absence of the T4 DNA ligase (figure 28,C) is striking and shows the influence of the ligase on phosphorylated dsDNA.

As a negative control, experiments were repeated with unphosphorylated dsDNA bound to the DNA origami. Nearly no difference between DNA samples in the presence or absence of the ligase was detected (figure 29). Donor- and acceptor-only species were removed using a 2CDE-filter (unfiltered data can be found in the appendix, Fig. A.2.) As expected, addition of the ligase did not lead to a FRET population. Thus, the T4 DNA ligase could not connect DNA double-strands without phosphorylated 5'-termini.

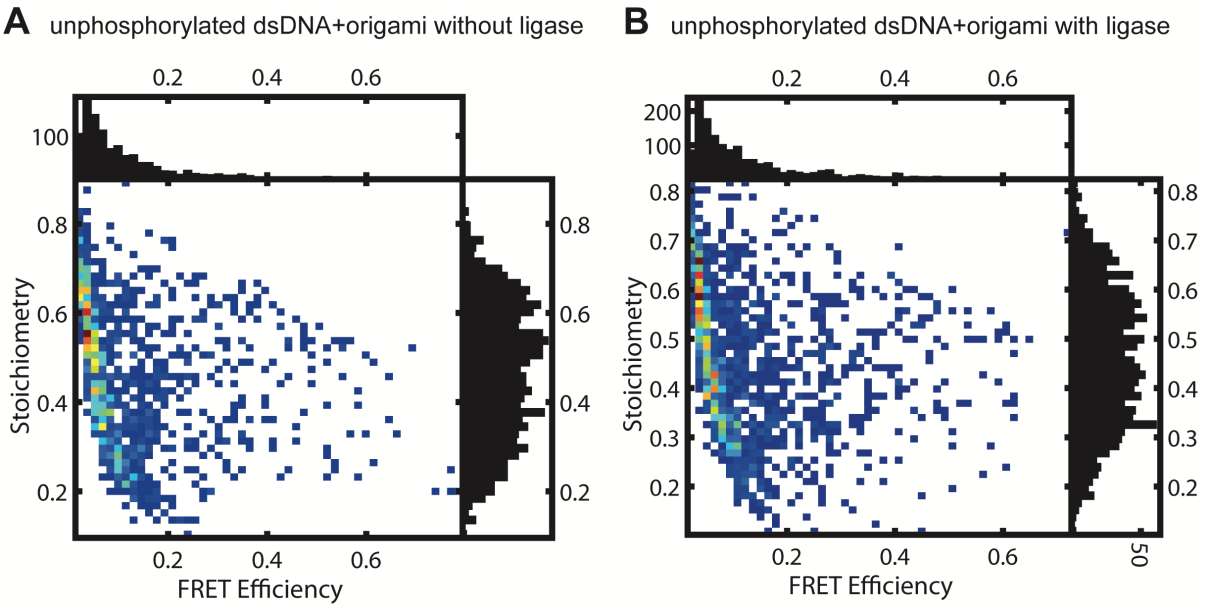

Figure 29: Without phosphorylated 5'-termini, dsDNA bound to the DNA origami can not be ligated. 2D histograms of the stoichiometry versus FRET efficiency are nearly identical for samples in the absence (**A**) and presence of the T4 DNA ligase (**B**). Double-labeled species in were selected using a 2CDE-filter ($ALEX_{2CDE} < 10$).

IV. Conclusion and Outlook

During this master's thesis, two DNA origami structures served as platforms for single-molecule fluorescence studies.

Firstly, to provide a scaffold for sarcomere assembly, rectangular DNA origami two-layer sheets were folded in the presence of either biotin-modified handles or staples containing single-stranded overhangs. Aggregation of the structures was considerably reduced by using endcaps with T_4-tails and freshly prepared scaffold.

To assemble sarcomere-like structures in solution, the actin-binding protein CapZ had to be connected to the DNA origami two-layer sheet. Besides using biotinylated CapZ, attempts were made to modify CapZ with a thiol-ssDNA complementary to the overhangs on the DNA origami. However, the two tested crosslinkers, SPDP and SMPH, could not connect the protein to the ssDNA. As the biotinylation protocol is also based on the reaction of an NHS-activated molecule with the amine groups of CapZ's lysine residues, the amine-reactive NHS groups of the crosslinkers should not be the reason for the unsuccessful crosslinking. The thiol-reactive groups are rather critical. Two scenarios are possible: The DNA was not fully reduced and existed as DNA dimers linked by disulfide bonds, displaying therefore no thiol-groups. Or sulfhydryl-reactive groups bound to cysteine residues and crosslinked two CapZ proteins or even two cysteines within the same protein instead of binding the protein to the handles on the DNA origami.

As the DNA-modification of CapZ was not successful, sarcomere assembly reactions were mainly performed in the presence of biotinylated CapZ and DNA origamis containing biotin-handles. Preliminary data aquired during a bachelor's thesis had suggested the successful formation of sarcomere-like structures under these conditions[30]. However, even after various modifications of the assembly protocol, no arrays of DNA origamis connected by actin filaments could be observed by TIRF. Thus, the preliminary results, which were based on single observations, could not be reproduced during this thesis, indicating that sarcomere assembly – at least for the tested experimental conditions - requires probably more components than an artificial Z-disc, CapZ, actin and myosin filaments. Crucial proteins might be nebulin, as it controls the length of actin thin filaments[45], or titin, as it connects myosin thick filaments with

the Z-disc[46]. Obviously, the current model system needs to be improved further to study the principles of skeletal muscle contraction.

For the second project of this thesis, a DNA origami two-layer sheet with gap containing two attachment sites for dsDNA was designed and successfully assembled. FCS and FRET data indicated the "repair" of phosphorylated dsDNA substrates bound to the DNA origami using the T4 DNA ligase and therefore the potential of this DNA origami as a platform for further DNA DSB repair studies.

The next step will be to investigate the system by TIRF. Four biotin-modified staples can be incorporated into the DNA origami and the structure therefore immobilized on a biotinylated surface. The ligation process could be monitored in real time by adding a ligase to already immobilized DNA origamis with bound DNA double-strands. An advantage of surface-immobilized origamis would be their reduced fluctuation. DNA origami systems with biotin and bound dsDNA were prepared and ready to measure. However, as the single-molecule TIRF setup was under construction, no data could be acquired.

Furthermore, the length of the complementary overhangs between the two dsDNA could be varied to test how longer overhangs influence the chance of spontaneous strand annealing in the absence of a ligase.

It is also possible to incorporate a fluorescently labeled staple strand during DNA origami assembly. The third color may help to indentify DNA origamis containing both a donor- and an acceptor-DNA double-strand through co-diffusion of the three colors. Donor-acceptor-origamis could thus be isolated from incompletely assembled structures or unbound dsDNA substrates in solution.

Although several experiments and modifications need to be done to better understand and optimize the DNA origami model system, I have shown that the designed DNA origami two-layer sheet with gap can be used to bring two DNA double-strand in close proximity and to ligate them with the help of the T4 DNA ligase. Therefore, this model system provides the basis for further studies with labeled proteins and DNA strands to investigate the underlying dynamical processes of DNA DSB repair by NHEJ or HR.

V. References

1. Stein, I. H., Schüller, V., Böhm, P., Tinnefeld, P. & Liedl, T. Single-molecule FRET ruler based on rigid DNA origami blocks. *Chemphyschem* **12,** 689–695 (2011).
2. Saccà, B. *et al.* Orthogonal protein decoration of DNA origami. *Angewandte Chemie International Edition* **49,** 9378–9383 (2010).
3. Pibiri, E., Holzmeister, P., Lalkens, B., Acuna, G. P. & Tinnefeld, P. Single-Molecule Positioning in Zeromode Waveguides by DNA Origami Nanoadapters. *Nano Lett.* **14,** 3499–3503 (2014).
4. Rothemund, P. W. K. Folding DNA to create nanoscale shapes and patterns. *Nature* **440,** 297–302 (2006).
5. Douglas, S. M. *et al.* Self-assembly of DNA into nanoscale three-dimensional shapes. *Nature* **459,** 414–418 (2009).
6. Castro, C. E. *et al.* A primer to scaffolded DNA origami. *Nat Meth* **8,** 221–229 (2011).
7. Seeman, N. C. Nucleic acid junctions and lattices. *J. Theor. Biol.* **99,** 237–247 (1982).
8. Castro, C. E. *et al.* A primer to scaffolded DNA origami. *Nat Meth* **8,** 221–229 (2011).
9. Ke, Y., Bellot, G., Voigt, N. V., Fradkov, E. & Shih, W. M. Two design strategies for enhancement of multilayer–DNA-origami folding: underwinding for specific intercalator rescue and staple-break positioning. *Chemical Science* **3,** 2587–2597 (2012).
10. Nakata, M. *et al.* End-to-end stacking and liquid crystal condensation of 6 to 20 base pair DNA duplexes. *Science* **318,** 1276–1279 (2007).
11. Stahl, E., Martin, T. G., Praetorius, F. & Dietz, H. Facile and scalable preparation of pure and dense DNA origami solutions. *Angewandte Chemie International Edition* **53,** 12735–12740 (2014).
12. Dietz, H., Douglas, S. M. & Shih, W. M. Folding DNA into twisted and curved nanoscale shapes. *Science* **325,** 725–730 (2009).
13. Alberts, B. *et al. Molecular Biology of the Cell, Fifth Edition.* (Garland Science, Taylor & Francis Group, New York, 2008).
14. Tanner, B. C. W., Daniel, T. L. & Regnier, M. Sarcomere Lattice Geometry Influences Cooperative Myosin Binding in Muscle. *PLoS Comput. Biol.* **3,** e115 (2007).
15. Lieber, M. R. The Mechanism of Double-Strand DNA Break Repair by the Nonhomologous DNA End Joining Pathway. *Annu. Rev. Biochem.* **79,** 181–211 (2010).
16. Limp-Foster, M. & Kelley, M. R. DNA repair and gene therapy: implications for translational uses. *Environ. Mol. Mutagen.* **35,** 71–81 (2000).
17. San Filippo, J., Sung, P. & Klein, H. Mechanism of eukaryotic homologous recombination. *Annu. Rev. Biochem.* **77,** 229–257 (2008).
18. Nick McElhinny, S. A., Snowden, C. M., McCarville, J. & Ramsden, D. A. Ku recruits the XRCC4-ligase IV complex to DNA ends. *Mol. Cell. Biol.* **20,** 2996–3003 (2000).
19. Gu, J. *et al.* XRCC4:DNA ligase IV can ligate incompatible DNA ends and can ligate across gaps. *EMBO J.* **26,** 1010–1023 (2007).

20. Reid, D. A. *et al.* Organization and dynamics of the nonhomologous end-joining machinery during DNA double-strand break repair. *PNAS* **112,** E2575–E2584 (2015).
21. Stokes, G. G. On the change of refrangibility of light. *Phil Trans R Soc London* **142,** 463–562 (1852).
22. Kasha, M. Characterization of electronic transitions in complex molecules. *Discussions of the Faraday society* (1950).
23. Lakowicz, J. R. *Principles of fluorescence spectroscopy. 3rd edn Springer*. (New York, 2006).
24. Förster, T. Zwischenmolekulare energiewanderung und fluoreszenz. *Ann Phys (Leipzig)* **2,** 55–75 (1948).
25. Stryer, L. Fluorescence energy transfer as a spectroscopic ruler. *Annu. Rev. Biochem.* **47,** 819–846 (1978).
26. Magde, D., Elson, E. & Webb, W. W. Thermodynamic fluctuations in a reacting system—measurement by fluorescence correlation spectroscopy. *Phys. Rev. Lett.* (1972).
27. Elson, E. L. & Magde, D. Fluorescence correlation spectroscopy. I. Conceptual basis and theory. *Biopolymers* **13,** 1–27 (1974).
28. Magde, D., Elson, E. L. & Webb, W. W. Fluorescence correlation spectroscopy. II. An experimental realization. *Biopolymers* **13,** 29–61 (1974).
29. Schwille, P., Meyer-Almes, F. J. & Rigler, R. Dual-color fluorescence cross-correlation spectroscopy for multicomponent diffusional analysis in solution. *Biophysical Journal* **72,** 1878–1886 (1997).
30. Böhm, D. Using a DNA origami two-layer sheet to build sarcomere-like structures. (bachelor's thesis at LMU München, supervised by Don C. Lamb). 1–60 (2015).
31. Green, N. M. A Spectrophotometric Assay for Avidin and Biotin Based on Binding of Dyes by Avidin. *Biochem. J.* **94,** 23C–24C (1965).
32. Fu, J., Liu, M., Liu, Y., Woodbury, N. W. & Yan, H. Interenzyme substrate diffusion for an enzyme cascade organized on spatially addressable DNA nanostructures. *J. Am. Chem. Soc.* **134,** 5516–5519 (2012).
33. Ngo, T. T. A simple spectrophotometric determination of solid supported amino groups. *J. Biochem. Biophys. Methods* **12,** 349–354 (1986).
34. Kron, S. J. & Spudich, J. A. Fluorescent actin filaments move on myosin fixed to a glass surface. *PNAS* **83,** 6272–6276 (1986).
35. Kuhn, J. R. & Pollard, T. D. Real-Time Measurements of Actin Filament Polymerization by Total Internal Reflection Fluorescence Microscopy. *Biophysical Journal* **88,** 1387–1402 (2005).
36. Aitken, C. E., Marshall, R. A. & Puglisi, J. D. An Oxygen Scavenging System for Improvement of Dye Stability in Single-Molecule Fluorescence Experiments. *Biophysical Journal* **94,** 1826–1835 (2008).
37. Lehman, I. R. DNA ligase: structure, mechanism, and function. *Science* **186,** 790–797 (1974).
38. Cordes, T., Vogelsang, J. & Tinnefeld, P. On the mechanism of Trolox as antiblinking and antibleaching reagent. *J. Am. Chem. Soc.* **131,** 5018–5019 (2009).
39. Nir, E. *et al.* Shot-noise limited single-molecule FRET histograms: comparison between theory and experiments. *J Phys Chem B* **110,** 22103–22124 (2006).
40. Kudryavtsev, V. *et al.* Combining MFD and PIE for accurate single-pair Förster resonance energy transfer measurements. *Chemphyschem* **13,** 1060–1078 (2012).

41. Tomov, T. E. *et al.* Disentangling Subpopulations in Single-Molecule FRET and ALEX Experiments with Photon Distribution Analysis. *Biophysical Journal* **102,** 1163–1173 (2012).
42. Yamashita, A., Maeda, K. & Maéda, Y. Crystal structure of CapZ: structural basis for actin filament barbed end capping. *EMBO J.* **22,** 1529–1538 (2003).
43. Casella, J. F., Maack, D. J. & Lin, S. Purification and initial characterization of a protein from skeletal muscle that caps the barbed ends of actin filaments. *Journal of Biological Chemistry* **261,** 10915–10921 (1986).
44. Greco, N. J. & Tor, Y. Synthesis and site-specific incorporation of a simple fluorescent pyrimidine. *Nat Protoc* **2,** 305–316 (2007).
45. Ottenheijm, C. A. C., Granzier, H. & Labeit, S. The Sarcomeric Protein Nebulin: Another Multifunctional Giant in Charge of Muscle Strength Optimization. *Front Physiol* **3,** 1–9 (2012).
46. Tskhovrebova, L. & Trinick, J. Roles of titin in the structure and elasticity of the sarcomere. *J. Biomed. Biotechnol.* **2010,** 612482–7 (2010).

VI. Abbreviations

A	adenine
ACF	auto-correlation function
AFM	atomic force microscopy
ATP	adenosine-triphosphate
BSA	bovine serum albumin
C	cytosine
CCF	cross-correlation function
DNA-PKcs	DNA-dependent protein kinase catalytic subunit
dsDNA	double-stranded deoxyribonucleic acid
ssDNA	single-stranded deoxyribonucleic acid
DSB	double-strand break
EGTA	ethylene glycol tetraacetic acid
FCS	fluorescence correlation spectroscopy
FRET	Förster resonance energy transfer
G	guanine
HABA	4'-hydroxyazobenzene-2-carboxylic acid
HR	homologous recombination
NA	numerical aperture
NHS	N-Hydroxy-succinimide
NHEJ	non-homologous end joining
PBS	phosphate buffered saline
PCA	3,4-dihydroxybenzoic acid
PCD	protocatechuate deoxygenase
PEG	(poly)ethylene glycol
PIE	pulsed interleaved excitation
RT	room temperature (usually 25° C)
SMPH	Succinimidyl 6-((beta-maleimidopropionamido)hexanoate
SPDP	succinimidyl 3-(2-pyridyldithio)propionate
T	thymine
T4 PNK	T4 polynucleotide kinase
TEM	transmission electron microscopy
TIRF-M	total internal reflection fluorescence microscopy
WF	wide-field
XLF	XRCC4-like factor
XRCC4	X-ray repair cross-complementing protein 4
2CDE	Two-Channel Kernel-Density Estimator

VII. Acknowledgments

First of all, I would like to thank Prof. Don C. Lamb for the great opportunity to write my master's thesis in his group.

I thank Prof. Hartschuh for agreeing to grade my thesis as a second corrector.

Next, I thank Dr. Alvaro Crevenna for his supervision and support and especially for the correction of my thesis.

A big thanks goes to the group of Prof. Tim Liedl and especially Dr. Mauricio Pilo-Pais, who introduced me to the assembly and purification of DNA origami structures. He also helped me a lot during the design process of the DNA origami two-layer sheet with gap.

I would like to thank the whole FAB lab group for the friendly and productive working atmosphere and for my nice birthday present (even if I am not a PhD student yet).

Further, I would like to thank my familiy and friends for their constant support, especially my sister Lara for her help in the lab that one day.

And last, but not least, I thank you, Anders, for everything.

VIII. Appendix

VIII.1. Annealing of ssDNA

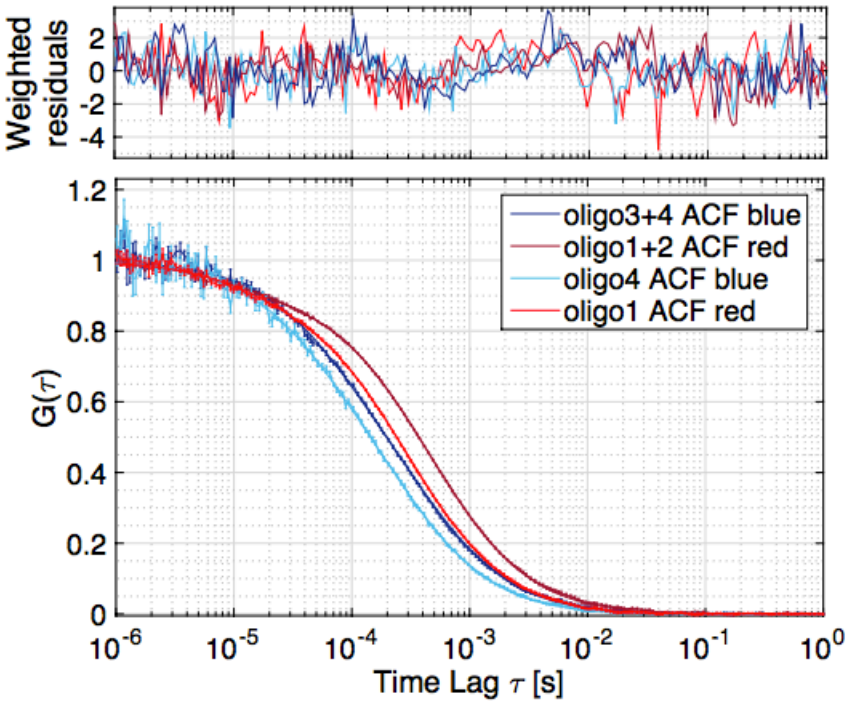

Figure A.1: DNA double-strands diffuse slower than Alexa488- (oligo 4) or Atto647N-labeled single strands (oligo1), as indicated by the respective autocorrelation functions

VIII.2. FRET data without 2CDE-filter

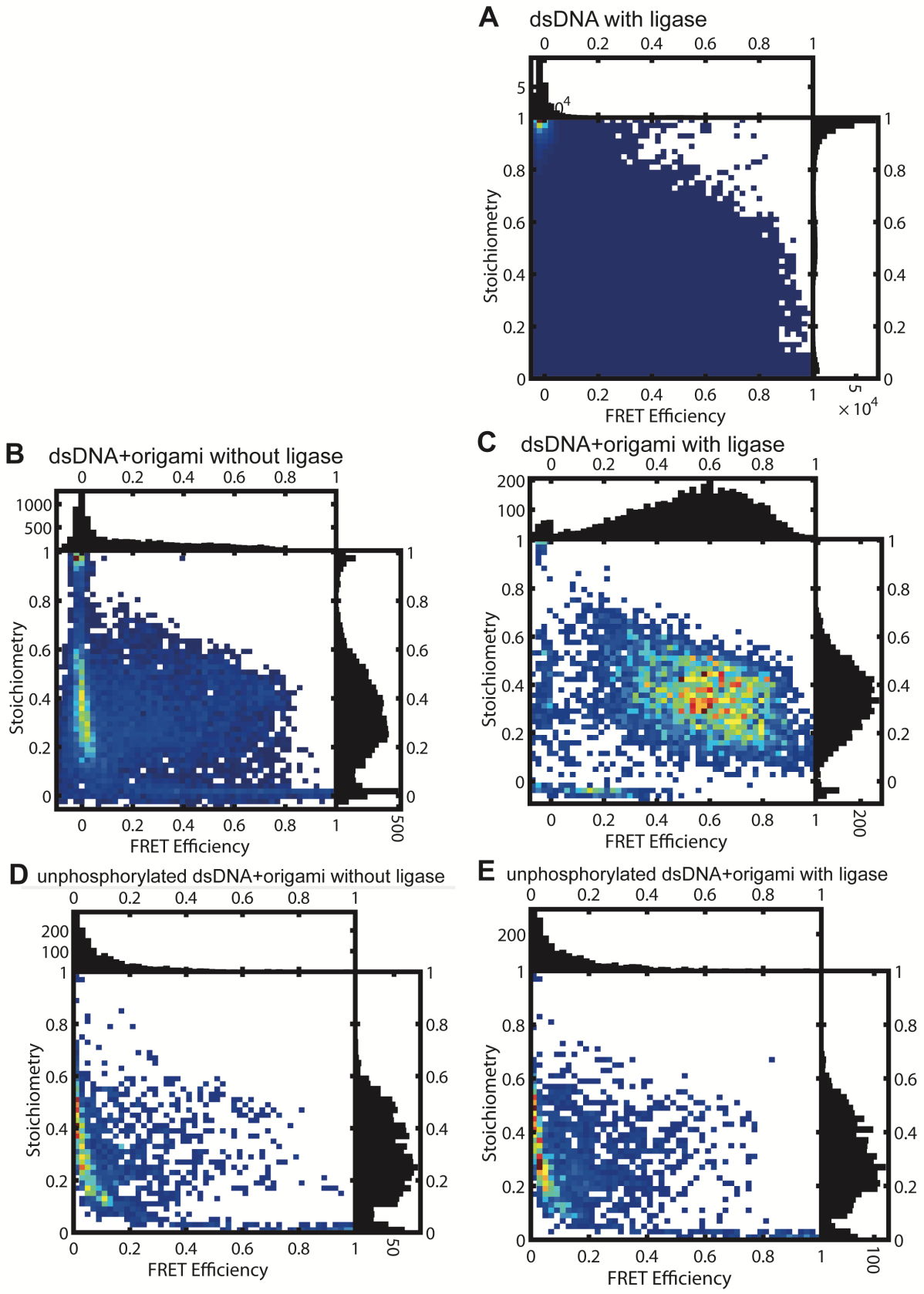

Figure A.2: 2D-histograms of stoichiometry versus FRET efficiency show donor- and acceptor species without the 2CDE-filter.

VIII.3. Lifetime and anisotropy plots

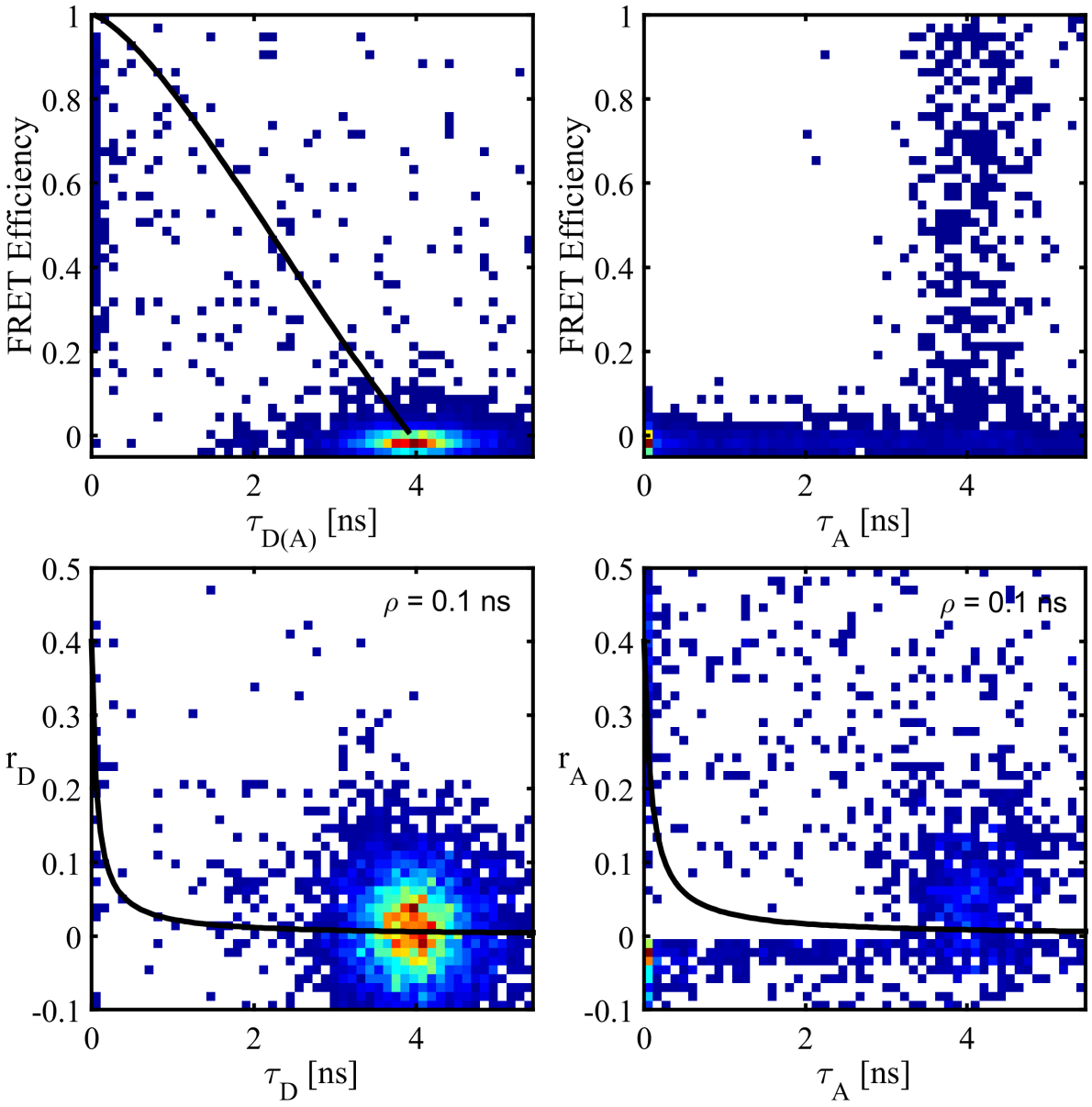

Figure A.3: Lifetime and anisotropy plots for dsDNA in solution. Top left: FRET efficiency versus donor lifetime. Top right: FRET efficiency versus acceptor lifetime. Bottom left: Anisotropy of the donor versus donor lifetime. Bottom right: Anisotropy of the acceptor versus acceptor lifetime.

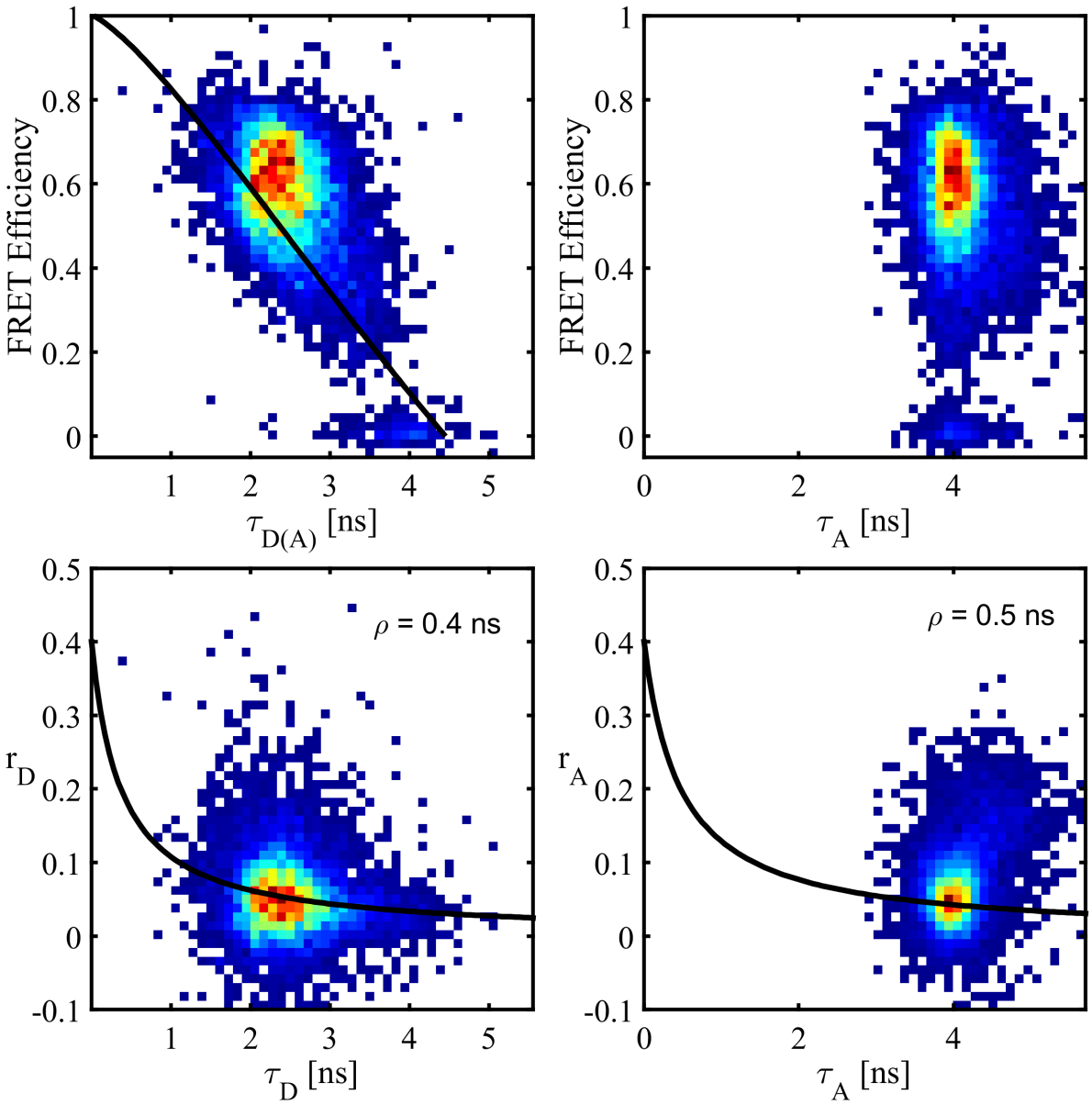

Figure A.4: Lifetime and anisotropy plots for dsDNA in the presence of the T4 DNA ligase. Top left: FRET efficiency versus donor lifetime. Top right: FRET efficiency versus acceptor lifetime. Bottom left: Anisotropy of the donor versus donor lifetime. Bottom right: Anisotropy of the acceptor versus acceptor lifetime.

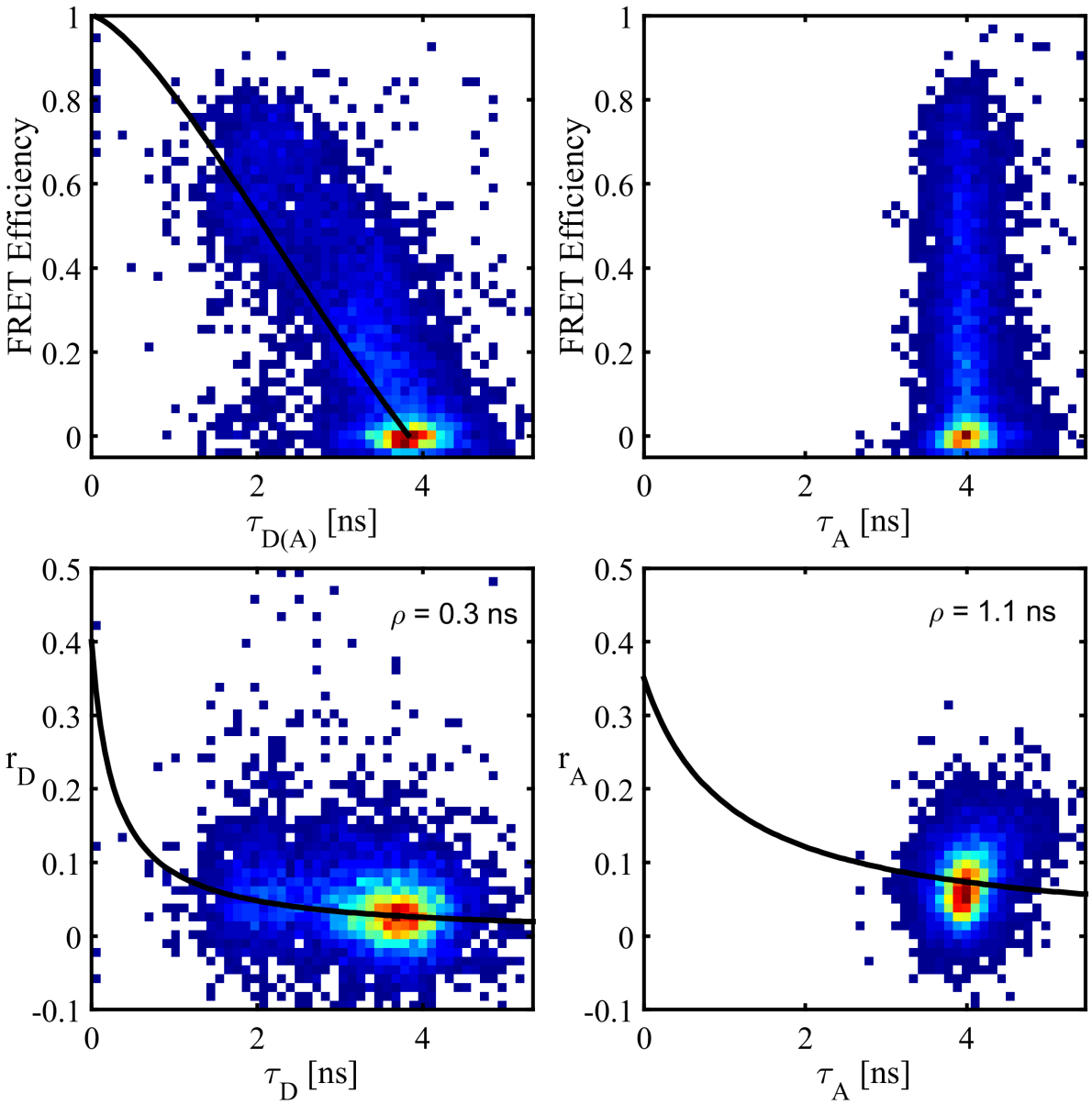

Figure A.5: Lifetime and anisotropy plots for dsDNA bound to the DNA origami. Top left: FRET efficiency versus donor lifetime. Top right: FRET efficiency versus acceptor lifetime. Bottom left: Anisotropy of the donor versus donor lifetime. Bottom right: Anisotropy of the acceptor versus acceptor lifetime.

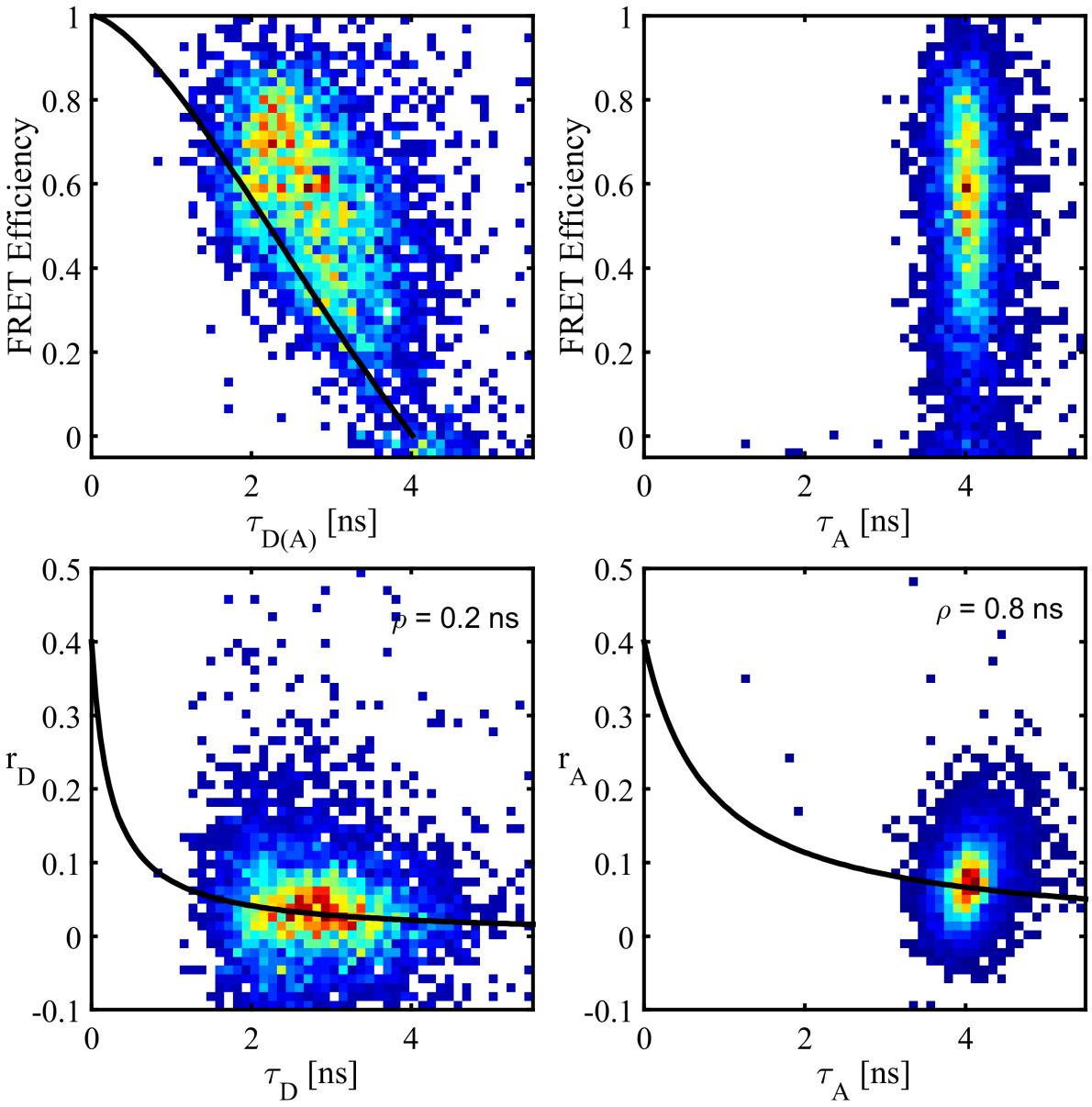

Figure A.6: Lifetime and anisotropy plots for dsDNA bound to the DNA origami in the presence of ligase. Top left: FRET efficiency versus donor lifetime. Top right: FRET efficiency versus acceptor lifetime. Bottom left: Anisotropy of the donor versus donor lifetime. Bottom right: Anisotropy of the acceptor versus acceptor lifetime.

VIII.4. Staple sequences for the DNA origamis

Table A.1: Overview of the staple strands used to assemble the DNA two-layer-sheet with gap (DNA DSB repair study).

Name	**Sequence 5'→3'**
Oligo 1	ATTGACCACCAGGAGGAAGGTTATCTAAAATATCTTGTAA
Oligo 2	GTGAGAAAGCAAAGAACGGAACAACATTATTACAGGTAGATCA
Oligo 3	ACATGATTAAGACGCTGAGAAGAGTCAATCCA
Oligo 4	GGCATCCGCTCACAATTCCCTTGAATCCG
Oligo 5	CAATATGAAGCATTAAATCAGTTGACCAGACG
Oligo 6	TAAAAAGAGAATCGATGAACATTGTATAGAAT
Oligo 7	AAATCAGTTCAGAAAACGAGAATGACCATAGACTGGATTT
Oligo 8	GCTGAAATCAGGTCTTTACCCTGACTATAGTT
Oligo 9	ATTGACAGGAGGTTGAGGCACAAA
Oligo 10	CCTAAATAAAGATAACGGATTCGCCTGAACCT
Oligo 11	GCTAAGCGAACACATCGGGCGAGGCATGATACATAACGCCAAACTGA
Oligo 12	AATCGATTATTCGCTCATGGAAATACAGAA
Oligo 13	CAACAAGAACCGAACTGACCAACTTTGAAAGAGGATATTAGACCAATTCGA
Oligo 14	ACAAAGCCCCCTTATTAGCGTTTGCCATGTGAATTAACCC
Oligo 15	AAGGTCAACAGTTTCAGCGG
Oligo 16	TGTAGCAAATCGGCCTCTTT
Oligo 17	TCAACGTCAGATAGTAACAGTACCTTTTCAGA
Oligo 18	TACATAAAACTATAAAAATTTTTAGAACAAAC
Oligo 19	TATAATGATGAATATAATCCTGATTGATCA
Oligo 20	AGGAACAGCCCTCATAGTTAGCGTAACGGTTGTGAAGACCTCCT
Oligo 21	AAAATGTTTAAATCAAAATATAATGCTG
Oligo 22	TAGGGCCCTGACCCGCGACCTGCTCCATGTTACTTAAAAGGCTCAAAAGG
Oligo 23	GAGTATAAGTATTTTTGTCGTCTTTCCATTTT
Oligo 24	ATCGACGGAGATTGAGATGGTTTAATTTGAT
Oligo 25	CCACCACCAATCCCTTATAAATCAAAAGAATAGCC
Oligo 26	AGAAATAATAAGAGCAAGAAACAATGAACGCCAGAAAAGGGATT
Oligo 27	CCGCACCGCCTGGCCCTGAGAGAGTTGCGCGGTTTGTCTGAATTAGAGGCTG
Oligo 28	GCAAGGAACCGCCTCCCTCAGAGCCGCCTACTGGTATCGG
Oligo 29	CCAGAACAACTTAACAACTAAAGGAATTTCCA
Oligo 30	CCATCTGTAAAGCCTGCAGTGCCCTAACGGGGTCAGTGCCGGT
Oligo 31	TTGCGCTAACGAGCGTCTTTCGGGAGGTATTC
Oligo 32	GTTTAATTTAGGATAAAGTACCGACAAAAGGTAAATAGGAGCAATTATCAT
Oligo 33	AGAGGAGGAAGCCCGAAAGACTTCAAATATCA
Oligo 34	TGACAATGGTCACCAGCCTCAGAACCGCCACCCCCC
Oligo 35	CAGAGTCCACGCTGGTTTGCCCCAGCACATTAATGTGGCTTTGAACCTAT
Oligo 36	TCGGTTCCTGTATTTTTTAACCAATAGGTTGT
Oligo 37	GAAGACTATATGTTACTAGA
Oligo 38	TAGGCTTTGCCCATAATACATTTGAGGATTTAGAAGCAGA
Oligo 39	TAACCTAATACGAATCTAATAGTAGTTATT
Oligo 40	TAAATAGCAACGGCTACAGACTGAGGCTCGGCGGATCGACGACA

Oligo 41	AATGGAAAAGAGGCGACAAGACAAGCGTTAAATAAGAATACTTA
Oligo 42	AATAGAACAATAATCGTTAGAACACCGAGTAAAAGAGT
Oligo 43	TCTTCCTGAACAATTACGCAGTATGTTAGCA
Oligo 44	ATGAAAATTGTTCAACGCGCGGGGAGAGAGCA
Oligo 45	GAGTGTTGTTCCAGTTAAATCGGATCACCGTCCAGCGCCA
Oligo 46	TTGGATAAAGCTTGACCATTAGATACATAATT
Oligo 47	CGAGAATCAAAATCACCGGAACCAGAG
Oligo 48	ACGATAAAAAGATTAATACCTTTAATTGCTCC
Oligo 49	TATAATCATAAGCCCAGGAAACCGAGGAAACGAATT
Oligo 50	GGGAGCTAAGAAAGGATGGTTTACACCGACTTGAGCCATTTCGG
Oligo 51	ATAACCGATGAGGGGATGACCGTAATGGGATA
Oligo 52	TTTTAACGCCAGGGTTCTAAGTGATCT
Oligo 53	TGGCGTCTTTAATGCGCGAAAGATAAAATTTC
Oligo 54	GCTTTAAAGATTATCAGGTCATTGCCTGAGAGTCTGGTCG
Oligo 55	ATCGATTATTCAGAATAATGGAAGGGTTACAA
Oligo 56	TATAACGTGCGCTAGGTTATTTTGGCAAAATCACCAGTAGGTCA
Oligo 57	CATAAGGGAAGGTGCCGTAAAGCACTTGGA
Oligo 58	GAATGAGATAACCCACAAGAATTGAGTGTGAGGCTCAGAGC
Oligo 59	ATTATGACCCTGATTCCCAATTCTGCGATTTT
Oligo 60	TGAACCTTCATCAAGAGTACAT
Oligo 61	CTACGTTAATATCCCCAAAAACAGGAAGGGTA
Oligo 62	TAAACCAGTGAGGATCCCCGGGTACCGATAAT
Oligo 63	TACCAACACCGCGAACCACCAGCAGACTGA
Oligo 64	GCAAAAGATATAGTCATTTTTGCGGATGGCT
Oligo 65	TTTTAGGTGAGGCGGAAAAATCTAACC
Oligo 66	CGACGATCGCACCGTCGGATTCTCCGTGGTCT
Oligo 67	CGAGAAAGCGAAAGGAGCGGGCTTTCCTAACG
Oligo 68	AAAAGCGATCGGAGGCAAAGCGCCATTCCTCA
Oligo 69	TAAATTGTGAGCAAACTGCAATGC
Oligo 70	TATTCTGCCTCAGAACGGCTGAGAATTGTCAACCTTA
Oligo 71	GGCCAACGAGGGGACTTTTTCATGAGGAGCCA
Oligo 72	AGTTAATGCTCAGAGCCGTCGGTGAAATAACCCCGCTTCT
Oligo 73	ACATAAATCCTGTGTGAAGTATTATACCGTTCCAGTAAGCCCCT
Oligo 74	TTTTAAATAATTCGCGGAACAAATGCA
Oligo 75	TTTTACGGGCAACAGCTGATTCTT
Oligo 76	AGTGAATATTGCTTTGATATATTTGGTTTGAAATACCGACCAAC
Oligo 77	GGCTTTGTATCATCGCCTGAAGGCAAAAAGCTTTT
Oligo 78	GGAATTGAGTAAGGGTGCCTGCGCTCACTGCCCGATCG
Oligo 79	CTGAGTAACTCAGAGCGAAGAAAAATCTACGTTAATAAAATAAG
Oligo 80	GGAATGCTCATTCAGTGAACGAA
Oligo 81	AATGTTACCAACCAGTTACAAAATAAACAAAC
Oligo 82	GGTCAGGACATCAATTCCTCGTTTAGATTTAGGAATACCAATCT
Oligo 83	GATGCAAATAGTGAATTTGAATTACCTTTTTT
Oligo 84	GAAACGGAAGCATAAAGTGTAAGCAACTCACC
Oligo 85	AGAAAACTAGCTTAAAATCAATATATGTG
Oligo 86	TTTTGCGATGGCCCACCCAT
Oligo 87	ATCCCCTAAAAACACGACCAGTAATACTGA
Oligo 88	TAGCGGTATTCTCTTAAATCAAGATTAGCCTG
Oligo 89	GATAGCCGAGGGCGACCGGGGAAAGGGAGCCC

Oligo 90	ACACTGATTAGCGCTACAGGGCGCGTCTGCGCGT
Oligo 91	ACCCCCATGTACCGTAACACTGAGTTTCTCCCGCCAGGCACGAA
Oligo 92	AATCTATTATAGGAACTCATTTTCAGGG
Oligo 93	ATCGCGAGAACAAGCAAGCCCATGTAGAAAATTTT
Oligo 94	ATCATAGGTCTGAGAGGTTA
Oligo 95	TGACCGTCAAATTTATCTAGCTGATAAATTAATGGGGA
Oligo 96	CCTTAAGTCAGAGGGTAATTATAGCAGCTGCTTTT
Oligo 97	CAATTTTTGTTTAGAGAATAACATAAAACTGA
Oligo 98	GAGCGCTACACGCAAACGAGCACG
Oligo 99	GGTTGGTGGCTCGAATGGATTAGGAAAGCCAGAATGGAAAGCCG
Oligo 100	GGGACAACCATCGCCCACGCTTGTATCGGGCTTTT
Oligo 101	TATTGCACTCATTAGGAATCATTACCGCGCTT
Oligo 102	TTTTTGGTAATATCCCTACATTTTAAT
Oligo 103	TTGGATGGTCATAGCTGTTTCATTTCTCACTC
Oligo 104	TAGCTCAACATGACGAGTAGATAG
Oligo 105	CTGTCCATATATCAGAACCCAAAAGAACTGGCGAAT
Oligo 106	CGTCTCATTATACCAGTCAGAGTAGTAAATTT
Oligo 107	CAACGTAGCGCGTTTTCATCGGCATTTTGGGAATGGGT
Oligo 108	ACACCAACCTAAAACGAAAGGGCTTTGACAATTTT
Oligo 109	AAGACAAAAACAAAGTGCCGATTATCCTGAGAAGTGTTTT
Oligo 110	AAAAAACCGCCACCCTCAGAGCCACCAGTCATACAAATC
Oligo 111	GTCAGAAGCAAAGCGGATTGCATCAAAAACC
Oligo 112	TATAGGGGCACACAACCTATTTCGTGATGATACAGGAGTGACCC
Oligo 113	CCACTACAAACTACAACGCCTGTAGCATTAGTGCTCGCATTTC
Oligo 114	TTCATCCTCATTATTAGCGG
Oligo 115	AAAGAGCCCGGAATAGGTGTCAAGAGAATCGT
Oligo 116	CAACTCGTAGGTTTAACTAATGCAAGTAAGAG
Oligo 117	TCTGAACGGTAATAGCAATAGTAAGCA
Oligo 118	AATCGCGCCAGGGTGGTTTTTGCCCTTCCAGC
Oligo 119	CCGATTTACTCACATTATTGACGGGATTGAGGGAG
Oligo 120	AAAATTGGGGCGAAATCATACAGGCAAGGGCC
Oligo 121	AGAAAGAATCGCGTCCAGACGACGACAA
Oligo 122	ATTCCATCCAATCGAGCTGAAAAGGTGGTTAG
Oligo 123	GACTGTCAAAGGGCGAAAAACCGTCTATCAGGTTTT
Oligo 124	TGAAAAGTGTAGCGGTCACGACTATGGTGACT
Oligo 125	TTTTAAATATTTAAAAACGCCATGGAC
Oligo 126	TTAGACAGATGATACCTTAAGAAAAGCTATCT
Oligo 127	CAACACTATCGCGTAAGCAAACTCCAACA
Oligo 128	AAGCAAGAACGCGAGGCGTTGTTTTTATCAGTTTT
Oligo 129	TAGCACGCAAAGACACCACGATGATTAATGCTTTGATTAACCGT
Oligo 130	AATTAAGGAGCGGAATTATCTTTGGATTAATCATAATAAATGCT
Oligo 131	ACCTTAATATCCAATAATCGGCTGTCTTCAAG
Oligo 132	ATTAAGAAACAAAATTGCGTAGATTTTCATTA
Oligo 133	TATTTAAAGCCACTAATGCAGAACGCGCAAGA
Oligo 134	AATCCATCCTAATTTACGAGTAAACAACAAGG
Oligo 135	TTCTTTTCAATTACCTGAGCAATTTCATTTATCAAA
Oligo 136	AAGTGCGCTGGCCCATCACCCAAATCAAACTC
Oligo 137	TTCTCATATTTAACAACGCCGT
Oligo 138	TTTTGATAATTTTCATTAGCGAGAGGCTTTT

Oligo 139	AAGTGTCCTTCCACAGGGTTTAGTACCGCCACAAAC
Oligo 140	ATAGGCCCTTTGACAGTGCGCCCTGGAGTGAC
Oligo 141	AAACGAAGGCACTAAAACACTCATCTTTAAAG
Oligo 142	AAATAATTGCGTTAATGAGTGAGCTAAGAGCTTGAATTCAACCAAATTATT
Oligo 143	CTAATTAGCAAAACCTGTTTAGCTATAGAG
Oligo 144	TCAGTCCTGTTTGATGGTGGTTCCGAACTTTCCAGATAAGTTTGTATAAAC
Oligo 145	AATCCTGGCTGACGGTGTACAGACCAGGCCAGTAATGTCAATAGGAACGTTA
Oligo 146	TAAAGCCGGCGAACGTGGCGAACAGGAGTACC
Oligo 147	TTTGCGGAAGAACCTATAAATAAGAGAACGCG
Oligo 148	TTGCTGGTCAATAATTAAGCAATAAAGCTGTG
Oligo 149	TTTTGCATCACCTTGACAGTTGAATGT
Oligo 150	AGACTCCTATCACCGTCGAACTCTTTCATGCGCACGACTT
Oligo 151	TCATGAGTCCACTATTAAAGAACGTGGGTTTTTTGTAGAGCCATCACAATC
Oligo 152	AAAACAAATATAGCCAGCAGCAAATGTCAG
Oligo 153	ACCGGATATTCATTACCCAAAAAG
Oligo 154	TCAGACGCTCAACAGTAGGGAACACCGGATAC
Oligo 155	TTAATTTTAAAACAGAAATTTAATTAGTTAATTTCATCTTAGGA
Oligo 156	GGAGAACAAAGCCGAGGCGCAGACGGTCAATCATAACCGGAGAGATCACCAT
Oligo 157	GTATCGGCGCCATTCAGTTT
Oligo 158	TTAGCGAAGGCTATTACAACAGAGATAGAACCC
Oligo 159	GGAAAATGACAAGTTAAAGGCCGCTTTTAGCA
Oligo 160	ACAGAACGTCAAAAATGAAACCAGAGCCTGATTTT
Oligo 161	TACCGAACAAGCCCATACGCTCGGCCCTG
Oligo 162	TTTTTGCGCAACTGTTTAAGTTGTAGA
Oligo 163	ACGTACAGTCAAGGTAGCTATTTTTGAGAGATCTACGCC
Oligo 164	AAGGAAAGGCTCGCTTGCTTTCGAGGTGGCGC
Oligo 165	TCAAAATACCAAAATTATTTGCACGTAAAA
Oligo 166	GATTATTACCGAGAAGAACTCAAACTTACT
Oligo 167	TTAGAGCCAAGAGAATCAGAGGCATTTTCGAGCGCA
Oligo 168	ATGTGAGTAACCTAACAACTAATAGA
Oligo 169	AGCGGCCGCCACCAGAACCACCACCAGAGCGCAGTCCGTA
Oligo 170	TAGAGCTTTTCGCAAACAGAGGGGGTAATAGT
Oligo 171	ATCACAAAAGGAGCCTTTAAAGTGAGAAGGTTTTT
Oligo 172	CTGCATACGAGCCCTGTCGTGCCAGCTGGGCG
Oligo 173	GTGACCATATCAAGTTACAAAATCGCGCCAGT
Oligo 174	TTTTCGCTCAATCGTAAAGGGACTTTG
Oligo 175	AGTTAAATCGGTTGTACCAACCTCATATATTG
Oligo 176	CCGGTTTAATTCGAGCTTCAATTAATTAATTTTCCCTCTGTAAATCGTC
Oligo 177	GCTATCACGACGATGTGCTGCAAGGCGATGGG
Oligo 178	CATTAAAGCTTTTCATATAGGGTT
Oligo 179	AAATGAGAAACACCAGAACGGACG
Oligo 180	TAGCGACAGAATCAAGTTTGCCTTTAGCCACCATTATACG
Oligo 181	TGCTTTAGAATCCTTGAAAACATAGCGATTTT
Endcap 1	TTTTACATACATAAAGGTGGCAAACGTAGAAAATTTTT
Endcap 2	TTTTGCCACGCTGAGCAAACCCTCAATTTT
Endcap 3	TTTTTCAGCAGCGAAAGACGCGGGATCGTCACCCTTTT
Endcap 4	TTTTTTCATTCCATATAACAGTTGTAATACTTTTGCGGGAGAAGTTTT
Endcap 5	TTTTATAGCAGCACCGTAACCAATGAAACCATCGTTTT

Endcap 6	TTTTAGATAAGTCCTGAACCTGTTTATCAACAATTTTT
Endcap 7	TTTTGGTAAAATACGTAATAGTTTCCATTAAACGTTTT
Endcap 8	TTTTAACAGGAAAAATACATTGGCAGTTTT
Endcap 9	TTTTCCCAATCCAAATAAGAGCCATATTATTTATTTTT
Endcap 10	TTTTTAAGTGCCGTCGAGATCAGTACCAGGCGGATTTT
Endcap 11	TTTTATTTTCTGTATGGGAGACGTTAGTAAATGATTTT
Endcap 12	TTTTATTCACCAGTCCATCGCCATTATTTT
Endcap 13	TTTTGCTTAATGCGCTAATAACATCATTTT
Endcap 14	TTTTAGAAAACAAAATTAATTACATTTAACAAAA
Endcap 15	TTTTCAGCTACAATTTTATTTGCTATTTTGCACCTTTT
Endcap 16	TTTTTCAATATCTGGATCAGATGATGTTTT
Endcap 17	TTTTTTCACGTTGAAAATCGCGAATAATAATTTTTTTT
Endcap 18	TTTTAATCAGATATAGAAGGCCCAATAGCAAGCATTTT
Endcap 19	TTTTGAATCCCCCTCAAATTCATAAATATTCATTTTTT
Endcap 20	TTTTAGACGGGAGAATTAAACAGGGAAGCGCATTTTTT
Endcap 21	AACCACCACACCCGCCGCTTTT
Endcap 22	TTTTAATGTGAGCGAGTAACAACCTCCAGCCAGCTTTCCGGCACTTTT
Endcap 23	TTTTTGAATTACCTTATGCCAACTTTAATCATTGTTTT
Endcap 24	TTTTGAACGGGTATTAAACTCCTTATCATTCCAATTTT
Endcap 25	TTTTCGTTATACAAATTCTGTTTAGTATCATATGTTTT
Endcap 26	TTTTGCAATTCATCAAACAAACATCATTTT
Endcap 27	TTTTATTTTTGTTAAATCAGCTCAGCCAGCTTTCATCAACATTATTTT
Endcap 28	TTTTCGCTTCTGGTGCCGGAAACCTGCGGGCCTCTTCGCTATTATTTT
Endcap 29	TTTTTACCAAGCGCGAAACGACCCCCAGCGATTATTTT
Endcap 30	TTTTCTTGCCTGAGTCCAGCCATTGCTTTT
Endcap 31	TTTTTTGATACCGATAGTTAATTTCTTAAACAGCTTTT
Endcap 32	TTTTCTTGATATTCACAAAGGTCAGACGATTGGCTTTT
Endcap 33	TTTTCCTTTATTTCAACGCAAGGAGCATGTCAATCATATGTACCTTTT
Endcap 34	TTTTAAAATACCGAACCTGCAACAGTTTTT
Endcap 35	TAAAATGCAACTAAAGTACGGTGTCTGGAAGTTTTT
Endcap 36	TTTTCGCCAGCTGGCGAAAGGGGGTTGTAAAACGACGGCCAGTGTTTT
Endcap 37	TTTTTCCGGCTTAGGTTGGACTACCTTTTTAACCTTTT
Endcap 38	TTTTCCAAGCTTTCTCAGGAGAAGCTTAAGCTACGTGGTGCTTGTTTT
Endcap 39	TTTTTTACCTCGATAAAGACGGAG
Endcap 40	TTTTCCGGTTGATAATCAGAAAAGTTTGTTAAAATTCGCATTAATTTT
Filler_Biotin 1	ACATATAAAAGAAAAGGCCGGAAACGTCATCAG
Filler_Biotin 2	AAAAGCCTTACCAGTACCTGATTTCAGTTGGCAAATCACTGA
Filler_Biotin 3	TTTAAGAACTGGCCAATACTGCGGAATCGGCTT
Filler_Biotin 4	GGTTTTGCGGGTTGATAAACAGGGCCAGGGTGGATGTTCTTTTC
Biotin 1	Biotin-TTTTT-ACATATAAAAGAAAAGGCCGGAAACGTCATCAG
Biotin 2	Biotin-TTTTT-AAAAGCCTTACCAGTACCTGATTTCAGTTGGCAAATCACTGA
Biotin 3	Biotin-TTTTT-TTTAAGAACTGGCCAATACTGCGGAATCGGCTT
Biotin 4	Biotin-TTTTT-GGTTTTGCGGGTTGATAAACAGGGCCAGGGTGGATGTTCTTTTC

Table A.2: Overview of the staple strands used to assemble the DNA two-layer-sheet (sarcomere project).

Name	**Sequence 5'→3'**
Core staple 1	ACGTGGCGGGAAGAAATGAGAATATGTACCGT
Core staple 2	CCGATTTACTGGCAAGTTGCTAAAAAACTACA
Core staple 3	AAGCACTACCACCACAACGTTAGTGCCCTCAT
Core staple 4	CAAATCAAAAAATCCCGACAGCATCGGAAAGT
Core staple 5	ATCAGCGATAGATAGGGTTTTGCGGAAGACTTT
Core staple 6	CTAGGGCGGAGCTTGAAAAATCTCCAAAAAAA
Core staple 7	AATCGGCGTTTTTTGCGAGGTGAATTTCTTA
Core staple 8	ATAGCCCGGGCCCACTATAGTTGCGCCGACAA
Core staple 9	GGGAGCTAGAACGGTATCAGAGCCAGGCTGAG
Core staple 10	GTATAACGTATAATCACCTCAGAATAGCGGGG
Core staple 11	GGGCGCGTCTGTCCATTCACCGTAAGTGCCGT
Core staple 12	ATCCTGTTCAACGCGCTTTGACCCCCAGCATA
Core staple 13	GGTCCACGGGCGCCAGAGAGGCAATTGTATCA
Core staple 14	AGTGTTTTTGCTTTCCACCAGTACCAACTTTC
Core staple 15	AAAAGAGTACTATGGTCACAGACAAAATGAAT
Core staple 16	AATCGGCTGATGGTGTAACGAGGGTAGCAAC
Core staple 17	GCGTATTGCTGGTTTGGAGGACTAGATCGTCA
Core staple 18	GTAATATCGAAAAACGGCCCCCTGTTGATATT
Core staple 19	GAGTAGAACGCTCAATCTTGAGTAAGCCAGAA
Core staple 20	CTTCTTTGTGGCAGATTACTGGTAACCGTTCC
Core staple 21	CTGTCGTGTAGCTGTTGAAAGAGGACAGATTT
Core staple 22	GCGCTCACTCACAATTCAATCATACCTTCATC
Core staple 23	CATTTTGAGAACTCAAATTAGGATCCGCCACC
Core staple 24	ATTTACATATTAGTAAGGCGGATACTCAGGAG
Core staple 25	ATGGTCACCAGCTGCAGTGATTATACCAAGC
Core staple 26	TTATCCGCTGCCCGCTACGGAGATAAGAATAC
Core staple 27	TTCTGACCACCGAACGCACCCTCATATTAGCG
Core staple 28	AGGGACATGAGGTGAGCCACCCTCATCACCGG
Core staple 29	TGTTACCTGGCTGACGTAAGGCTTGAATTACC
Core staple 30	ATAAAACATCTGGCCACTGAATTTATAAGTTT
Core staple 31	CAACTCGCTCGAATTGGCTGAACGGTGTACA
Core staple 32	CTTGAATCCGATAAAGCTGGCTGAAGGGAACC
Core staple 33	GTTATCTAAAGCATCAAGCCCCCTGAGCCGCC
Core staple 34	ACTAATAGCGCTGAGATAATCAAAAGAACCGC
Core staple 35	GAAGCCACCTGCCATGGAGGCTTGAGATGGT
Core staple 36	TGTGAATTTGGAGTGAATCATTGTGCCCTGAC
Core staple 37	TTAATTTTCAAAGAAAATAGAAAACCAGAAGG
Core staple 38	CAACTCGTTCATATTCCACCACGGGGAATACC
Core staple 39	TTAGAAGTCATCAATAAAGGTGGCCTCCTTAT
Core staple 40	GTTTTCCCAAGGGCGAACCAAAATATACTGCG
Core staple 41	GAAATTGCACAGTAACCTTACCGACCTTTACA
Core staple 42	TCAAAATTAATAACGGAGAGCAAGAGCGCATT
Core staple 43	CTGAATAACAAGTTACACCCACAACCTGAACA
Core staple 44	GCTTCTGGTTCTCCGTATAGTCAGAAGCACGC

Core staple 45	AAGATCGCTAATGGGAAATCAAAAAAAGACTT
Core staple 46	CGTCGGATGCCGGAAAAAGGGTAATAGTAAA
Core staple 47	AACAAACATGCTTCTGTTACAAAAGGTTTTGA
Core staple 48	CTGGCCTTGTTAATATGAGAGTACTAGCTCAA
Core staple 49	AATAACCTTCAAGAAAAACAGGGAAAACAATG
Core staple 50	AATTAATTACCTGAGCCTGAACACGAATTGAG
Core staple 51	ACAGGAAGAGCGAGTGAGAAGCGGATTGCAT
Core staple 52	TTGTAAACCCTGTAGCGAAGCCCGATCAGGTC
Core staple 53	CTTTTTAAGTAAATGCATAGCAAGGTCCTGAA
Core staple 54	AATTTATCAAGAACGCTATTTTCAATTTACGA
Core staple 55	TAGATTAATTAGTTAACCGCACTCCGGCTGTC
Core staple 56	TGATAATCCGTTCTAGGATACATTTCGCAACG
Core staple 57	AACTAGCGTAGCTATCTGCGAACGGGCGCGA
Core staple 58	GCAAGACAAAAATCATTTGCGGGATAAACAGC
Core staple 59	AATATATTGACGCTGATTAGTTGCCTTTCCAG
Core staple 60	ATTCAACAGAAAAGCATCGGATGGCTTAGAG
Core staple 61	CGGAGAGGATGTCAATTAATGCTGCTTTAATT
Core staple 62	TACTAGAAATTCTTACACAACATGTTCAGCTA
Core staple 63	CGTTAAATTAGGGCTTGTAAAGTAATTCTGTC
Core staple 64	TTTGAAAAACGCCAAGTAATAAGAGAATATA
Core staple 65	AGTCAAATACCAAAAAAGAGCATA
Core staple 66	AGATTCAGCGGGAGAAAGAATTAGCAAAATTA
Core staple 67	CTCAACAGAAGAATAACCATCCTATCGTAGGA
Core staple 68	TTTAGGCAGTCGGTTGTCACCATCAAGAAATGG
Core staple 69	ATACTTTTAAAGGGTGTTCATTTGGAGTAGAT
Core staple 70	CAGACGACATAATATCACACCGGAATCCAATC
Core staple 71	AAGCTAAAAGGCATTTTCATTCCAATACCTAAATTTAATGG
Core staple 72	AGCAATAGCTATATTAGAAAGGTTAATGC
Core staple 73	CCAATAAATCATACAGGGTGGCATGAGTAATGGATCTACA
Core staple 74	CAAGAAAAGACAATAACAGTATAAAGCCAACG
Core staple 75	GCATGTAACAAAAGAATTGAGAATCGCCA
Core staple 76	TTTCCTTATCGAGCCACATGTAA
Core staple 77	TCAATAACCTGTTTAAAGCCTCCATTATGACCCTGTA
Core staple 78	GCTGAAAAGCAAGGCAAGCCTTTATTTCAACG
Core staple 79	ATCATTACCTCCCGACAGGTCTGATGTGAGTG
Core staple 80	CAAGCAAGAATCAAGAGAAGAGTCGCTATT
Core staple 81	GGTATTAAACAATTTTCCCCATAGCGATAGCT
Core staple 82	TTAGTTTGGCTGAATACATATGTATTTAAA
Core staple 83	CAGTTGATAAATATGCATGAACGGAATTCGCA
Core staple 84	TAGCGAACCGCGCCCATGATGCAAATCATAAT
Core staple 85	AGCCTTACCGTTTTGAGAAAACAAATAAGG
Core staple 86	ACCCAGCTACCAAGTATTTCATCTTCTGATGAT
Core staple 87	CATGTTTTTCCCAATTTTTTGAGATGTAGGTAA
Core staple 88	CATATTATAACATAAAACAAAATTTTACATCG
Core staple 89	AGCCTAATAGAATTAAAAAAGAAGATTGCT
Core staple 90	AATCTTACGGGTAATTAACGGCGAATTATTCA
Core staple 91	GCTCCTTTATTAAGAGCAGCTTTACGGCGG
Core staple 92	CAACAGGTGCGTTTTACAAAAATAGTTGGTGT
Core staple 93	AGACGGGTTGCCAGTAAATCGTCAATAGTG

Core staple 94	AAGTCAGACAACGCTAGAATCCTTGAAAAAAAA
Core staple 95	CAAATATCCAGGATTATTTGTTAATAATCGTAA
Core staple 96	TAATATCAATGTTAGCACCTTGGATTATACTT
Core staple 97	AAACCGAGATAGCTATAGTACCTTAATTACAT
Core staple 98	CAAAAGAAATAATAATTCGCCTGATGATGA
Core staple 99	TACGCAGTGAGAGATAAAAATCGCGCAGAAACC
Core staple 100	ATGTTTAGACTATTGGGAACAACATCAACA
Core staple 101	GAATCGTCTGACCATATAGGTCACATTCGCGT
Core staple 102	GAGGGAGGCACAATCACCACCAGAGAAATAAA
Core staple 103	TTCATTAGCAAAGACTGATTATCTACCATA
Core staple 104	ATACCACAAAAGAAATTCAGGCCCGGCACC
Core staple 105	GCCAAAAGCGATAAAATCGGTGCGGCCTCAGG
Core staple 106	ATCGATAGTCGGTCATCCTTGCTGCATCGCCA
Core staple 107	TAGCAAGGTCTTTTCAGCCAGCAGCAGAAG
Core staple 108	GCCAGCAACCACCACCCTGACACCGCCTGCAA
Core staple 109	CATTATTACAACTTTACTCTATGTAGGGGC
Core staple 110	ATCTACGTTTTTAAGACTTCTAATATAAATCA
Core staple 111	ACCAGAACAATAAATCTAAGAATAAATACCTA
Core staple 112	CACCCTCACGCAGTCTACAGAGAATGGATT
Core staple 113	GCCTCCCTTCATACATCGTGACCAGTAATAAA
Core staple 114	GAGAAACACGCATAGGACGGAGGGAAATTG
Core staple 115	CTGCTCATTCTTGACATAAGCTACCATACGAG
Core staple 116	TGGAAAGGAGCCACAACCACCAGCAAATGA
Core staple 117	AGTAAGCGCAGAGCCGGCGGTCAGTATTATAAG
Core staple 118	AAGAGTAATCAGTGAACATTTCACCTATTTAC
Core staple 119	CGTATAAAAGAGAAGGACTATCGGTCCTGAGA
Core staple 120	TAACGGGGCAGTACCATAACATCACCGAGT
Core staple 121	TGATGATATTGATATAATTCGTTGTAGCAATA
Core staple 122	GAACTGACAAAGTACATTCCAGTGCGGTTT
Core staple 123	ACGAGGCGTAAATTGTTCACATTATTCTTTTC
Core staple 124	ACTCCTCACAGTTAATCTCATGGACGTGGCAC
Core staple 125	TTTTGCTTCAGTGCCGTCTGAATAGAACCC
Core staple 126	CGAGAGGGCAGGAGTGTCACCAGTCACACAATC
Core staple 127	GCGAAACCAACTTTTCCTGTGTATCCCCGG
Core staple 128	TCGCCTGACAGACGGTCCACACAAGTGGTGCT
Core staple 129	CTCAGAACGTTTCGTCTCGTTAGAAGCGGGCG
Core staple 130	GTTTAGTATAGCATTCTGCTTTGTCACGCT
Core staple 131	GCCCGGAATAACGATCGTTATGCGCCGCTACA
Core staple 132	ACTAAAACGAGGCTTTCCCCAGCCAAAAGA
Core staple 133	ACCAACCTGAAGTTTCGAGAGTTGTGTTCCAG
Core staple 134	AACACTGACGCCACCCCGCCAGAACCTTGCTG
Core staple 135	ACGCCTGCCGCCACGTGAGGCCACTTGCCT
Core staple 136	AGTTAGCGTAGGTGTACACGCAAATTAACAATG
Core staple 137	GGCTACAACTCATCGGGGAGAGCGGGAAAC
Core staple 138	TTCATGAGAAAACGAAGGTGGTTTATTGCGTT
Core staple 139	AACAGTTTTCACGTTGCGGGGAAAGCCGGCGA
Core staple 140	TTTGTCGTCTTGCTTTGGGTCGAGGTGCCGTA
Core staple 141	CCCTCAGCTGATACCGACGTGAACCATCACC
Core staple 142	GGGAGTTAACCATCGCGGCGAAAAACCGTCT

Core staple 143	GCGAATAATAATTTTTCAGCGGAGGCGAAAGGATCAGAGC
Core staple 144	AGGCTCCTGGGATTTGTAGCGGACGAGCAC
Core staple 145	TTTATCAGCTTTCCAGCCCGCCGCGCTTACCGA
Core staple 146	AACAGCTAGCGAAATTATAAATAGGCGAAA
Core staple 147	TGACAACAAAGGCCGCTTGAGTGTCAGCAAGC
Core staple 148	ATATCAAAAACAGTTGTAATCAGTAACCGATT
Core staple 149	AATTATCAATTAAATCATATTGACATGAAACC
Core staple 150	GGAGAAACATTTGCACATAATAACAATAAGTT
Core staple 151	AAAATCTAAAATATCTCGTCACCAGGAAATTA
Core staple 152	TGGCAATTATTAGACTTTATCACCATTACCAT
Core staple 153	TTGAATACTGGAAGGGGATTAAGAAACATATA
Core staple 154	CAGTGCCAATTAGAGCGTAGCACCGTCACCGA
Core staple 155	AGTGCGGCGGGTGGATAAAGATTCATCAGAGA
Core staple 156	GCCAGTGCCATTCGCCGTTTTGCCAGAGGCGT
Core staple 157	AAAGCGCCAAGCTTTATTTTGAGATTTAGGA
Core staple 158	CTGTTGGGAGTCACGAAATGCAGACGGAACAA
Core staple 159	ATTGACCGACTCCAGCAGCGTCCAAGCGAGAG
Core staple 160	GCTCGCCCCATGCGCACGAACTAATACATAAC
Core staple 161	CGCTATTAGCGATTAAAGGCATAGGAAGAAAA
Core staple 162	AGATGGGCGACGACGATCATTGAACTCGTTTA
Core staple 163	AAATAGCAGAAACGCAGTAAAACAAGGAGCGG
Core staple 164	TATTTTGTGAAGGTAACTTTGCCCTGAGGAAG
Core staple 165	CGGCATTTCAGCACCGAAAGGAATGAACGTTA
Core staple 166	TTAAGCCCACTGGCATTTAGAACCAGATGA
Core staple 167	AAAGAAACAAGGTGAATTACAAAACTAACA
Core staple 168	AGAAAATAATTTGGGACTCTACATTTGAGGAT
Core staple 169	CTTGAGCCCATACATATAATCCTGATTGTAGGC
Core staple 170	AACCAGAGAATCACCACGTCAATAGATAAAGGA
Core staple 171	TTTACCCTGACTGGATCAGCTTTTGCGCAA
Core staple 172	GCTTTTGCATTCAACTCGTTGTAAAGTGGT
Core staple 173	TTAATTTCAGGTAGGTTCTTCTAAACGACG
Core staple 174	AACGAGAAATAAATATCAGTATCGGGCCTCTT
Core staple 175	CCAGACGAGAATTACGGTTGGGTAGTGTCCTT
Core staple 176	TTATGCGATAATAAAACGACTTAAACGCCAGG
Core staple 177	TTTGGAACCGTCAAAGCCACGCAT
Core staple 178	ACCAGTGAGGCCCTGACATTAAACGGCTTGCA
Core staple 179	CCGGAAGCGAGCTAACGTCGAAATACGAAGGC
Core staple 180	TTTCTCCGACAGGGCTAGAACCGGTAGCCGGA
Core staple 181	AGTGCTGATAACCCCGACTGGCTCTAACAAAG
Core staple 182	TTAAATTTAACGCCATATTCGAGCGTTCAGAA
Core staple 183	AAGGCTATGAGAATCGAACTAAAGGCAAACTC
Core staple 184	CAAGGATACAATGCCTCAATTCTACCATATAA
Cy5 staple 1	Cy5-TTTTTTTAAAAATTGAAAGCGCTCATTAAACAGTGCC
Cy5 staple 2	Cy5-TTTTTTTTCAATTTTCCCTTAACGAGCGTTATTTTGC
Cy5 staple 3	Cy5-TTTTTCTTAATTACCATTACTGATAAACCGGAGAC
Cy5 staple 4	Cy5-TTTTTTTTGCCACCGGAAATTAGGAGCCAATTCGA

Biotin/ACC_5 staple 1	Biotin-TTTTT- or $(ACC)_5$-GCGCGTAAAATCGGAACCTTTAATTGTATCGG
Biotin/ACC_5 staple 2	Biotin-TTTTT- or $(ACC)_5$-AGACAATAACTGATAGGAGCCGCCGTTTTCAT
Biotin/ACC_5 staple 3	Biotin-TTTTT- or $(ACC)_5$-GTACCGAGTCGGTGGGGAGTAGTAAATTGACC
Biotin/ACC_5 staple 4	Biotin-TTTTT- or $(ACC)_5$-TTAACAATTACATAAAATCCAAATAGGCGTTT
Biotin/ACC_5 staple 5	Biotin-TTTTT- or $(ACC)_5$-TTAAATGTGATTGTATAGGTCATTTTTGCCTG
Biotin/ACC_5 staple 6	Biotin-TTTTT- or $(ACC)_5$-TATTTAACTACCGACCTCAATAATATCGAGAA
Biotin/ACC_5 staple 7	Biotin-TTTTT- or $(ACC)_5$-AAGTACCGGAAACCAAGTGTGATTTTTTCA
Biotin/ACC_5 staple 8	Biotin-TTTTT- or $(ACC)_5$-GAGAGAATTTATCCCATCAATATAGAGACTAC
Biotin/ACC_5 staple 9	Biotin-TTTTT- or $(ACC)_5$-CAAAAAGTGATAAGAAGCAAATACCCCGGT
Biotin/ACC_5 staple 10	Biotin-TTTTT- or $(ACC)_5$-CACAAACACACCACCACCCTAAAAAACCTCAA
Biotin/ACC_5 staple 11	Biotin-TTTTT- or $(ACC)_5$-GACCAGGCCAGAACCACGAATAATACCGAC
Biotin/ACC_5 staple 12	Biotin-TTTTT- or $(ACC)_5$-TTTCTGTAAAAAGGAGCCCTAAAGGGAGCCC
Endcap 1	TTTTAAAGACAAAAGGGCGACATTCAGCGACAGAATCAAGTTTGCCTTTT
Endcap 2	TTTTGGGGATGTGCTGCAAGCGCCAGCTGGCGAAAGTTTT
Endcap 3	TTTTTTTTTAATGGAAACAGTTCATTTGAATTACCTTTTT
Endcap 4	TTTTTTATCATTTTGCGGAAAAAAGTTTGAGTAACATTTT
Endcap 5	TTTTAGGCAGGTCAGACGATTGGCCCCTATTTCGGAACCTATTATTTTTT
Endcap 6	TTTTAGAACGTGGACTCCAAAAGAGTCCACTATTAATTTT
Endcap 7	TTTTCCAGACCGGAATACGGTGTCTGTTTT
Endcap 8	TTTTTTTAGCGTCAGACTGTAGCGCGCCAGCATTGACAGGAGGTTGTTTT
Endcap 9	TTTTCAATGTCCCGCCAAAAATTGTCAACCTTATGATTTT
Endcap 10	TTTTTCGGTCGCTGAGGGTAAAATACTTTT
Endcap 11	TTTTGGGGTGCCTAATGAGTATAAAGTGTAAAGCCTTTTT
Endcap 12	TTTTTTGCCCTTCACCGCCTGACGGGCAACAGCTGATTTT
Endcap 13	TTTTCTGAAACATGAAAGTATTAAGACCACCCTCATTTTCAGGGATTTTT
Endcap 14	TTTTGTAATGCCACTCCGCGACCTGCTTTT
Endcap 15	TTTTCTGTTTATCAACAATAGATAACAAATCAGATATAGAAGGCTTTTTT
Endcap 16	TTTTCAGGACGTTGGTAAGAGCAACATTTT
Endcap 17	TTTTCCAAATCAACGATTATACCAGTTTTT
Endcap 18	TTTTTTGGTGTAATGAGTAAAACTCTGACCTCCTGGTTTT
Endcap 19	TTTTTCATATATTTTAAATGAAAATTTTTAGAACCCTTTT
Endcap 20	TTTTATCCGGTATTCTAAGAACGCGAAGAAACGATTTTTTGTTTAATTTT
Endcap 21	TTTTAACGTCAGATGAATATGTAGATTTTCAGGTTTTTTT
Endcap 22	TTTTTCTGCCAGTTTGAGGGGCATCGTAACCGTGCATTTT
Endcap 23	TTTTAGCAAGCCCAATAGGAACCCA
Endcap 24	TTTTCGTCAAAAATGAAAATAGCAGAGCCCTTTTTAAGAAAAGTAATTTT

Endcap 25	TTTTTCCATGTTACTATATTCATTACTTTT
Endcap 26	TTTTAGTCTGGAGCAAACAACAGGTCATTGCCTGAGTTTT
Endcap 27	TTTTGGTCAGTTGGCAAATCCCCTCAATCAATATCTTTTT
Endcap 28	TTTTTTTTTTAACCAATAGGTTGTTAAATCAGCTCATTTT
Endcap 29	TTTTAGTCTTTAATGCGCGATTTTTGAATGGCTATTTTTT
Endcap 30	TTTTCTATCATAACCTCCCCCTCAAATTTT
Endcap 31	TTTTCCAGCCATTGCAACAGCAGAACAATATTACCGTTTT
Endcap 32	TTTTGCAGATAGCCGAACAAAGTTATTCATATGGTTTACCAGCGCCTTTT
Endcap 33	TTTTTGCTTTAAACATTCAAAGCGAATTTT
Endcap 34	TTTTAAGGGATTTTAGACAGAACAGGAGGCCGATTATTTT
Endcap 35	TTTTGAAGTTTCATTCTAATAGTAGTTTTT
Endcap 36	TTTTCATATGCGTTATACAAAAAGCCTGTTTAGTATTTTT
Endcap 37	TTTTGGTTATATAACTATATCCTCCGGCTTAGGTTGTTTT